Republic of Iraq
Ministry of Higher Education & Scientific Research
University of Babylon
College of Education for Pure Sciences
Department of Physics

Quasi Elastic Scattering Calculations in some Heavy-Ion Systems

A Dissertation

Submitted to the Council of College of Education for Pure Sciences, University of Babylon in Partial Fulfillment of the Requirements for the Degree of Doctor of Philosophy in Education / Physics.

by

Farah Jabbar Hamood Abd-Alhussain

B.Sc. in Physics
(University of Babylon, 2004)
M.S.c. in Physics
(University of Babylon, 2016)

Supervised by

Prof. Dr.Khalid Salih Jassim

College of Education for Pure Sciences

Department of Physics

2023 A.D **1445 A.H**

بسم الله الرحمن الرحيم

﴿ ويسألونك عن الروح قل الروح من أمر ربي وما أوتيتم من العلم إلا قليلا ﴾

صدق الله العلي العظيم

سورة الإسراء – الآية (٨٥)

Certification of Scientific Expert

I certify that I have read the scientific content of this dissertation " **Quasi Elastic Scattering Calculations in some Heavy-Ion Systems**" and I have approved this dissertation is qualified for debate.

Signature:

Name: Dr. Ali A. Abo Jasem

Title: Professor.

Address: Al-Kufa University, College of Science

Date: / / 2023

Certification of Scientific Expert

I certify that I have read the scientific content of this dissertation **"Quasi Elastic Scattering Calculations in some Heavy-Ion Systems"** and I have approved this dissertation is qualified for debate.

Signature: Fadhil I. Sharrad.

Name: Dr. Fadhil I .Sharrad

Title: Professor.

Address: Al-Kafeel University, College of Health and Medical Technology.

Date: / / 2023

Certification of linguistic Expert

I certify that I have read this dissertation entitled " **Quasi Elastic Scattering Calculations in some Heavy-Ion Systems**" and corrected its grammatical mistakes; therefore, it has qualified for debate.

Signature: Name: Dr. Ahmed Rawdhan Salman

Title: Asst. Prof

Address: AL- Mustaqbal University

Date: / 9 / 2023

Supervisor's Certification

I certify that the preparation of this thesis, entitled " ***Quasi Elastic Scattering Calculations in some Heavy-Ion Systems*** " by " ***Farah Jabbar Hamood Abd-Alhussain*** " under my supervision at the College of Education for Pure Sciences, University of Babylon as partial fulfillment of the requirement for the Degree Doctor of philosophy Education / Physics.

Signature:
Name: **Dr. Khalid Salih Jassim** Title: Professor
Address: University of Babylon
College of Education for Pure Sciences
Date: / / 2023

Head of the Department Certificate

In view of the available recommendations, I forward this thesis for debate by the examining committee.

Signature:
Name: **Dr. Khalid Haneen Abass**
Title: Professor
Head of Physics Department
Address: University of Babylon
College of Education for Pure Sciences
Date: / / 2023

Examination Committee Certification

We certify that we have read this thesis entitled " ***Quasi Elastic Scattering Calculations in some Heavy-Ion Systems*** " and as an examine committee, we examined the student (***Farah Jabbar Hamood***) in its contents, and that in our opinion it meets the standards of a thesis for the Degree of Doctor of philosophy Education / Physics.

Signature:
Name: **Dr. Fouad A. Majeed**
Title: Professor
Address: University of Babylon
Date: / / 2023
(Chairman)

Signature:
Name: **Dr. Mohsin Kadhim Muttaleb**
Title: Professor
Address: University of Babylon
Date: / / 2023
(Member)

Signature:
Name: **Dr. Mohanad H. Oleiwi**
Title: Professor
Address: University of Babylon
Date: / / 2023
(Member)

Signature:
Name: **Dr.Murtadha Shakir Aswood**
Title: Professor
Address: University of Al-Qadisiyah
Date: / / 2023
(Member)

Signature:
Name: **Dr. Inaam Hani Kadhim**
Title: Assist .Professor
Address: University of Babylon
Date: / / 2023
(Member)

Signature:
Name: **Dr. Khalid Salih Jassim**
Title: Professor
Address: University of Babylon
Date: / / 2023
(Supervisor)

Approved by the Council of the College of Education for Pure Sciences.

Signature:
Name: **Dr. Bahaa Hussien Salih Rabee**
Dean of the College of Education for Pure Sciences
Title: Professor
Address: University of Babylon
Date: / / 2023

Dedications

To My parents who I knew the meaning of success by them, especially my Mother who dreams at this moment.

To My husband… Who bore with me all the difficulties and stood with me and supported me step by step

To the source of my happiness in life … who their hearts with me…

My sister…

My brothers…

My sons…

My real friends…

To all who helped me and prayed for me.

Farah

Acknowledgments

First and foremost, praise be to Allh Almighty, who gave me the strength and patience to complete this work ,and blessings be upon his Prophet Mohammed, who sent mercy to the world and all his family and companions.

then I would like to thank my supervisor, Prof. Dr. Khalid Salih Jassim, for his supervision, his continuous follow-up, and his suggestions for the completion of this thesis .

I also extend my thanks to the head and members of the Department of Physics, especially Prof .Dr. Khalid Haneen Abass for his valuable observations and for the lessons in life that I learned from him throughout the study period and before. I thank, the Dean of the College of Education for Pure Sciences Prof .Dr. Bahaa Hussein Rabee and the staff of the College of Education for Pure Sciences at the University of Babylon for allowing them to complete the study .

Finally, I wish I could have a better word of thanks to express my feelings to my family: dear parents, my husband, my sister, and my sons for their understanding, constant encouragement, and support throughout this work, with apologies to them for any shortcomings I may have appeared to them .

Farah

Abstract

In this study, an essential component of comprehending a nucleus-nucleus collision is knowing the nuclear potential between the two colliding nuclei. The nucleus-nucleus potential for some heavy-ion reactions can be studied by using large-angle quasi-elastic scattering at deep sub-barrier energies close to the Coulomb barrier height, which is considered a suitable method to study the nuclear potential . The nuclear potential has been described using the Woods-Saxon (WS) form, which is characterized by the surface diffuseness parameter, the potential depth, and the radius parameter. Single channel (SC) and coupled channel (CC) calculations were performed to investigate the relative movement of colliding nuclei and their internal movements and their impact on computing the ratio of quasi-elastic scattering cross sections to Rutherford scattering cross sections, as well as the investigation of the surface diffusion method to find the best suitable value for diffusion parameters in comparison to empirical data.

A systematic study and analysis of the nuclear potential (the surface diffusion parameters, potential depth) for heavy ion systems following: $^{24}Mg+^{90}Zr$,$^{28}Si+^{120}Sn$,$^{28}Si+^{150}Nd$,$^{16}O+^{160}Gd$,$^{12}C+^{197}Au$, $^{6}Li+\ ^{144}Sm$,$^{28}Si+\ ^{124}Sn$, $^{6}Li+^{159}Tb$,$^{22}Ne+^{248}Cm$,$^{10}B+^{232}Th$ .By using the CQEL computer program, which is regarded as the most recent version of the CCFUL computer program. That was developed by Hagino and his fellow Japanese scientists was employed .The chi-square χ^2 method has been used to find the best-fit values to (diffuseness parameters a_0 and potential depth V_0) based on the comparison of theoretical calculations and experimental data.

In the systems ($^{6}Li+\ ^{144}Sm$, $^{6}Li+^{159}Tb$, and $^{10}B+^{232}Th$), it is found that the diffuseness parameters best-fitted values of the parameters is

determined by using the coupled-channels calculation using an inert projectile and an excitation target, except for the $^{28}Si+^{150}Nd$ system, where an inert target and an excitation projectile .for the systems $^{16}O+^{160}Gd$,$^{12}C+^{197}Au$, ^{28}Si + ^{124}Sn, $^{24}Mg+^{90}Zr$,$^{28}Si+^{120}Sn$ and ^{22}Ne + ^{248}Cm, the projectile and the target is taken as excited

In the systems (^{6}Li + ^{144}Sm, ^{6}Li +^{159}Tb, and $^{10}B+^{232}Th$), it is found that the diffuseness parameters best-fitted values of the parameters is determined by using the coupled-channels calculation using an inert projectile and an excitation target, except for the $^{28}Si+^{150}Nd$ system, where an inert target and an excitation projectile .for the systems $^{16}O+^{160}Gd$,$^{12}C+^{197}Au$, ^{28}Si + ^{124}Sn, $^{24}Mg+^{90}Zr$,$^{28}Si+^{120}Sn$ and ^{22}Ne + ^{248}Cm, the projectile and the target is taken as excited

In the second part of the calculations, for some of the systems studied, the effect of changing the potential depth (V_0) on the calculated ratio of quasi-elastic scattering to the Rutherford cross section was in agreement with the potential depth that has been adopted as a standard value or at a value less than it.

Contents

Chapter Three

3 The Coupled Channel Formalism 3

Chapter Four

4 Calculations, Results and Discussion 4

Chapter Five

5 Conclusions and Future works 5

List of Symbols

Symbols	Definition
^{24}Mg	The stable isotope of Magnesium
^{90}Zr	The stable isotope of Zirconium
^{28}Si	The stable isotope of Silicon
^{120}Sn	The stable isotope of Tin
^{150}Nd	The stable isotope of Neodymium
^{16}O	The stable isotopes of Oxygen
^{160}Gd	The stable isotope of Gadolinium
^{12}C	The stable isotope of Carbon
^{197}Au	The stable isotope of Gold
^{6}Li	The stable isotope of Lithium
^{144}Sm	The stable isotope of Samarium
^{124}Sn	The stable isotope of Tin
^{159}Tb	The stable isotope of Terbium
^{22}Ne	The stable isotope of Neon
^{248}Cm	The stable isotope of Curium
^{10}B	The stable isotope of Boron
^{232}Th	The stable isotope of Thorium
WS	The Woods-Saxon
SC	The single-channel.
CC	The coupled-channels
$V_N(r)$	The Nuclear potential.
$V_c(r)$	The Coulomb potential.
$V(r)$	The bare potential in the absence of coupling.
R_o	The radius parameter of the system.

Symbols	Definition
r_0	The radius parameter
a	The surface diffuseness parameter.
V_0	The potential depth.
A_T	The mass number of the target nucleus.
A_P	The mass number of the projectile nucleus.
Z_P	The atomic number of the projectile.
Z_T	The atomic number of the target.
e	The electron charge.
R_C	The radius of the ball equivalent to the nuclei of the target and the projectile.
$V_{eff}(l,r)$	The effective potential
l	The orbital angular momentum.
r	The center- of-mass distance between the projectile and target nuclei.
μ	The reduced mass of the system.
V_B	The Coulomb barrier height.
R_B	The position of the Coulomb barrier.
H	The Hamiltonian operator.
E	The Eigen value of the Hamiltonian operator.
$\psi(\vec{r})$	The wave function of the incoming plane wave.
$\psi(r,\theta)$	The wave function of the sum of incoming plane wave and The outgoing spherical wave.
$\vec{k}$	The wave number vector of the incoming wave.
P_l	The Legendre polynomials.
θ	The angle between $\vec{r}$ and $\vec{k}$.
$H_l^{(-)}(kr)$	The incoming Coulomb wave.

Symbols	Definition
$H_l^{(+)}(kr)$	The outgoing Coulomb wave.
S_l	The complex quantity nuclear S-matrix.
A_{lm}	The expansion coefficient of expanding the wave function $\psi(\vec{r})$, represents the capacity of the wave function.
$U_l(r)$	The diagonal part of the wave function $\psi(\vec{r})$.
$Y_{lm}(\vec{r})$	The angular part of the wave function $\psi(\vec{r})$.
σ_{el}	The total elastic cross section.
$f(\theta)$	The scattering amplitude.
$\mathrm{H}(\vec{r},\xi)$	The Hamiltonian of the system.
$H_0(\xi)$	The Hamiltonian for the intrinsic motion.
ξ	The internal degree of freedom.
$V_{coup}\,(\vec{r}.\xi)$	The coupling Hamiltonian of the system.
$f_\lambda(r)$	The coupling form factor.
$Y_{\lambda\mu}(\hat{\mathrm{r}})$	The spherical harmonics.
$\mathrm{T}_{\lambda\mu}(\xi)$	The spherical tensors.
J	The total angular momentum.
$\varphi_{nIm_I}(\xi)$	The wave function for the intrinsic motion
I	The intrinsic angular momenta.
$V^J_{nlI;\acute{n}\,l'\acute{I}}(r)$	The coupling matrix elements.
$k_{nlI}(r)$	The local wave number .
$\mathcal{T}^{\mathrm{J}}_{\mathrm{n}lI}$	The transmission coefficients.
k_{nIi}	The wave number for the entrance channel.
$P^J_{liIi}(E)$	The penetrability during the Coulomb barrier.

Symbols	Definition
σ_l	The Coulomb phase shift.
f_c	The Coulomb scattering amplitude.
η	The Summerfield parameter.
σ_R	The Rutherford cross section.
$\alpha_{\lambda\mu}$	The coordinate of the surface vibration.
$R_T(\theta,\phi)$	The radius of the vibrating target nucleus.
R_T	The equivalent sharp radius.
$a_{\lambda\mu}$	The phonon annihilation operator
$a^{\dagger}_{\lambda\mu}$	The phonon creation operator
α_o	The amplitude of the zero-point motion
β_λ	The deformation parameter
B(Eλ) ↑	The electromagnetic transition probability.
R_C	The Coulomb radius.
$\hat{O}_\lambda$	The dynamical operator.
R_T	The target radios.
$V^N_{mn}(r)$	The nuclear coupling matrix elements.
$V_N^{coup(vib)}(r,\hat{O}_\lambda)$	The nuclear vibrational coupling potential.
ρ_T	The charge density of the target nucleus
$Q_{\hat{\lambda}\hat{\mu}}$	The electric multiple operator.
$V_C^{coup(vib)}(\vec{r},\alpha_{\lambda\mu})$	The Coulomb vibrational coupling potential.
$f^C_\lambda(r)$	The Coulomb coupling form factor.
$V^C_{nm}(r)$	The Coulomb coupling matrix elements.
$V_{coup}(r)$	The total coupling matrix elements.

Symbols	Definition
$\hat{O}_{\lambda_P}$	The excitation operators for the projectile.
$\hat{O}_{\lambda_T}$	The excitation operators for target
λ_P	The multi-polarity of the vibrations in the projectile.
λ_T	The multi-polarity of the vibrations in the target.
$V_{nm}(r)$	The coupling potentials.
$\xi_{\alpha(\gamma)}$ and $\|\alpha(\gamma)\rangle$	The eigenvalues and the eigenvectors for the operators $\hat{O}_{P(T)}$
ϕ_d, θ_d, χ_d	The Euler angles.
$V_{mn}^{N}(r)$	The nuclear coupling matrix elements.
$V_N^{coup(rot)}(r, \hat{O}_\lambda)$	The nuclear rotational coupling potential
λ_μ , $\|\mu\rangle$	The eigenvalue and the eigenvector of the operator $\hat{O}_\lambda$.
$V_C^{coup(rot)}(r, \hat{O}_\lambda)$	The Coulomb rotational coupling potential .
$V_{nm}^{C}(r)$	The matrix elements for the rotational coupling potential.
SC	Single Channel
CC	Coupled Channel
HI	Heavy Ione

List of Tables

List of Figures

Chapter One

General Introduction

And Literature survey

Chapter 1
General Introduction

1.1 Introduction

Knowing the potential between two colliding nuclei is of fundamental importance in order to describe nucleus-nucleus collisions. The nucleus-nucleus potential is the sum of a short range attractive nuclear potential V_N (r) and a long range repulsive Coulomb potential V_C(r).Although the Coulomb contact between two nuclei is widely understood, describing the nuclear component is far more challenging [1]. The simplest nuclear reaction process, elastic scattering, is frequently used to explain more intricate nuclear reactions. The nuclear reactions at sub-barrier energies play an extremely important role fundamental behavior of stars, their evolution, and many aspects of the production of the elements , which have a huge impact on nature [2].

In the study of nuclear structure, the Woods-Saxon potential is often used to represent the nuclear component, which is characterized by the deepness(V_0), radius r_0, and diffuseness parameters a_0. within regarded as the most realistic short - range potential in nuclear physics[3]. that it is reasonably straightforward, making study theoretical calculations easy. The study of nuclear particle elastic and quasi-elastic scattering has resulted in the discovery of several extended variants of this potential[1].

There are benefits to understanding the nuclear potential using experimental data from quasi-elastic scattering instead of fusion. For instance, measuring fusion cross sections necessitates a specialized recoil separator (electrostatic deflector/velocity filter), often with low acceptance and efficacy. On the other hand, measuring quasi-elastic cross

sections just requires a very basic charged particle detector. This implies that the experimental data for quasi-elastic scattering are likely to be more precise and less prone to mistakes than the experimental data for fusion. So, by using experimental data from quasi-elastic scattering, evaluations of the nuclear potential may be done with more accuracy[1] . There are a variety of distinct reaction modes produced by collisions between two heavy nuclei at energies over the Coulomb barrier, but two processes are noticeable: direct reactions and compound nucleus synthesis. Other processes, such as deep-inelastic reactions, incomplete fusion, and quasi-fission events, have been discovered through research on heavy-ion reactions. The interaction gradually evolves with increasing impact parameter from fusion and fission-like reactions, which require a significant overlap of the two nuclei [4]. The total of elastic scattering, inelastic scattering, and transfer reaction may be used to compute quasi-elastic scattering[5]. Fusion is defined as a reaction where two separate nuclei combine together to form a composite system, fusion and quasi-elastic scattering are both recognized as complete procedures that complement each other. As a result, both interactions have the same potential and share the same understanding of the interaction process, and both are susceptible to the effects of channel coupling (owing to reciprocal inelastic excitations of colliding nuclei) at energies close to the Coulomb barrier. [1] .

The coupling channel (CC) model is an ideal tool to reproduce the experimental data at the same time for several processes, such as elastic and inelastic scattering, particle transfers, and fusion, within a unified framework. Many interactions between two nuclei are possible when they get closer to one another. In the first approximation, they may be thought of as a cluster of nucleons, and the inter nuclear two-body force would be

the main source of their interaction. The period that the responding nuclei are together during the collision, however, may result in one or many rearrangement events. It is possible for inelastic excitations to take place. For instance, before fusion can occur, one or both of the interacting nuclei may be stimulated to a higher energy state. There are two types of excitations to take into account: rotational and vibrational. Single-particle excitation can also happen when a particle in one of the nuclei is stimulated during a reaction from one state to another. Moreover, single nucleons or groups of nucleons may move from one nucleus to another[6]. The strong interaction between the attractive nuclear force and the repulsive Coulomb force results in a potential barrier for the relative motion between the colliding nuclei in a basic model. Due to couplings of the relative motion to intrinsic degrees of freedom (such as collective inelastic excitations of the colliding nuclei and/or transfer processes), this barrier in the coupled channel is split into a number of distributed barriers [7].

The quasi-elastic scattering is connected to the reflection probability at the Coulomb barrier, but the fusion is related to the transmission probability. This is a key distinction between the two processes.The excitation function data reveals the most fundamental features of the underlying reaction process and is very often used for extracting the other relevant observable such as the extraction of barrier distribution. It is worthwhile mentioning that the barrier distribution of a given system obtained from both the quasi-elastic scattering and fusion excitation function measurements is found to be very similar in nature. However, the quasi- elastic excitation function measurement is relatively easier to carry out from the technical point of view [12]. It is now well-known that the coupled-channel calculations for the heavy-ion reaction at

energies close to and below the Coulomb barrier can explain the experimental data of fusion reactions as well as the quasi-elastic scattering of the medium-heavy mass systems, heavy mass systems, and a very heavy mass systems. It is demonstrated that the collective excitations (rotations and surface vibrations), and nucleon transfer of the colliding nuclei have a significant impact on the cross section and barrier distribution for fusion reactions and quasi-elastic scattering [9]. It is generally acknowledged that the barrier distribution idea offers a potent tool for analyzing the effects of channel coupling on heavy-ion fusion events as well as quasi-elastic scattering at sub-barrier energies even for very heavy mass systems. Channel couplings also affect the scattering process. It was suggested that the same information as the fusion cross section may be obtained from the cross section for quasi-elastic scattering (as elastic ,inelastic ,and transfer cross sections) at large angles. It is known that the single-barrier elastic cross section falls off smoothly from a value close to that for Rutherford scattering at low energies to very small values at energies high above the barrier. Therefore, it is proposed to use the first derivative of the ratio of the quasi-elastic cross section σ_{qel} to the Rutherford cross section σ_R with respect to energy, $D_{qel}(E) = -\frac{d}{dE}\left[\frac{d\sigma_{qel}}{d\sigma_{Ruth.}}\right]$,as an alternative representation of the barrier distribution [10] .

1.2 Heavy-Ion Reactions

the nuclear reaction is the process by which a nucleus changes from one species to another . In these reactions, a target nucleus is struck by an accelerating projectile. So, the original system is changed into the reaction's new system , heavy-ion collisions occur when relatively heavy projectiles collide with targets. A composite nucleus with a high atomic

number would be formed. Many fascinating events can occur in heavy-ion collisions by carefully selecting targets and projectiles [6]. The range of events produced by heavy ion collisions close to the Coulomb barrier is particularly intriguing. The barrier splits as a result of many channels coupling with one another, creating the sub-barrier region [11]. Throughout the past several decades, interest in heavy ion collisions at near-barrier energies, in particular fusion and quasi-elastic processes, has developed from an experimental and theoretical perspective. Such studies offers a great chance to learn about nuclear structure and nucleus-nucleus interaction. [12].

1.3 Quasi Elastic Scattering and Heavy Ion Reaction

First emerged in the early 1970s the term quasi-elastic reaction, which entails inelastic scattering and few-nucleon transfer reactions populating , in order to distinguish peripheral collisions associated with energy losses from the more violent deep-inelastic reactions, which showed substantial amounts of energy and mass transfer a clear distinction between quasi-elastic and deep-inelastic reactions ,as a result of this coupling, reaction modes associated with central collisions, such as fusion, can be influenced peripheral quasi-elastic reactions. These reactions (inelastic scattering and few nucleon transfer reactions) depend through strongly on the structure of the interacting nuclei. Fusion reactions were once thought to be mainly a macroscopic process, but channel coupling makes them strongly dependent on nuclear structure. For inelastic heavy-ion scattering, experimental and theory data are usually in good agreement [4]. Heavy-ion quasi-elastic scattering and fusion reactions at energies near the Coulomb barrier have received a lot of attention because they provide an excellent opportunity to learn about nuclear structure and nucleus-nucleus interaction, as well as investigate

the mechanism of heavy-ion reactions at near-barrier energies, which is important for the synthesis of super-heavy nuclei. The quasi-elastic scattering is a good counterpart to the fusion reaction . As a result, it is expected that the fusion and quasi-elastic scattering cross sections of a heavy-ion process at energies near the Coulomb barrier may be characterized by the same nucleus-nucleus potential[13].

1.4 Literature Survey

K.Hagino *et al.*, 2004 [10] were discussed in great detail the barrier distributions derived from large-angle quasi-elastic scattering of heavy ions at energies close to the Coulomb barrier. The quasi-elastic barrier distribution was compared to the fusion test function. In coupled channel calculations of quasi-elastic scattering ,they find that it works well for backward angles, lending credence to the idea of a barrier distribution for scattering processes. This approach is a useful tool for studying unstable nuclei.

K. Hagino *et al.*, 2005 [14] have analyzed highly precise experimental results for heavy-ion reactions in order to explain the data at sub-barrier energy. An unexpectedly large surface diffuseness parameter is necessary in order to fit the experimental data for the $^{16}O + ^{154}Sm$ system at sub-barrier energies. found that the divergence of the ratio of the quasi-elastic to Rutherford cross sections from unity provides a simple method for calculating the value of the surface diffuseness parameter in the nucleus-nucleus potential. They proved that surface diffuseness parameter is indeed more influential in the coupling channel for quasi-elastic scattering at low energies.

K. Washiyama *et al.*,2006 [15]conducted study on the surface properties of nuclear potential in heavy ion interactions for $^{32,34}S+^{197}Au$, $^{32,34}S+^{208}Pb$, $^{16}O+^{154}Sm$, ^{186}W and ^{208}Pb systems. By employing large-angle quasi elastic scattering at energies much below the Coulomb barrier. have extensively investigated experimental data for quasi-elastic scattering at deep sub-barrier energies in order to extracting the surface diffuseness parameter of inter nuclear potential. have been got a diffuseness parameter commensurate with the conventional value of roughly a is 0.63 fm for systems containing spherical nuclei.

L. R. Gasques *et al.*,2007 [16] have measured highly precise quasi-elastic scattering for ^{32}S reactions with ^{208} Pb, ^{197}Au, ^{186}W, and ^{170}Er at energies much below the Coulomb barrier. The diffuseness parameter of the nuclear potential was calculated using single-channel SC and coupled channels. Both theoretical analyses provide the same diffuseness parameter for reactions with near-spherical targets. Coupling channels are essential for deformed systems, even at high sub-barrier energies. The effect of coupling channels is to reduce the diffuseness parameter value extracted from a single-channel potential. Single-channel fits to quasi-elastic scattering data result in a = 0.72,0.82 fm, whereas coupled-channel calculations give diffuseness parameters in the range 0.58–0.75 fm.

M. Zamrun F *et al.*,2008 [17] proved that the coupled-channels method is effective for large-angle quasi-elastic scattering in complex systems. have investigated the effects of single, double, and triple phonon excitations on quasi-elastic scattering experimental cross-section systems ^{48}Ti,^{54}Cr,^{56}Fe, ^{64}Ni, and $^{70}Zn+^{208}Pb$.have demonstrated that the experimental barrier distribution for the overall width of these systems is well represented by the coupled-channel computations in use.

C. J. Lin *et al.*,2009 [18] have been measured the high precision excitation data of large-angle quasi-elastic scattering for the systems of $^{16}O+^{208}Pb$, ^{196}Pt, ^{184}W, and $^{154,152}Sm$ at energies much less than the Coulomb barrier. The surface diffuseness parameters of the real part of the Woods-Saxon potential have been extracted from the single-channel and coupled-channels calculations .By considering the effect of couplings, the extracted diffuseness parameters are in the range from 0.64 to 0.69 fm, which is close to the values extracted from the systematic analyses of elastic and inelastic scattering data. On the other hand, single-channel calculations give somewhat larger values in the range from 0.68 to 0.77 fm, especially for systems with deformed target nuclei.

C. J. Lin *et al.*,2011[19] have measured the quasi-elastic scatterings at backward angles to explore the heavy ion reaction processes at close to sub-barrier energies. Single-channel(SC)and coupled-channel(CC) calculations were used to measure the surface diffuseness parameters for the systems $^{16}O+^{144,152,154}Sm$,^{170}Er,^{174}Yb, $^{184,186}W$, $^{194,196}Pt$, and ^{208}Pb. For SC, the diffuseness parameters are larger than the baseline value of 0.65 fm, especially for deformed systems. After accounting for the CC effects, these values are quite near 0.65 fm.

M. L. I. Ibrahim *et al.*,2013 [1]studied the surface diffuseness parameter of the nuclear potential for the reactions of ^{208}Pb with ^{48}Ti, ^{54}Cr, ^{56}Fe, ^{64}Ni, and ^{70}Zn using large-angle quasi-elastic scattering. Their study's diffuseness parameters were lower than the typical value of roughly 0.63 fm. However, as compared to SC computations, diffuseness parameters determined by CC analysis at sub-barrier energies were superior to the standard value.

K. S. Jassim *et al.*,2014 [20] have studied large-angle quasi-elastic scattering at sub-barrier energies for the nuclear potential of heavy ion systems, specifically ^{48}Ti, ^{54}Cr, and ^{64}Ni + ^{208}Pb systems. Around the Coulomb barrier's height, using an inert target and a vibrational projectile, the value of the diffuseness parameter that best fits a system was calculated using the coupled-channel method. The calculated ratio of the quasi-elastic to the Rutherford cross sections for systems yields good agreement when a = 0.44 fm, 0.67 fm, and 0.67 fm, respectively.

K. S. Jassim *et al.*,2015 [21] studies the nuclear potential's surface diffuseness parameter for the heavy-ion reactions involving the systems ^{32}S + ^{208}Pb and^{34}S + ^{208}Pb ,which were made feasible by deep sub-barrier energies near the Coulomb barrier height by using large-angle for quasi elastic scattering .have been computed the diffuseness parameter of the nuclear potential using single-channel (SC) and coupled-channel (CC) methods. Surface diffuseness parameters calculated with an inert projectile and a vibrational target agree exactly with the standard value of 0.63 fm to find the diffuseness parameter value that best matches the experimental data, while single-channel calculations produce slightly higher values in the 0.64 fm to 0.65 fm range.

Q.J. Tarbool *et al.*,2019 [22] investigated the surface characteristics of the inter nucleus potential in heavy-ion reactions for the ^{63}Li + ^{64}Zn and ^{73}Li + ^{64}Zn systems at sub-barrier energies around the Coulomb barrier height. A ground-state rotational band and the rotational deformation of the nucleus ^{64}Zn were both present. The diffuseness parameter of the nuclear potential as well as the potential depth were computed using single-channel (SC) and coupled-channel(CC) computations with an inert projectile and a rotating target for those systems, it was found that the

diffuseness parameter was entirely consistent with the standard value of 0.63 fm.

S. Biswas *et al.*,2020 [23] studied Large-angle quasi elastic scattering data were used to calculate barrier distributions for the $^{28}Si+^{142,150}Nd$ systems. The measurements were made across a wide range of incoming beam energies near the Coulomb barriers. The experimental data were compared with coupled-channel calculations performed using various coupling techniques. The experimental and theoretical results agreed rather well.

A. J. Hassan *et al.*,2020 [24]studied the impacts of the surface diffuseness parameter on quasi-elastic scattering using nuclear potential Woods-Saxon (WS) for $^{6}He+^{64}Zn$, $^{7}Li+^{64}Zn$, and $^{8}Li+^{90}Zr$ systems. For the nuclei ^{64}Zn, the effect of rotational deformation was included with the ground state rotational band up to the 4^{+} states. The single-channel (SC) and coupled-channel (CC) computations were performed. It has been found that the best-fitting value of the diffuseness parameter is obtained from a coupled-channel calculation with an inert target and an energized projectile.

P. Biswas *et al.*,2021 [25] measured the Quasi elastic scattering excitation data at large backward angle has been measured for the system, $^{7}Li+^{159}Tb$ at energies around the Coulomb barrier. The corresponding quasi elastic barrier distribution has been derived from the excitation data, the α-particles produced in the reaction .The centroid of the barrier distribution obtained after inclusion of α-particles was found to be shifted higher in energy ,compared to the distribution excluding the α-particles .The quasi elastic data ,excluding the α-particles ,have been analyzed in the framework of continuum discretized coupled channel calculations .

The quasi elastic barrier distribution for $^{7}Li+^{159}Tb$, has also been compared with the fusion barrier distribution for the system.

N. H. Hayef *et al.*,2023 [26] studied effects of the surface diffuseness parameter on quasi-elastic scattering using the Woods-Saxon (WS) potential for the systems $^{6}Li+^{64}Zn$, $^{23}Na+^{90}Zr$, and $^{11}C+^{208}Pb$. demonstrated the results of theoretical examinations of the impacts of deformation rotational for the nucleus ^{64}Zn with ground state rotational band up to the 2^{+} levels. The best suitable value of the diffuseness parameter is obtained by using a coupled-channel approximation with an inert target and an energized projectile.

Aim of the present study

The primary objective of preparing this dissertation is to study the effect of changing the diffuseness parameter a_0, nuclear potential (potential depth)V_0, and the influence of coupling on quasi-elastic scattering using a large angle for the energies near the Coulomb barrier for the following systems: $^{24}Mg + ^{90}Zr$, $^{28}Si+^{120}Sn$, $^{28}Si+^{150}Nd$, $^{16}O + ^{160}Gd$, $^{12}C + ^{197}Au$, $^{6}Li + ^{144}Sm$, $^{28}Si + ^{124}Sn$, $^{6}Li + ^{159}Tb$,$^{22}Ne+^{248}Cm$ and$^{10}B+^{232}Th$.

Find the best-fit values for the quasi-elastic scattering and the distribution by using the chi-square method for comparison between theoretical calculations and experimental data.

Thesis outline

This thesis is organized as follows:

Chapter1: General introduction about the nucleus-nucleus potential include the definition and its components and the model that can be described it, in addition to know the cross-section of the quasi-elastic scattering. As well as review the aim of the research and most important previous studies concerning the subject matter.

Chapter2: Reviews The Coulomb Barrier and the basic theory of scattering and Rutherford scattering

Chapter3 : The theory of coupled channel with all order of coupling. The concept of barrier distribution were also reviewed.

Chapter 4: Presents our theoretical calculations and the comparison of our present work with the available experimental data for the Quasi elastic scattering and barrier distribution.

Chapter 5: Concludes the research, provides a summary of key findings, and gives suggestions for future researches.

Chapter Two
Theoretical Part

Chapter 2

Theoretical Part

2.1 Introduction

The most important experimental technique in quantum physics is the scattering experiment. Where in nuclear physics, the first clear evidence of nuclear structure came from Rutherford's observation of the scattering reaction. The theoretical tool for the analysis of scattering experiments is scattering theory. Scattering theory is the study of an interacting system on a time and/or distance scale which is large compared to the scale of the actual interaction[27]. The scattering process is defined as a change in a particle's motion due to a collision with another particle. According to the definition of collision in physics, a collision can happen between particles that repel one another, such as positive or negative ions. Experiments with subatomic particles show that the electric repulsive force between the particles meets Coulomb's law, which stipulates that the force varies as the inverse square of the distance between the particles. The nuclear collision can often lead to one of a variety of reactions, each of which gives insight into a specific feature of nuclear structure or behavior. To examine the nuclear force, create new nuclei, ascertain the size and structure of the nuclei, and learn more about the characteristics of excited nuclei. According to the classical picture, the projectile can induce various kinds of reactions depending on the impact parameter or the corresponding angular momentum and the dynamical behavior of nuclear matter during different types of collision in the classical picture of Heavy-Ion [28,29],as shown in Fig.

2.1 [30] The eventual aim of every scattering experiment is to determine the true forces at work between colliding particles.

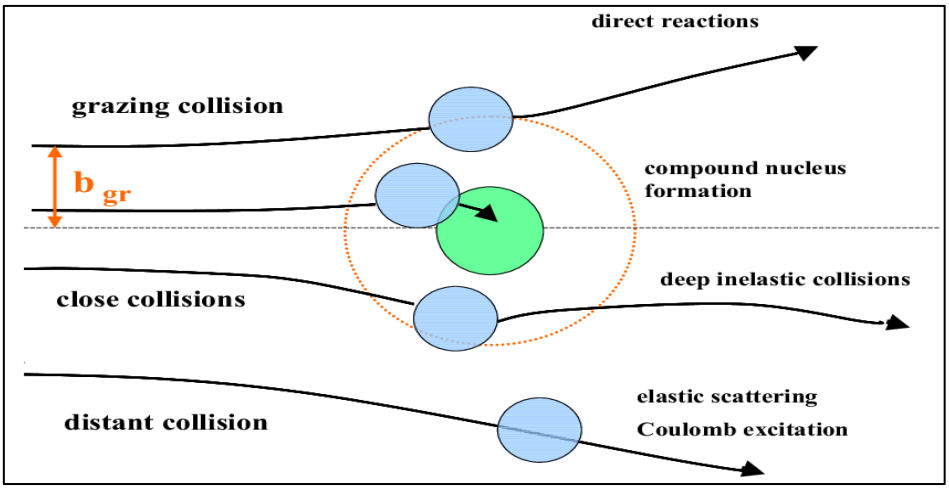

Figure 2.1 : Distant, grazing and close collisions in the classical picture of heavy ion collisions [6,30].

2.2 The Coulomb Barrier

The Coulomb barrier is the most familiar barrier to penetrate , present because of the electrostatic repulsion between the positively charged target nucleus and the positively charged projectile and the nuclear force between the two nuclei can be expressed as the interaction potential. By using a simple model, nuclear reactions can be described by considering the two nuclei as rigid spherical objects that interact via a potential which depends only on the relative distance (r) between the canter of mass (c.m.) of two nuclei. The total potential between the target and projectile nuclei have been illustrated in Eq (2.1) [31].

$$V(r) = V_C(r) + V_N(r) \qquad (2.1)$$

where V_C is the Coulomb and V_N is the nuclear potential Fig. 2.1[6]provides examples of them.

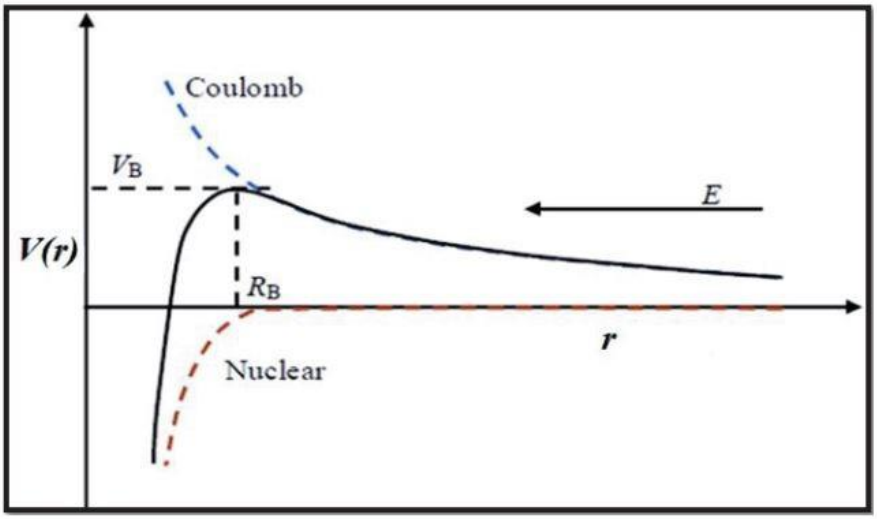

Fig 2.2 : The illustration of the potentials that form a barrier between the participating nuclei in a nuclear reaction [6].

The radial Schrödinger equation comprises an effective potential, which defined by the following equation[1]

$$V_{eff}(l,r) = V_N(r) + V_C(r) + \frac{\hbar^2 l(l+1)}{2\mu r^2}, \qquad (2.2)$$

Effective potential is the sum of nuclear, Coulomb, centrifugal components. When angular momentum l = 0, the compound centrifugal vanish.

There are two components to the nucleus-nucleus potential: the nuclear part V_N, which is well and properly defined by the WS form, which is given by[31]:

$$V_N(r) = -\frac{V_0}{1+\exp\left[\frac{r-R_0}{a}\right]}, \qquad (2.3)$$

where a_0 is the surface diffuseness parameter and V_0 is the potential depth R_0 is the radius parameter of the system ,defined as follows.

$$R_0 = r_0(A_T^{\frac{1}{3}} + A_P^{\frac{1}{3}}), \qquad (2.4)$$

where the radius parameter is r_0. It is important to note that the possible values for V_0, a_0, and r_0 are not all the unique[32]. They are usually adjusted by fitting experimental data.While r denotes the center of mass distance between the projectile's mass number A_P and the target's mass number A_T [33,34]. The Coulomb part $V_C(r)$ between two spherical nuclei with normal charge density distributions when they do not interact is given by[35]:

$$V_c(r) = \frac{Z_P Z_T \ e^2}{r}, \qquad r > R_c \tag{2.5}$$

where Z_P and Z_T are the atomic number of the projectile and target, respectively, and r is the distance between the centers of mass of the colliding nuclei. The Coulomb radius parameter R_c is the radius of the ball that corresponds to the projectile and target nuclei. where $R_c = r_c(A_T^{\frac{1}{3}} + A_P^{\frac{1}{3}})$ and r_c is a Coulomb radius parameter[36].

when the nuclei interact. The Coulomb potential is produced[20][35]

$$V_c(r) = \frac{Z_P Z_T \ e^2}{2R_C}\left[3 - \left(\frac{r}{R_C}\right)^2\right], \qquad r \leq R_c \tag{2.6}$$

2.3 Types of Scattering Reactions

In heavy ion systems, the products of the various reaction channels include the following phenomena elastic scattering, inelastic scattering, transfer reactions, fusion reactions, fission reactions, and quasi-fission reactions [6] .

2.3.1 Elastic Scattering

Elastic scattering is defined to be a collision in which the colliding particles only change their direction. In this reaction no kinetic energy of the projectile is used to take the target into an excited state. The projectile and the target remain in their ground states [6].

2.3.2 Inelastic Scattering

Inelastic scattering differs from elastic scattering in that the target nucleus is raised to an excited state as a result of the collision. Classically, the projectile only touches the target nucleus, or it may enter the nucleus and exit at a reduced energy. When the excited target nucleus returns to its ground state, the excess energy is released by the emission of particles like -γ-rays[6].

2.3.3 Transfer Reactions

One or more nucleons are transferred between the projectile and the target in transfer reactions when the projectile crosses over the target's perimeter, for example, when an incoming deuteron transforms into an outbound proton or neutron, adding nucleons to the target A to create a nucleus, B[6].

2.3.4 Quasi Elastic Scattering

In quasi elastic scattering, the projectile loses a moderate amount of energy, and a small number of nucleons are exchanged with the target nucleus. Quasi-elastic processes are thought to correlate. The term "quasi-elastic" refers to the total of all transfer processes, elastic scattering, and inelastic scattering.[6 ,37].

2.3.5 Deep Inelastic

This reaction entails substantial damping of kinetic energy and mass exchange. The larger fragments are highly deformed and excited while retaining partial memory of target and projectile masses and charges. This process takes place at energies above the Coulomb barrier[6] .

2.4 Scattering Theory

In this section, a Single Channel SC potential model is used to derive the basic formula for calculating the elastic and the fusion cross sections. Through finding the solution of Schrödinger equation $H\psi = E\psi$, we can describe elastic scattering between two nuclei [1].

$$\left[-\frac{\hbar^2}{2\mu}\nabla^2 + V(r) - E\right]\psi(\vec{r}) = 0, \qquad (2.7)$$

where μ is the reduced mass of the system, if there is no potential V(r), can be clearly solve this equation with $\psi = e^{i\vec{k}.\vec{r}}$, where $k = \sqrt{2\mu E/\hbar^2}$ is the wave number of the incoming wave. This solution has asymptotic form as follows [38]:

$$\psi(r,\theta) = e^{i\vec{k}.\vec{r}} \rightarrow$$
$$\frac{i}{2k}\sum_{l=0}^{\infty}(2l+1)(i)^l\left(\frac{e^{-ik(r-l\pi/2)}}{r} - \frac{e^{ik(r-l\pi/2)}}{r}\right)P_l(\cos\theta)\,, r \rightarrow \infty, \qquad (2.8)$$

the wave function $\psi(r,\theta)$ is sum of the incoming plane wave and the outgoing spherical wave. P_l stands for the Legendre polynomials, θ is the angle between $\vec{r}$ and $\vec{k}$. When the potential is presence the characteristic of the solution is change.

However, the asymptotic form of the wave function can be written down in a similar way to Eq. (2.8). because of the fact that the potential

vanishes at infinity. By replacing the plane waves with the corresponding Coulomb waves, the asymptotic form becomes [37].

$$\psi(r,\theta) \to \frac{i}{2k}\sum_{l=0}^{\infty}(2l+1)(i)^l\left(\frac{H_l^{(-)}(kr)}{r} - S_l\frac{H_l^{(+)}(kr)}{r}\right)P_l(\cos\theta)\; r \longrightarrow \infty, \qquad (2.9)$$

where $H_l^{(-)}(kr)$ and $H_l^{(+)}(kr)$ are the incoming and the outgoing Coulomb waves, respectively. S_l represents the nuclear S-matrix and generally is a complex quantity.

Can be determine the S-matrix, by expanding the wave function $\psi(\vec{r})$ in terms of the spherical harmonics as[39].

$$\psi(\vec{r}) = \sum_{l=0}^{\infty}\sum_{m=-l}^{l} A_{lm}\ \frac{u_l(r)}{r}\ Y_{lm}(\hat{r}), \qquad (2.10)$$

When the expansion coefficient is A_{lm}, the Schrödinger equation's solution is $u_l(r)$, with [39]

$$\left[-\frac{\hbar^2}{2\mu}\frac{d^2}{dr^2} + V(r) + \frac{l(l+1)\hbar^2}{2\mu r^2} - E\right]u_l(r) = 0, \qquad (2.11)$$

Where $\frac{l(l+1)\hbar^2}{2\mu r^2}$ represent the centrifugal potential [6].

Equation (2.11) can be solved by imposing the boundary conditions[34].

$$u_l(r) \sim r^{l+1} \qquad r \to 0 \qquad (2.12)$$

$$u_\ell(r) = H_l^{(-)}(kr) - S_l\, H_l^{(+)}(kr) \quad r \to \infty \qquad (2.13)$$

The nuclear S-matrix S_l, can be used to evaluate the differential elastic cross section, as [40].

$$\frac{d\sigma_{el}}{d\Omega} = |f(\theta)|^2, \qquad (2.14)$$

where $f(\theta)$is the scattering amplitude, the differential scattering cross section is defined as the number of particles emitted per solid angle $d\Omega$ divided by the incident flux of particles per unit time [41].

$$f(\theta) = \frac{i}{2k}\sum_{l=0}^{\infty}(2l+1)\,(1 - S_l)P_l(cos\,\theta). \qquad (2.15)$$

The total elastic cross section is given by:

$$\sigma_{el} = 2\pi \int_{-1}^{1} d(\cos\theta)\frac{d\sigma}{d\Omega} = \frac{\pi}{k^2}\sum_{l=0}^{\infty}(2l+1)|S_l - 1|^2 \qquad (2.16)$$

2.5 Reaction Cross Sections and Differential Cross Section

Reaction cross-section is the most important quantity in nuclear reaction study. It is a measure of the probability for particular reaction to occur. The larger the nuclear cross sections the more probable the reactions. This factor can be viewed as the target area effectively presented to the incident particles by each nucleus, such that if the incident particle passes through this area reaction will take place. The cross-section of a react ion is defined by [42].

$$\sigma = \frac{\text{number o f events o f given type per unit time per nucleus}}{\text{number o f incident particles per unit area per unit time}} \qquad (2.17)$$

Nuclear cross-section or the probability of any interaction has diminution of area that is so called cross-section and measured in a unit of cm^2 or barn. 1barn $=10^{-24}$ cm^2[43]. Cross sections are the central observable of nuclear and particle physics. In some areas of nuclear physics (e.g. HI physics) reactions (scattering) are often treated semi classically. Likewise, the historically important Rutherford scattering can be treated classically. The classical description implies that particles and their

trajectories are localized. However, in each case it must be checked whether a classical description is valid. A criterion for classicists is (like in geometrical light optics) the wavelength of the radiation used is small as compared with some characteristic object dimension (d). In agreement with Heisenberg , s uncertainty relation this means[42].

$$\lambda_{debroglie} = \frac{h}{p} << d \qquad (2.18)$$

When choosing for a typical object dimension half the distance of the trajectory turning point (d_0) for a central collision the Somerfield criterion for classical scattering is obtained [44].

$$\eta_s = \frac{Z_P Z_T e^2}{\hbar v} = \frac{Z_P Z_T e^2}{\hbar c} \cdot \frac{c}{v} = Z_P Z_T \cdot \frac{\alpha}{\beta} >> 1 \qquad (2.19)$$

with $\alpha = e^2/\hbar c$ Somerfield's fine-structure constant and β a short notation for v/c. Z_P and Z_T are the atomic number for the projectile and target nuclei, respectively.

There exist more refined criteria, which take into account that the wave nature of the radiation leads to diffraction phenomena, especially where the scattering potential changes strongly, e.g. at the nuclear surface. Therefore, a requirement is postulated that the de-Broglie wavelength not change substantially by the potential gradient. For Coulomb scattering this provides a scattering-angle dependent criterion[45].

$$\eta_s^2 \gg \eta_{crit}^2 = \left[\frac{\sin^2\left(\frac{\theta}{2}\right)}{\cos\left(\frac{\theta}{2}\right)\left(1-\sin\left(\frac{\theta}{2}\right)\right)}\right]^2 \qquad (2.20)$$

Thus, a classical description is always possible at $\theta = 0^{\circ}$ but never at $\theta = 180^{\circ}$. Definition of the differential cross section is the number of particles of a given type from a reaction, which, per target atom and unit time, are scattered into the solid-angle element $d\Omega$ (formed by the angular interval θ....θ + dθ and ϕ....ϕ + dϕ), divided by the incident particle flux j (a current density is number of particles passing a unit area per unit time)[45]. In the following we assume azimuthal (i.e. ϕ) independence of the scattering. The classical scattering situation is characterized by a definite trajectory and a unique relation between each particle incident from r → (−∞) at a definite perpendicular distance b (the impact parameter) from the z-axis and its (asymptotic) of a given type from a reaction, which, per target atom and unit time, are scattering angle at r → (+∞) after the interaction. This definition yields the classical formula for the cross section. With the number of particles per unit time $jd\sigma = j.2\pi\, bdb$ one obtains[42].

$$\left(\frac{d\sigma}{d\Omega}\right)_{\text{class}} = \frac{2\pi b db}{2\pi \sin\theta d\theta} = \frac{b}{\sin\theta} \cdot \left|\frac{db}{d\theta}\right| \qquad (2.21)$$

$b = b(\theta,E)$ contains the influence of the interaction (the dynamics). $\theta(b)$ is called deflection function. Its knowledge determines the scattering completely as shown in Fig. 2.3.

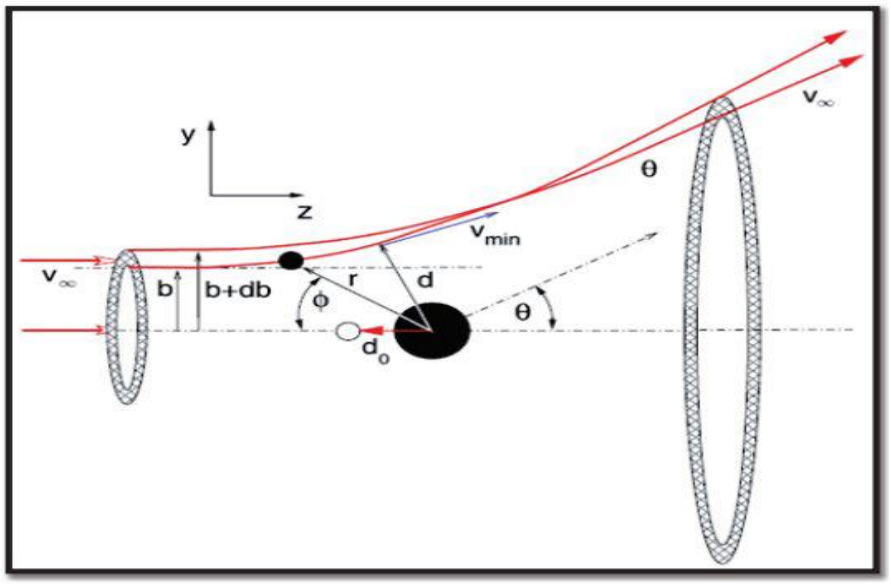

Fig (2.3): Classical Rutherford scattering. b is the impact parameter, *(r,ϕ)* are the polar coordinates of the projectile, *θ* the polar scattering angle, d is the distance of closest approach, and d_0 its minimum for a central collision[44].

2.6 Rutherford Scattering

2.6.1Classical-Mechanical Derivation of Rutherford's Formula

General approaches to describe elastic scattering like partial wave decomposition or the Born-approximation are of quantum-mechanical nature and lack a certain clearness. On the other hand one likes to imagine Coulomb-scattering using a model based on classical trajectories [46]. In fact it is often possible to describe elastic scattering processes well in a semiclassical or classical approximation. This is particularly true for heavy ion scattering experiments. As for heavy projectiles the Coulomb barrier is very high though, it is necessary to perform calculations on the peak of the Coulomb-wall (V_C) with the reduced kinetic energy of the projectile : $E = E_{c.m.} - V_C$ [46]. A classical derivation of the differential cross section for the elastic scattering of a

charged particle by the electrostatic potential given by a point charge. It is also commonly referred to as Rutherford scattering. In Fig 2.3 a particle is shown being deflected through an angle θ by a scattering center of charge Z_{Te}. the particle has charge Z_{Pe}, mass m, speed υ_∞, impact parameter b and energy $E = \frac{1}{2} mv^2$. We assume, for simplicity, that the scatterer remains at rest that is, we shall take the scatterer to be infinitely heavy [47]. The angle of the position vector $(\overrightarrow{r})$ to the y-axis is ϕ and we can use conservation of angular momentum to write [44].

$$L = mv_\infty b = mr^2 \frac{d\phi}{dt} = mv_{\min} d \tag{2.22}$$

We can also calculate $P = mv$ as the integral over the trajectory of the y component of the impulse on the particle due to the Coulomb force F_C acting on it, as following [42].

$$F_C = \pm \frac{1}{4\pi\varepsilon_0} \cdot \frac{Z_P Z_T e^2}{r^2} = \pm \frac{C}{r^2} \tag{2.23}$$

Where

$$C = \frac{1}{4\pi\varepsilon_0} \cdot Z_P Z_T e^2$$

$$dt = r^2 d\phi / v_\infty b \tag{2.24}$$

$$\Delta P = \int F_y dt$$

$$v_\infty \sin\theta = \frac{C}{mv_\infty b} \int_{-\infty}^{\infty} \sin\phi \frac{d\phi}{dt} dt$$

$$\frac{C}{mv_\infty b} \int_0^{\pi-\theta} \sin\phi d\phi = \frac{C}{mv_\infty b} (1 + \cos\theta) \tag{2.25}$$

After transformation to half the scattering angle the deflection function is

$$\cot(\theta/2) = mv_\infty^2 b/C = v_\infty L/C \tag{2.26}$$

and

$$b = \frac{C}{2E_\infty} \cdot \cot\left(\frac{\theta}{2}\right) \tag{2.27}$$

the derivative of Eq.(2.13) is [42][44].

$$\frac{db}{d\theta} = \frac{C}{2mv_\infty^2} \cdot \frac{1}{\sin^2(\theta/2)} = \frac{C}{4E_\infty} \cdot \frac{1}{\sin^2(\theta/2)} \tag{2.28}$$

and thus for the Rutherford cross section[44]

$$\frac{d\sigma}{d\Omega} = \left(\frac{Z_P Z_T e^2}{4E_\infty}\right)^2 \cdot \frac{1}{\sin^4(\theta/2)} \tag{2.29}$$

Numerically[44].

$$\frac{d\sigma}{d\Omega} = 1.296\left(\frac{Z_P Z_T}{E_\infty(MeV)}\right)^2 \cdot \frac{1}{\sin^4(\theta/2)}\left[\frac{mb}{sr}\right] \tag{2.30}$$

for finding the minimal scattering distance d one needs additionally the energy-conservation law is (d) [44].

$$\frac{mv_\infty^2}{2} = \frac{mv_{\min}^2}{2} + \frac{C}{d} \tag{2.31}$$

The absolutely smallest distance d_0 is obtained in central collisions with [44].

$$E_\infty = \frac{mv_\infty^2}{2} = \frac{C}{d_0} \tag{2.32}$$

From this and the angular-momentum conservation the relation is given[42].

$$b^2 = d(d - d_0) \tag{2.33}$$

is obtained with the solution[42].

$$d = \frac{C}{2E_\infty}\left(1 + \sqrt{1 + b^2 \frac{4E_\infty^2}{c^2}}\right) \tag{2.34}$$

$$= \frac{d_0}{2}\left(1 + \frac{1}{\sin(\theta/2)}\right) \tag{2.35}$$

2.6.2 Quantum-Mechanical Derivation of Rutherford's Formula

In the nonrelativistic limit, the scattering of one particle off another is described by the Schrodinger equation. In the c.m., the wave function is the solution of the equation[42].

$$-\frac{\hbar^2}{2\mu}\nabla^2\psi + (V - E)\psi = 0 \tag{2.36}$$

where μ is the reduced mass of the two-nucleon system and V is the central potential. The scattered particle outside the interaction region is described by a spherical wave e^{ikr}/r radiating outward from the center of the interaction region. The particles density in the incident beam is usually sufficiently low that we may ignore any collision between the incident and scattering particles. As a result, the wave function at large r is a linear combination of a plane wave, made of the incident beam and particles not scattered by the potential, and a spherical wave, made of scattered particles. The result may be

expressed as[42].

$$\psi(r) \underset{r\to\infty}{\longrightarrow} e^{ikz} + f(\theta,\phi)\frac{e^{ikr}}{r} \qquad (2.37)$$

here, $f(\theta,\phi)$ is the scattering amplitude which measures the fraction of incident wave scattered in the direction with polar angle θ and azimuthal angle ϕ. In general, both $\psi(r)$ and $f(\theta,\phi)$ are also functions of the incident wave vector k and scattered wave vector $\acute{}k$. Furthermore, the probability for scattering is sufficiently small that the normalization of the incident wave is not affected by particles removed from the incident beam due to scattering. Since the z-axis is chosen to be along the direction the two particles approaching each other outside the interaction zone, the zy-plane is fixed by requiring it to be perpendicular to the z-axis [42 ,46].

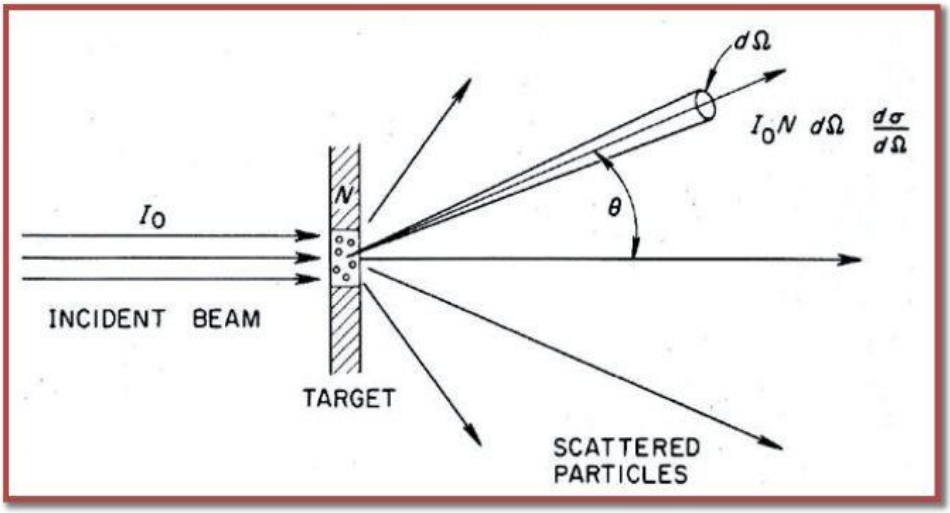

Fig 2.4: Diagram for the definition of differential cross-section. Usually the size of the irradiated area of the target is small, very much smaller than the distance to the detector, so that the scattering angle θ is well defined[42].

From Fig. 2.4, the relation between wave function and intensity of the incident beam is given by the quantum-mechanical probability current density [42] .

$$\vec{j}_i = \frac{\hbar^2}{2i\mu}\left[\psi^*\overrightarrow{\nabla}\,\psi - \ \psi\overrightarrow{\nabla}\,\psi^*\ \right] = Re\left\{\psi^*\frac{\hbar}{i\mu}\overrightarrow{\nabla}\,\psi\right\}$$
$$\vec{J}_{sc} = Re\left\{e^{-ikz}\ \frac{\hbar}{i\mu}\frac{d}{dz}\ e^{ikz}\right\} = \frac{\hbar k}{\mu} \qquad (2.38)$$

where Re denotes the real part . The differential scattering cross section can be stated in terms of the scattering amplitude $f(\theta)$. The probability current density for the scattered spherical wave is given by the equation[48,49].

$$J_{sc} = R_e\left\{\left(f(\theta)\frac{e^{ikr}}{r}\right)^*\frac{\hbar}{i\mu}\frac{d}{dr}\left(f(\theta)\frac{e^{ikr}}{r}\right)\right\} = \vec{j}_i\frac{|f(\theta)|^2}{r^2} \qquad (2.39)$$

If the scattered particle is detected by a detector with effective area *da* situated at *r* from the scattering center, the solid angle subtended by the detector at the origin is[42].

$$d\Omega = \frac{da}{r^2} \qquad (2.40)$$

and the number of particles recorded per unit time is[49]

$$N_{sc} = \vec{j}_{sc}da = \vec{j}_{sc}r^2 d\Omega$$

$$N_{inc} = \frac{\hbar k}{\mu}d\Omega$$

The differential scattering cross section, $\frac{d\sigma}{d\Omega}$ sometimes represented also as *σ(θ)*, is defined as the number of particles scattered into a solid angle $d\Omega$ at angle θ divided by the incident flux[50,51].

$$\frac{d\sigma}{d\Omega} = \frac{\vec{j}_{sc}\,r^2}{\vec{j}_i} = |\,f(\theta)|^2 \qquad (2.41)$$

The scattering cross section is the integral of the differential cross section over all solid angles [50].

$$\sigma = \int \frac{d\sigma}{d\Omega} d\Omega = \int_0^{\pi} |f(\theta)|^2 \, 2\pi \, \sin\theta \, d\theta \qquad (2.42)$$

where

$$d\Omega = \sin\theta \, d\theta \, d\phi$$

If the interaction potential is a central one, *V = V(r)*, that depends only on the relative distance *r*, angular momentum is a constant of motion. In this case, it is convenient to decompose the wave function *ψ(r)* into a product of radial and angular parts and write it as a sum over components with definite orbital angular momentum l, or partial waves [44,49].

$$\psi(r,\theta) = \sum_{l=0}^{\infty} a_l \, R_l(r) Y_{l0}(\theta) \qquad (2.43)$$

where a_l are the expansion coefficients. Only spherical harmonics $Y_{l\mathrm{m}}(\theta,\phi)$ with *m = 0* are involved here, as we are considering systems independent of the azimuthal angle ϕ in terms of the modified radial wave function [42].

$$u_l(r) \equiv r \, R_l(r) \qquad (2.44)$$

The equation simplified of differential equation[42].

$$\frac{d^2 u_l(r)}{dr^2} - \left\{ \frac{l(l+1)}{r^2} + \frac{2\mu}{\hbar^2} V(r) - k^2 \right\} u_l(r) = 0 \qquad (2.45)$$

For short-range potentials, V(r) goes to zero as r → ∞. The same is also true for the l (l + 1)/ r^2 term. In the asymptotic regions, we are left with

a simple second-order equation of the form differential equation of the form [42] .

$$\frac{d^2u_l\,(r)}{dr^2} + k^2u_l\,(r) = 0 \qquad (2.46)$$

The solution for this equation is the familiar linear combination of *sin(kr)* and *cos(kr)*. That is, at large *r*, the function $u_l(r)$ must take on the form[42]:

$$u_l(r) \xrightarrow[r\to\infty]{} A_l \sin(\, kr - \frac{1}{2}l\pi) + B_l \cos(\, kr - \frac{1}{2}l\pi)$$

$$= C_l \sin(\, kr - \tfrac{1}{2}l\pi + \delta_l) = C_l' \left\{e^{-i(kr-\frac{1}{2}l\pi)} - \, e^{2i\delta_l}e^{i(kr-\frac{1}{2}l\pi)}\right\} \qquad (2.47)$$

where A_l and B_l, or C_l (C_l'),are two constants that must be determined from boundary conditions and δl is the phase shift. The phase factor $\frac{1}{2}l\pi$ is included here so that it is more convenient to compare with the asymptotic form of spherical Bessel functions. Its physical meaning can be seen by comparing Eq.(2.47) with the partial wave expansion of a plane wave [44].

$$e^{ikz} = \sum_{l=0}^{\infty}\sqrt{4\pi(2l+1)}\; i^l j_l(kr)Y_{l0}(\theta) \qquad (2.48)$$

The spherical Bessel function, $j_l(kr)$, asymptotically has the following shape[52].

$$j_l(kr) \xrightarrow[r\to\infty]{} \frac{\sin\left(kr - \frac{1}{2}l\pi\right)}{kr}$$

in comparison to Eq. (2.47). In the asymptotic region, a plane wave can be expressed as the following [53].

$$e^{ikz} \xrightarrow[r\to\infty]{} \sum_{l=0}^{\infty}\sqrt{4\pi(2l+1)}\;\frac{i^l}{kr}\sin(kr - \frac{1}{2}l\pi)Y_{l0}(\theta)$$

$$= \sum_{l=0}^{\infty} \sqrt{4\pi(2l+1)} \left\{ \frac{e^{ikr}}{2ikr} - \frac{i^l e^{-i\left(kr-\frac{1}{2}l\pi\right)}}{2ikr} \right\} Y_{l0}(\theta) \quad (2.49)$$

Asymptotic form of the same wave function as given earlier in Eq.(2.37), we arrive at the equality [53].

$$e^{ikz} + f(\theta)\frac{e^{ikr}}{r} = \sum_{l=0}^{\infty} \acute{a}_l Y_{l0}(\theta) \frac{1}{r} \sin\left(kr - \frac{1}{2}l\pi + \delta_l \right)$$

$$= \sum_{l=0}^{\infty} \acute{a}_l Y_{l0}(\theta) \left\{ (-i)^l e^{i\delta_l} \frac{e^{ikr}}{2ikr} - e^{-i\delta_l} \frac{e^{-i\left(kr-\frac{1}{2}l\pi\right)}}{2ikr} \right\} \quad (2.50)$$

Where

$$\acute{a}_l = \sqrt{4\pi(2l+1)}\, i^l e^{i\delta_l}$$

The scattering amplitude may be expressed in terms of phase shifts as

$$f(\theta) = \frac{\sqrt{4\pi}}{k} \sum_{l=0}^{\infty} \sqrt{(2l+1)}\ e^{i\delta_l} \sin\delta_l Y_{l0}(\theta) \quad (2.51)$$

The differential scattering cross section can be written as[49,53].

$$\frac{d\sigma}{d\Omega} = \frac{4\pi}{k^2} \left| \sum_{l=0}^{\infty} \sqrt{(2l+1)}\ e^{i\delta_l} \sin\delta_l Y_{l0}(\theta) \right|^2 \quad (2.52)$$

From the orthonormal condition on spherical harmonics[49].

$$\int_0^{2\pi}\int_0^{\pi} Y_{lm}^{*}(\theta,\emptyset)Y_{\acute{l}\acute{m}}(\theta,\emptyset)\sin\theta\, d\theta\, d\emptyset = \delta_{l\acute{l}}\delta_{m\acute{m}} \qquad (2.53)$$

The scattering cross section may be reduced to an extremely basic form. at $l = \acute{l}$ [42,49].

$$\sigma_{sc} = \frac{4\pi}{k^2}\sum_{l\acute{l}}\sqrt{(2l+1)\left(2\acute{l}+1\right)}\; e^{i(\delta_l-\delta_{\acute{l}})}\sin\delta_l\sin\delta_{\acute{l}}\int_0^{\pi} Y_{l0}(\theta)Y_{\acute{l}0}(\theta)\sin\theta d\theta$$

$$\sigma_{sc} = \frac{4\pi}{k^2}\sum_{l=0}^{\infty}(2l+1)\sin^2\delta_l \qquad (2.54)$$

In this case, $4\sin^2\delta_l = |1-\eta_l|^2$, and η_l is reflection coefficient.

$$\sigma_{sc} = \frac{\pi}{k^2}\sum_l(2l+1)\,|1-\eta_l|^2 \qquad (2.55)$$

Only elastic scattering may occur. where $4\sin^2\delta_l = |1-\eta_l|^2$, $|\eta_l| = 1$.

Chapter Three
Coupled-channel formalism

Chapter 3

The Coupled Channel Formalism

3.1 Introduction

The coupled-channels calculations for the heavy-ion reaction at energies near and below the Coulomb barrier can explain the experimental data of fusion reactions as well as the quasi-elastic scattering of medium-heavy mass systems and heavy mass systems. It is revealed that the cross section and the barrier distribution for fusion reactions and quasi-elastic scattering are very sensitive to the structure of the colliding nuclei, the collective excitations (rotations and surface vibrations), and/or nucleon transfer. Those effects can be more easily visualized through the so-called barrier distribution concept[54].

3.2 Coupled-channels equation with full angular momentum

The coupled channel (CC) method is the most powerful tool to study. multi-channel scattering. The coupling to intrinsic degrees of freedom affects heavy ion collisions. This issue can be resolved by directly solving the Schrodinger equation. At collision energies below the Coulomb barrier, it has been demonstrated that the coupling between the relative motion and a number of intrinsic movements of the nuclei causes significant increases in the fusion cross sections. Numerous experimental and theoretical studies have shown this [1,54]. The collision between two nuclei has a coupling between the nuclear intrinsic motion ξ and the relative motion of the nuclei's centers of mass, $\vec{r} = (r, \hat{r})$. the Hamiltonian for the system is [1,34]**.**

$$\mathrm{H}(\vec{r}, \xi) = -\frac{\hbar^2}{2\mu}\nabla^2 + V(r) + H_0(\xi) + V_{coup}(\vec{r}, \xi), \qquad (3.1)$$

where r refers to the center of mass distance between the colliding nuclei, V(r) is the bare potential in the absence of the coupling, $H_0(\xi)$ represents the Hamiltonian for the intrinsic motion and V_{coup} is the coupling Hamiltonian. The Schrodinger equation for the total wave function would be given by[34]:

$$\left(-\frac{\hbar^2}{2\mu}\nabla^2 + V(r) + H_0(\xi) + V_{coup}(\vec{r}.\xi)\right)\psi(\vec{r},\xi) = E\psi(\vec{r},\xi). \quad (3.2)$$

The internal degree of freedom ξ principally has a finite spin. The coupling Hamiltonian in complications can be written as [1].

$$V_{coup}(\vec{r}.\xi) = \sum_{\lambda>0.\mu} f_\lambda(r) Y_{\lambda\mu}(\hat{r}).T_{\lambda\mu}(\xi), \quad (3.3)$$

Where $f_\lambda(r)$denotes the coupling form factor, $Y_{\lambda\mu}(\hat{r})$ denotes the spherical harmonics, and $T_{\lambda\mu}(\xi)$ denotes the spherical tensors that are constructed from the internal coordinate, the dot denotes a scalar product. Since it was first taken into account in V (r), the sum has taken all values of λ , excluding for λ = 0. since it is originally considered in V (r). For a given total angular momentum J and its z component M, one can define the channel wave functions as [1,34].

$$\langle\hat{r}\xi|(nlI)JM\rangle = \sum_{m_l m_I}\langle lm_l\, Im_I|JM\rangle Y_{lm_l}(\hat{r})\,\varphi_{nIm_I}(\xi), \quad (3.4)$$

where $\langle lm_l Im_I|JM\rangle$ is Clebsch-Gorden coefficient, *l* refers to the orbital angular momenta, *I* represents the intrinsic angular momenta, and $\varphi_{nIm_I}(\xi)$represents the wave function for the intrinsic motion which probes[1,34]

$$H_0(\xi)\,\varphi_{nIm_I}(\xi) = \epsilon_{nI}\,\varphi_{nIm_I}(\xi) \quad (3.5)$$

where n any quantum number despite angular momentum.

The total wave function $\psi(\vec{r},\xi)$ has been expanded with this basis[1].

$$\psi(\vec{\mathrm{r}},\xi) = \sum_{\mathrm{n},l,\mathrm{I}} \frac{\mathrm{u}^{\mathrm{J}}_{\mathrm{n}l\mathrm{I}}(\mathrm{r})}{\mathrm{r}} \langle \hat{\mathrm{r}}\xi | (\mathrm{n}l\mathrm{I})\mathrm{JM} \rangle. \qquad (3.6)$$

The Schrödinger equation [Eq. (3.2)] can be written as a set of coupled equations for $u^J_{nlI}(r)$ [1]

$$\left[-\frac{\hbar^2}{2\mu}\frac{d^2}{dr^2} + V(r) + \frac{l(l+1)\hbar^2}{2\mu r^2} - E + \epsilon_{nI}\right] u^J_{nlI} + \sum_{\acute{n},l',\acute{I}} V^J_{nlI;\acute{n}l'\acute{I}}(r) u^J_{\acute{n}l'\acute{I}}(r) = 0, \qquad (3.7)$$

where the coupling matrix elements $V^J_{nlI;\acute{n}\,l'\acute{I}}(r)$ is given by[1, 55]

$$V^J_{nlI;\acute{n}\,l'\acute{I}}(r) = \langle (nlI)JM | V_{coup}(\vec{r}.\xi) | (\acute{n}l'\acute{I})JM \rangle$$
$$= \sum_{\lambda} (-1)^{I-\acute{I}+l'+J} f_\lambda(r) \langle l \| Y_\lambda \| l' \rangle \langle nI \| T_\lambda \| n'I' \rangle$$
$$\times \sqrt{(2l+1)(2I+1)} \begin{Bmatrix} I' & l' & J \\ l & I & \lambda \end{Bmatrix}. \qquad (3.8)$$

The reduced matrix elements in Eq. (3.8) are defined by :

$$\langle l_{ml} | Y_{\lambda\mu} | l'_{ml'} \rangle = \langle l'_{ml'}\, \lambda\mu | l_{ml} \rangle \langle l \| Y_\lambda \| l' \rangle. \qquad (3.9)$$

Since $V^J_{nlI;\acute{n}\,l'\acute{I}}(r)$ is freelance of the coefficient M, the coefficient has been suppressed as seen in Eq.(3.8). Equation (3.7) is called CC equations. These equations are commonly resolved using the incoming wave boundary conditions[1],

$$u^J_{nlI}(r) \sim \mathcal{I}^J_{nlI}\, exp\left(-i \int_{r_{abs}}^{r} k_{nlI}(\acute{r}) d\acute{r}\right) \; r \leqslant r_{abs}\,, \qquad (3.10)$$

$$u_{nlI}^{J}(r) \rightarrow \frac{i}{2}\begin{pmatrix} H_l^{(-)}(k_{nI}r)\delta_{n,n_i}\delta_{l,l_i}\delta_{I,I_i} \\ +\sqrt{\frac{k_{nI_i}}{k_{nI}}}\, S_{lI}^{J} H_l^{(+)}(k_{nI}r) \end{pmatrix} \quad r \longrightarrow \infty , \qquad (3.11)$$

where $k_{nI} = \sqrt{2\mu(E-\epsilon_{nI})/\hbar^2}$, $k_{nI_i} = k = \sqrt{2\mu E/\hbar^2}$ is the wave number for the entrance channel nl_i. $\mathcal{T}_{\mathrm{n}lI}^{\mathrm{J}}$ is the transmission coefficient, the local wave number $k_{nlI}\,(r)$ is defined as [1, 34].

$$k_{nlI}(r) = \sqrt{\frac{2\mu}{\hbar^2}\left(E - \epsilon_{nI} - \frac{l(l+1)\hbar^2}{2\mu r^2} - V(r) - V_{nlI;\acute{n}\,l'\acute{\imath}}^{J}(r)\right)}. \qquad (3.12)$$

Unlike to the calculation of fusion cross sections, the calculation of quasi-elastic cross sections usually requires a large value of angular momentum so as to obtain converged results. The potential pocket at (r = r_{abs}) becomes superficiality or even disappears for such large angular momentum. Hence, the incoming flux in Eq. (3.10) cannot be correctly identified. Therefore, the quasi-elastic problem commonly performs the regular boundary conditions at the origin rather than using the incoming wave boundary conditions. When using the regular boundary conditions, a complex potential $V_N(r) = V_N^0(r) + iw(r)$, is needed to simulate the fusion reaction. Once the nuclear S-matrix in Eq. (3.11) is obtained, the scattering amplitude can then be calculated as [1].

$$f_{lI}^{J}(\theta,E) = i\sum_{Jl}\sqrt{\frac{\pi}{kk_{nI}}}\, i^{J-l}\, e^{i[\sigma_J(E)+\sigma_J(E-\epsilon_{nI})]}\sqrt{2J+1}\, Y_{l0}(\theta)\big(S_{lI}^{J} - \delta_{I.I_2}\delta_{l.l_2}\big) + f_c(\theta.E)\delta_{I.I_2}\delta_{l.l_2}\,, \qquad (3.13)$$

where σ_J is the Coulomb phase shift which is given by [1].

$$\sigma_J = |\Gamma(l+1+i\eta)|. \qquad (3.14)$$

While f_c is the Coulomb scattering amplitude which is given by [1]

$$f_c(\theta, E) = \frac{\eta}{2k\sin^2\left(\frac{\theta}{2}\right)} e^{\left[-i\eta \ln\left(\sin^2\left(\frac{\theta}{2}\right)\right)+2i\sigma_0(E)\right]}, \qquad (3.15)$$

where η is the Summerfield parameter, which is given by $\eta = Z_1 Z_2 e^2/\hbar v$, the differential cross section can be evaluated by using Eq.(3.13) [1].

$$\frac{d\sigma_{qel}(\theta, E)}{d\Omega} = \sum_{Jl'} \frac{k_{nI}}{k} |f_{ll'}^J(\theta, E)|^2. \qquad (3.16)$$

We can assess the Rutherford cross section using Eq.(3.15)

$$\frac{d\sigma_R(\theta,E)}{d\Omega} = |f_C(\theta.E)|^2 = \frac{\eta^2}{4k^2} csc^4\left(\frac{\theta}{2}\right). \qquad (3.17)$$

3.3 Coupled-Channels Equations in the Rotating Frame approximation

The full CC calculations have often been considered very difficult to manage when we take into account many of the physical channels. As a result, the dimension of the CC equations generally becomes too large for the practical purposes. To get rid of this problem, an approximation has been used one known as the rotating frame approximation which is also called as the no-Coriolis approximation or the iso-centrifugal approximation[34,53]. The no-Coriolis approximation was used primarily in the fields of chemistry under the name of centrifugal sudden approximation [1]. Let us say that the initial intrinsic spin is zero. In the no-Coriolis approximation, the whole system is transformed to the rotating frame such that the z-axis is along the direction of the relative motion $\vec{r}$ at every instance [56,58].

In the rotating frame approximation to the CC equations, Eq. (3.7), one first replaces the angular momentum of the relative motion in each channel by the total angular momentum J, that is,

$$\frac{l(l+1)\hbar^2}{2\mu r^2} \approx \frac{J(J+1)\hbar^2}{2\mu r^2}. \tag{3.18}$$

This means the change of the orbital angular momentum between the colliding nuclei because of the excitation of the intrinsic degree of freedom is negligible. The transformation to the rotating frame can be applied without leading to any complication since the operator for the rotational coordinate transformation in the whole space commutes with the centrifugal operator for the relative motion[1,34].

3.4 Coupling to Low-Lying Collective States

3.4.1 Vibrational Coupling

3.4.1.1 Nuclear Coupling

In this section, we will study the evident form of the coupling Hamiltonian (V_{coup}). We suppose that the nuclear potential has a Wood Saxon (WS) form, as in Eq. (2.3). Consider couplings of the relative motion to a 2^{λ} pole surface vibration of the target nucleus. The radius of the vibrating target nucleus in the geometrical model of Bohr and Mottelson is characterized as [34,59]

$$R_T(\theta,\phi) = R_T\left(1 + \sum_{\lambda} \alpha_{\lambda\mu}\, Y_{\lambda\mu}(\theta,\phi)\right), \tag{3.26}$$

where $\alpha_{\lambda\mu}$ is the coordinate of the surface vibration while R_T is the equivalent sharp radius.

A harmonic oscillator can be used to approximate the surface oscillation which is given by[34].

$$\mathrm{H}_o = \hbar\omega_\lambda \left(\sum_\mu a^\dagger_{\lambda\mu}\, a_{\lambda\mu} + \frac{2\lambda+1}{2} \right), \tag{3.27}$$

where $a_{\lambda\mu}$ is phonon annihilation operator, $a^\dagger_{\lambda\mu}$ is the phonon creation operator, $\hbar\omega_\lambda$ is the oscillator quanta.

The surface coordinate $\alpha_{\lambda\mu}$ is related to the phonon creation and annihilation operators by[34].

$$\alpha_{\lambda\mu} = \alpha_o\left(a^\dagger_{\lambda\mu} + (-)^\mu a_{\lambda\mu}\right), \tag{3.28}$$

where $\alpha_o = \beta_\lambda/\sqrt{2\lambda+1}$ is the amplitude of the zero-point motion, β_λ is the deformation parameter, which can be evaluated from the measured electromagnetic transition probability *B(Eλ)* ↑ using [35].

$$\beta_\lambda = \frac{4\pi}{3Z_T R_C^\lambda}\left[\frac{B(E\lambda)\uparrow}{e^2}\right]^{\frac{1}{2}}, \tag{3.29}$$

where R_C is the Coulomb radius, and is taken to be the same as R_T, therefore α_o is given by[35].

$$\alpha_o = \frac{1}{\sqrt{2\lambda+1}}\frac{4\pi}{3Z_T R_C^\lambda}\left[\frac{B(E\lambda)\uparrow}{e^2}\right]^{\frac{1}{2}}. \tag{3.30}$$

In the no-Coriolis approximation, the angular momentum of the relative motion does not change. Evaluating the associated spherical harmonics in

Eq.(3.26) at angle $\hat{r}$ = 0 leads to the factor $\sqrt{(2\lambda + 1)/4\pi}$. Thus, Eq. (3.26) reads[60].

$$R_T(\theta, \alpha_{\lambda 0}) = R_T\left(1 + \sqrt{\frac{2\lambda+1}{4\pi}}\,\alpha_{\lambda 0}\right). \qquad (3.31)$$

Using Eqs. (3.28), (3.30) and (3.31), the nuclear coupling potential can be written as[57].

$$V_N^{coup(vib)}\left(r, \hat{O}_\lambda\right) = \frac{-V_o}{1 + e^{[(r - R_o - R_T\hat{O}_\lambda/\sqrt{4\pi})/a]}}, \qquad (3.32)$$

where the dynamical operator $\hat{O}_\lambda$ is given by [41].

$$\hat{O}_\lambda = \beta_\lambda\left(a_{\lambda 0}^{\dagger} + a_{\lambda 0}\right). \qquad (3.33)$$

In order to obtain the matrix elements of the nuclear coupling Hamiltonian between the n-phonon state and the m-phonon state, the eigenvalues and the eigenvectors of the operator $\hat{O}_\lambda$ must be determined. The operator $\hat{O}_\lambda$ satisfies[34].

$$\hat{O}_\lambda|\alpha\rangle = \xi_\alpha|\alpha\rangle. \qquad (3.34)$$

The eigenvalues and eigenvectors can be obtained by diagonal the matrix elements of the operator between the phonon states[34]

$$O_{nm} = \beta_\lambda\left(\sqrt{m}\,\delta_{n,m-1} + \sqrt{m+1}\,\delta_{n,m+1}\right). \qquad (3.35)$$

After the eigenvalues and eigenvectors are determined, the nuclear matrix elements of Eq (3.32) can be assessed as [34].

$$V_{mn}^{N}(r) = \langle m\left|V_N^{coup(vib)}\right|n\rangle - V_N(r)\delta_{n,m}.$$

$$= \sum_{\alpha} \langle m|\alpha\rangle \ \langle \alpha|n\rangle \frac{-V_o}{1+e^{[(r-R_o-R_T\xi_\alpha/\sqrt{4\pi})/a]}} - V_N(r)\delta_{n,m}. \quad (3.36)$$

To ensure that coupling interaction vanishes in the entrance channel, the last term in Eq. (3.36) is introduced.

3.4.1.2 Coulomb Coupling

One may now consider the Coulomb part of the coupling Hamiltonian. The Coulomb potential between a point-like spherical projectile and a vibrating target is given by [34]:

$$V_C(\vec{r}) = \int d\vec{\acute{r}} \ \frac{Z_P Z_T e^2}{|\vec{r}-\vec{\acute{r}}|} \ \rho_T(\vec{\acute{r}}).$$

$$= \frac{Z_P Z_T e^2}{r} + \sum_{\acute{\lambda}\neq 0} \sum_{\acute{\mu}} \frac{4\pi Z_P e}{2\acute{\lambda}+1} \ Q_{\acute{\lambda}\acute{\mu}} Y^*_{\acute{\lambda}\acute{\mu}}(\hat{r}) \frac{1}{r^{\acute{\lambda}+1}}, \quad (3.37)$$

where ρ_T is the charge density of the target nucleus, Z_P and Z_T are the atomic numbers of the projectile and the target nuclei respectively, and $Q_{\acute{\lambda}\acute{\mu}}$ is the electric multipole operator defined by[1,34].

$$Q_{\acute{\lambda}\acute{\mu}} = \int d\vec{\acute{r}} \ Z_T e \rho_T(\vec{r}) r^{\acute{\lambda}} Y_{\acute{\lambda}\acute{\mu}}(\hat{r}). \quad (3.38)$$

The first term on the right hand side of Eq (3.37) is the named Coulomb potential, while the second term is the Coulomb component of the coupling Hamiltonian. Eq (3.37)is obtained by using the following formula[34, 41].

$$\frac{1}{\left|\vec{r}-\vec{\acute{r}}\right|}=\sum_{\acute{\lambda}\acute{\mu}}\frac{4\pi}{2\acute{\lambda}+1}\frac{r_{<}^{\acute{\lambda}}}{r_{>}^{\acute{\lambda}+1}}\,Y_{\acute{\lambda}\acute{\mu}}(\hat{\acute{r}})Y_{\acute{\lambda}\acute{\mu}}^{*}(\hat{r}). \tag{3.39}$$

The relative coordinate r is considered to be bigger than the charge radius of the target nucleus. If the target nucleus is supposed to have a sharp matter distribution, the electric multiple is given by[34, 41].

$$Q_{\acute{\lambda}\acute{\mu}}=\frac{3Z_{T}e}{4\pi}\,R_{T}^{\acute{\lambda}}\alpha_{\lambda\mu}\delta_{\lambda,\acute{\lambda}}\delta_{\mu,\acute{\mu}}. \tag{3.40}$$

Up to the first order in the surface coordinate $\alpha_{\lambda\mu}$. Thus, we can write the coupling component of the Coulomb interaction as [34, 41].

$$\begin{aligned}V_{C}^{coup(vib)}\left(\vec{r},\alpha_{\lambda\mu}\right)&=\sum_{\lambda\mu}\frac{3Z_{P}Z_{T}e^{2}}{\sqrt{2\lambda+1}}\frac{R_{T}^{\lambda}}{r^{\lambda+1}}\alpha_{\lambda\mu}Y_{\lambda\mu}^{*}(\hat{r})\\&=\sum_{\lambda\mu}f_{\lambda}^{C}(r)\alpha_{\lambda\mu}Y_{\lambda\mu}^{*}(\hat{r}),\end{aligned} \tag{3.41}$$

where $f_{\lambda}^{C}(r)$ is called the Coulomb coupling form factor, which is given by:

$$f_{\lambda}^{C}(r)=\frac{3Z_{P}Z_{T}e^{2}}{\sqrt{2\lambda+1}}\frac{R_{T}^{\lambda}}{r^{\lambda+1}}. \tag{3.42}$$

Conversion to the rotating frame according to the no-Coriolis approximation, the Coulomb coupling is given by [1,61].

$$\begin{aligned}V_{C}^{coup(vib)}\left(\vec{r},\hat{O}_{\lambda}\right)&=\sum_{\lambda}3Z_{P}Z_{T}e^{2}\frac{R_{T}^{\lambda}}{r^{\lambda+1}}\frac{\alpha_{\lambda0}}{\sqrt{4\pi}}\\&=\sum_{\lambda}\frac{3Z_{P}Z_{T}e^{2}}{2\lambda+1}\frac{R_{T}^{\lambda}}{r^{\lambda+1}}\frac{\hat{O}_{\lambda}}{\sqrt{4\pi}},\end{aligned} \tag{3.43}$$

where $V_{nm}^{C}(r)$ represents the Coulomb coupling matrix elements, $\hat{O}_{\lambda}$ is given by Eq. (3.33), then we may be evaluated similar to the nuclear coupling Hamiltonian, with[1, 61].

$$V_{nm}^{C}(r) = \left\langle m \middle| V_{C}^{coup(vib)} \middle| n \right\rangle$$
$$= \sum_{\lambda} \frac{3Z_P Z_T e^2}{2\lambda+1} \frac{R_T^{\lambda}}{r^{\lambda+1}} \frac{\beta_{\lambda}}{\sqrt{4\pi}} \left[\sqrt{m}\,\delta_{n,m-1} + \sqrt{m+1}\,\delta_{n,m+1}\right] \quad (3.44)$$

The total coupling matrix elements essentially represent the sum of the nuclear and Coulomb couplings as follows[41][61].

$$V_{coup}(r) = V_{mn}^{N}(r) + V_{nm}^{C}(r). \quad (3.45)$$

3.4.1.3 Projectile and Target Excitations

When the relative motion couples to the vibrational excitation of the projectile nucleus in addition to the vibrational excitation of the target nucleus, the above formulation can also be extended, where the coupling potential can be written as [62].

$$V_{coup}\left(r, \hat{O}_{\lambda_P}, \hat{O}_{\lambda_T}\right) = V_N\left(r, \hat{O}_{\lambda_P}, \hat{O}_{\lambda_T}\right) + V_C\left(r, \hat{O}_{\lambda_P}, \hat{O}_{\lambda_T}\right). \quad (3.46)$$

$$V_N\left(r, \hat{O}_{\lambda_P}, \hat{O}_{\lambda_T}\right) = \frac{-V_o}{\left[1 + e^{\frac{\left[r - R_o - \left(R_P \hat{O}_{\lambda_P} + R_T \hat{O}_{\lambda_T}\right)/\sqrt{4\pi}\right]}{a}}\right]} - V_N(r) \quad (3.47)$$

$$V_C\left(r, \hat{O}_{\lambda_P}, \hat{O}_{\lambda_T}\right) = \frac{Z_P Z_T e^2}{r}\left(\frac{3R_P^{\lambda_P}\hat{O}_{\lambda_P}}{(2\lambda_P+1)r^{\lambda_p}} + \frac{3R_T^{\lambda_T}\hat{O}_{\lambda_T}}{(2\lambda_T+1)r^{\lambda_T}}\right). \quad (3.48)$$

The $\hat{O}_{\lambda_P}$ and $\hat{O}_{\lambda_T}$ are the excitation operators for the projectile and target nuclei respectively, and have a form of Eq. (3.33). λ_T and λ_P represent the multi-polarity of the vibrations in the target and the

projectile nuclei, respectively. In order to avoid double counting, the term $V_N(r)$ in Eq. (3.47) is subtracted. The matrix elements of the coupling potential of Eq. (3.46) is evaluated in a similar way as Eqs. (3.36) and (3.44). Firstly, the operators $\hat{O}_{\lambda_P}$ and $\hat{O}_{\lambda_T}$ are diagonalize in the physical space in order to obtain their eigenvalues and eigenvectors. The coupling potentials are then accounted as[62].

$$V_{nm}(r) = \langle m|V_{coup}|n\rangle - V_N(r)\delta_{n,m}$$

$$= \sum_{\alpha,\gamma} \langle m|\alpha\rangle\langle\alpha|n\rangle\langle m|\gamma\rangle\langle n|\gamma\rangle \times \frac{-V_o}{\left[1 + e^{\frac{[r-R_o-(R_P\xi\alpha+R_T\xi\gamma)/\sqrt{4\pi}]}{a}}\right]}$$

$$+ \sum_{\lambda_P,\lambda_T} \left[\frac{3Z_PZ_Te^2}{2\lambda_T+1}\frac{R_T^{\lambda_T}}{r^{\lambda_T+1}}\frac{\beta_{\lambda_T}}{\sqrt{4\pi}} + \frac{3Z_PZ_Te^2}{2\lambda_P+1}\frac{R_P^{\lambda_P}}{r^{\lambda_P+1}}\frac{\beta_{\lambda_P}}{\sqrt{4\pi}}\right]$$

$$\times \left[\sqrt{n}\ \delta_{n,m+1} + \sqrt{n+1}\ \delta_{n,m-1}\right]$$

$$- V_N(r)\delta_{n,m}, \qquad (3.49)$$

where $|\alpha(\gamma)\rangle$ and $\xi_{\alpha(\gamma)}$ are the eigenvectors and the eigenvalues for the operators $\hat{O}_{P(T)}$, respectively.

In the former section, we have shown that the dimension of the CC equations can be greatly reduced when the no-Coriolis approximation is used. One can achievement a further lowering by introducing the n-phonon channels [8]. The multi-phonon states are distinguished from each other by the angular momentum and seniority, have generally several levels at the same energy [55]. As an example, for the quadrupole surface vibrations, the two-phonon state is degenerate in the excitation energy. One can then replace the coupling to all the member of the two phonon state by the coupling to a single state given by [63]

$$|2\rangle = \sum_{I=0,2,3} \langle 2020|I0\rangle |I0\rangle = \frac{1}{\sqrt{2!}} \left(a_{20}^{\dagger}\right)^2 \qquad (3.50)$$

Similarly, one can introduce the n-phonon channel for a general multi-polarity λ as[41,62].

$$|n\rangle = \frac{1}{\sqrt{n!}} \left(a_{\lambda 0}^{\dagger}\right)^n |0\rangle. \qquad (3.51)$$

If we mutilate at the two-phonon states, the operator $\hat{O}_{\lambda}$ of Eq. (3.33) corresponds to the matrix elements which are given by[62].

$$O_{mn} = \frac{1}{\sqrt{4\pi}} \begin{pmatrix} 0 & \beta_{\lambda} & 0 \\ \beta_{\lambda} & 0 & \sqrt{2}\beta_{\lambda} \\ 0 & \sqrt{2}\beta_{\lambda} & 0 \end{pmatrix}. \qquad (3.52)$$

3.4.2 Rotational Coupling

3.4.2.1 Nuclear Coupling

Here, we will look into the couplings to the ground state rotational band of the target nucleus. It is convenient to discuss them in the body fixed frame where the z-axis is along the orientation of the deformed target. The surface coordinate $\alpha_{\lambda\mu}$ is then transformed to [34].

$$\alpha_{\lambda\mu} = \sum_{\acute{\mu}} D^{\lambda}_{\mu\acute{\mu}} (\phi_d, \theta_d, \chi_d) a_{\lambda\acute{\mu}}, \qquad (3.53)$$

where ϕ_d, θ_d, χ_d are the Euler angles which describe the orientation of the target. If one considers a permanently deformed nucleus with the axial symmetry is about the body-fixed axis (z-direction), the deformation parameter $a_{\lambda\mu}$ have the form[1].

$$a_{\lambda\mu} = \beta_\lambda \delta_{\mu 0}, \tag{3.54}$$

where β_λ is a constant which specifies the static deformation of the nucleus. In the space fixed frame, we have[1]

$$\alpha_{\lambda\mu} = \beta_\lambda \, D^{\lambda}_{\mu 0}(\phi_d, \theta_d, \chi_d). \tag{3.55}$$

Using Eqs. (3.26), (3.53) and (3.54), we have

$$R_T(\theta, \beta_\lambda) = R_T \left(1 + \sum_{\lambda\mu} \sqrt{\frac{4\pi}{2\lambda+1}} \beta_\lambda \, Y_{\lambda\mu}(\theta_d, \phi_d) Y^*_{\lambda\mu}(\hat{r}) \right). \tag{3.56}$$

In getting Eq. (3.56), we have used the conformity[34].

$$D^{L}_{M0}(\phi, \theta, \chi) = \sqrt{\tfrac{4\pi}{2\lambda+1}} Y^*_{\lambda\mu}(\theta, \phi). \tag{3.57}$$

Using the rotating frame, Eq. (3.56) becomes[1].

$$R(\theta, \beta_\lambda) = R_T \left(1 + \sum_{\lambda} \beta_\lambda Y_{\lambda 0}(\theta) \right). \tag{3.58}$$

Using this equation, the nuclear coupling has a similar form as Eq. (3.32) with[1].

$$V_N^{coup(rot)}\left(r, \hat{O}_\lambda\right) = \frac{-V_o}{1 + e^{[(r - R_o - R_T \hat{O}_\lambda)/a]}} - V_N(r) \tag{3.59}$$

However, the dynamical operator $\hat{O}_\lambda$ is now given by[62]:

$$\hat{O}_\lambda = \sum_{\lambda} \beta_\lambda Y_{\lambda 0}(\theta). \tag{3.60}$$

Now we need to know the matrix elements of the operator $\hat{O}_\lambda$ between the $|n\rangle = |I0\rangle$ and $|m\rangle = |\acute{I}0\rangle$ states of the ground states rotational band for the target nucleus, and are given as[62].

$$O_{I\acute{I}} = \sum_\lambda \beta_\lambda \sqrt{\frac{(2\lambda + 1)(2I + 1)(2\acute{I} + 1)}{4\pi}} \begin{pmatrix} I & \lambda & \acute{I} \\ 0 & 0 & 0 \end{pmatrix}^2. \quad (3.61)$$

This matrix is diagonalized to determine its eigenvalues and eigenvectors. Again, the nuclear matrix elements are evaluated in the same way as Eq. (3.36). Hence, the matrix elements of Eq. (3.59) are calculated as[61].

$$V_{\acute{I}\,I}^N(r) = \langle \acute{I}0 \left| V_N^{coup(rot)} \right| I0\rangle - V_N(r)\delta_{\acute{I},I}$$
$$= \sum_\alpha \langle \acute{I}0|\mu\rangle \, \langle \mu|I0\rangle \frac{-V_o}{1 + e^{\left[\frac{(r - R_o - R_T\lambda_\mu)}{a}\right]}} - V_N(r)\delta_{\acute{I},I}, \quad (3.62)$$

where λ_μ and $|\mu\rangle$ are the eigenvalue and the eigenvector of the operator $\hat{O}_\lambda$ in Eq. (3.60), respectively. As before, we introduce the last term in Eq. (3.62) in order to avoid double counting of the diagonal components.

3.4.2.2 Coulomb Coupling

For the Coulomb interaction, the coupling component is given by[64]:

$$V_C^{coup(rot)}(r, \hat{O}_\lambda) = \sum_\lambda \frac{3Z_P Z_T e^2}{2\lambda + 1} \frac{R_T^\lambda}{r^{\lambda+1}} \hat{O}_\lambda, \quad (3.63)$$

where the operator $\hat{O}_\lambda$ is given by Eq. (3.60).

Using Eq. (3.61), the matrix elements for the rotational coupling potential of Eq. (3.63) reads[64].

$$V_{nm}^{C}(r) = \langle I\acute{0} \left| V_{C}^{coup(rot)} \right| I0\rangle$$

$$= \sum_{\lambda} \frac{3Z_P Z_T e^2}{2\lambda+1} \frac{R_T^{\lambda}}{r^{\lambda+1}} \beta_{\lambda} \sqrt{\frac{(2\lambda\ +\ 1)(2I\ +\ 1)(2\acute{I}\ +\ 1)}{4\pi}}$$

$$\times \begin{pmatrix} I & \lambda & \acute{I} \\ 0 & 0 & 0 \end{pmatrix}^2 . \qquad (3.64)$$

The total coupling matrix elements are the sum of the nuclear and Coulomb coupling matrix elements. To explain the difference between the vibrational and the rotational couplings, let us consider a system coupled to a ground state rotational band up to 2^+ state of the target nucleus which has a quadruple deformation β_2. The wave function for the $|I0\rangle$ state in the ground state rotational band is given by $|I0\rangle = Y_{I0}$. Thus, the matrix elements of the operator in Eq. (3.61) is given by[64].

$$O_{ij} = \frac{1}{\sqrt{4\pi}} \begin{pmatrix} 0 & \beta_2 \\ \beta_2 & \frac{\beta_2 2\sqrt{5}}{7} \end{pmatrix}. \qquad (3.65)$$

In obtaining this matrix elements, we truncate the ground states of the rotational bands up to 2^+ state. One of the main differences between the rotational coupling matrix and the vibrational coupling matrix is that the former has a diagonal component which is proportional to the deformation parameter β_2. This is known as the 'reorientation effect'. This effect has been used in the Coulomb excitation experiment in order to determine the sign of the deformation parameter[61,65].

3.5 Barrier Distribution of Scattering

Information on the impacts of couplings may be learned from the distribution of barrier that was recovered from the observed fusion's

excitation function. Fusion's cross-section is a result of several channels contributing. The following is a definition of the barrier of fusion's distribution[10].

$$D_{fus}(E) = \frac{d^2}{dE^2}\left[E\,\sigma_{fus}(E)\right] \tag{3.66}$$

The fusion cross sections must be measured with extreme precision in order to obtain the barrier distribution by taking the second derivative of the quantity $(E\,\sigma_{fus}(E))$ with respect to E. Estimates of absolute scattering at back angles provide information on the function of channel couplings in fusion reactions[66].Complete scattering is the total scattering caused by all direct reactions, including transition and breakdown, as well as the contributions of elastic and inelastic reactions. The large-angle total scattering is connected to the probability of reflection, $R_0(E)$, and the probability of transmission across the angular momentum barrier is related to fusion $\ell = 0$, $T_0(E)$. The backscattering of total scattering can be thought of as complementary to the fusion since the reaction flux is retained and $T_0(E) + R_0(E) = 1$for this situation. The definition of the total scattering barrier distribution $D_{tot}(E)$ is [57, 58].

$$D_{tot}(E) = -\frac{d}{dE}\left[\frac{\sigma_{tot}}{\sigma_R}(E)\right] \tag{3.67}$$

the ratio of total scattering cross sections to Rutherford cross sections is expressed as σ_{tot}/σ_R. These approaches have the advantage of requiring a numerical assessment First derivatives rather than second derivatives ,as in mergers. Additionally, total and elastic scattering measurements are typically simpler to perform than fusion experiments[53].

Chapter Four
Calculations, Results and Discussion

Chapter 4
Calculations, Results and Discussion

4.1 Introduction

Large-angle quasi-elastic scattering is a suitable method to study the nuclear potential. Several studies have used this method, and it has been applied to find the nuclear potential surface diffuseness parameter for heavy-ion systems [1]. Heavy ion collisions at near-barrier energies and, in particular, fusion and quasi-elastic reactions have been of increased interest from experimental and theoretical points of view over the last few decades. Such studies provide an ideal opportunity to obtain information on nuclear structure and nucleus-nucleus interaction [12]. Both are inclusive processes and are sensitive to channel coupling effects at energies close to the Coulomb barrier. [67]. These computations were carried out by making use of a Wood-Saxon WS form for the nuclear potential. This form's overall composition is made up of both real and imaginary components. [20]. This chapter is summarized our theoretical calculations for both (quasi elastic scattering ,distribution) calculations and the effect of changing the Wood Saxon potential parameters with including the single channel (SC) and coupled channel (CC) effects to investigate the importance this effects on the Coulomb barrier , for systems:-

1. $^{24}Mg+^{90}Zr$
2. $^{28}Si+^{120}Sn$
3. $^{28}Si+^{150}Nd$
4. $^{16}O+^{160}Gd$
5. $^{12}C+^{197}Au$

6. $^{6}Li+^{144}Sm$
7. $^{28}Si + ^{124}Sn$
8. $^{6}Li + ^{159}Tb$
9. $^{22}Ne+^{248}Cm$
10. $^{10}B+^{232}Th$

4.2 Calculations, Results and Discussion

The calculations in this work have been performed using CQEL code as a main code of calculations, which is a modified version of the computer code CCFULL[8].

The first part of the calculations is performed using CQEL code and discusses the effect of changing the value of the surface diffusion parameter (a_0) at a certain potential depth on quasi-elastic scattering. The chi-squared method χ^2 is applied to compare the best-fit value of the diffuseness parameter and get a correspond between the theoretical calculations and the experimental data[20]. The data with $d\sigma_{qel}/d\sigma_R > 1$ are excluded from the fitting procedures but included in the figures for completeness. This is because theoretically, it is clear that $d\sigma_{qel}/d\sigma_R$ cannot be larger than one.

The second part of the results studied the effect of changing the potential depth on the quasi-elastic scattering after determining the value of the surface diffusion parameter(a_0) in the first part of the results. A higher and lower value of the potential depth fixed in the first part of the results was taken , and using the (χ^2) method, The best potential depth value was determined at which the best convergence was achieved between theoretical calculations and experimental data.

4.2.1 The ^{24}Mg + ^{90}Zr system

The first part for the results In this system, were processed in two cases: the first, where both the projectile and target nuclei were considered inert (SC) at different values of the diffusion parameter (0.57, 0.63, and 0.69) fm, and we considered the diffusion parameter 0.63 fm is to be the standard value [9]. The second case, the projectile nucleus was ^{24}Mg rotated with a deformation coefficient of $\beta_2 = 0.374$ and $\beta_4 = -0.053$ [68] to the state 2^+(1.368672MeV), and this was deduced according to the ratio $E_{4^+}/E_{2^+} = 3.012$, while the target nucleus was ^{90}Zr vibrating with a deformation coefficient of $\beta_2 = 0.089$ [68] to the state 2^+(2.186273 MeV), where $E_{4^+}/E_{2^+} = 1.4$ at coupled-channel (CC) The single phonon state of the quadruple excitation of the target nuclei, with the radius parameter r_0 is 1.2 fm.

Table (4.1): The fitted **WS** parameters (radius r_0, depth potential V_0, and the diffuseness parameters a_0), which were obtained from SC and CC calculation, and the values of the χ^2 between experimental and theoretical data for the ^{24}Mg + ^{90}Zr system.

System	Channel	V_0 (MeV)	r_0 (fm)	a_0 (fm)	$\theta_{c.m.}$ $(deg.)$	χ^2	
						σ_{qel}/σ_R	D_{qel}
^{24}Mg + ^{90}Zr	SC	58.8	1.2	0.57	158	0.2817738	0.0734226
				0.63		3.4713360	0.3349851
				0.69		12.6813900	0.8826095
	CC	58.8	1.2	0.57	158	0.0107140	0.0457186
				0.63		0.0217765	0.0203603
				0.69		0.0730525	0.0201489

From table (4.1), in the single-channel SC calculation ,where the projectile ^{24}Mg nucleus and target ^{90}Zr nucleus are inert, the best-fitting diffuseness parameter a_0 is 0.57 fm. The potential depth V_0 is 58.8 MeV.

Based on the chi-squared χ^2 data, the ratio of quasi-elastic scattering to Rutherford cross sections $d\sigma_{qel}/d\sigma_R$ is 0.2817738 denoted by the red line in Fig. 4.1. It is the curve nearest to the curve of the experiment data. The best value of the barrier distribution D_{qel} is 0.0734226 at the same value of a_0, and it is represented by the red curve in Fig. 4.1. The channel couplings start to play an important role in the energies in the sub-barrier region and therefore should be taken into account in our analyses here. The best-fitting diffuseness parameter obtained through a coupled-channels calculation with a rotating projectile (P) and vibrating target (T) is 0.57 fm, as shown by the red line in Fig. 4.2. It is considerably lower than the standard value. The best fit for χ^2 is 0.0107140, while the best value of the distribution D_{qel} is 0.0201489 at the diffuseness parameter a_0 is 0.69 fm, represented by the black curve in Fig. 4.2. Therefore, the best-fitting diffuseness parameter obtained through a coupled-channels calculation should be accepted over the one obtained through a single channel calculation, which is expected.

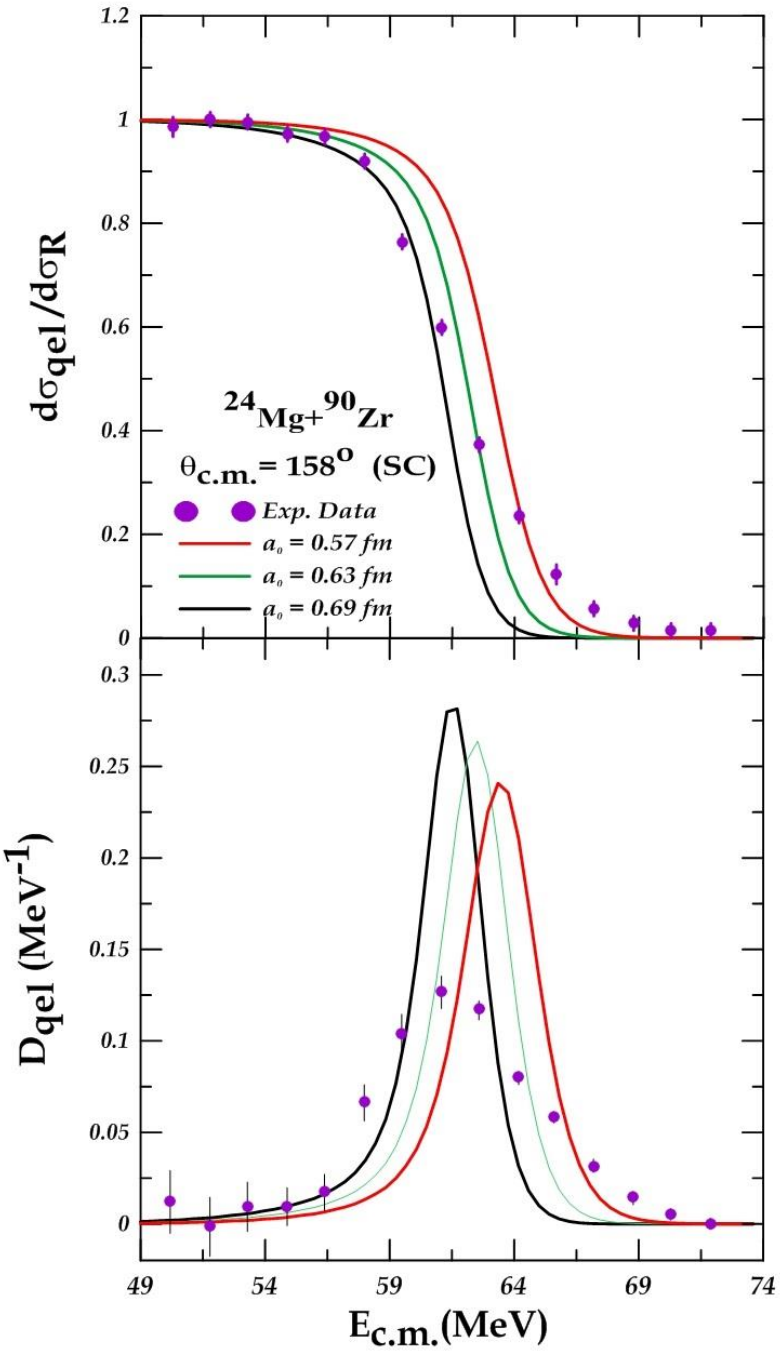

Fig. 4.1. The comparison of the calculated quasi-elastic scattering ratio to the Rutherford cross sections and the distribution at the sub-barrier energies with the corresponding experimental data taken from [54] for the system $^{25}Mg+^{90}Zr$. in the single channel (SC) calculations at a_0 = (0.57, 0.63, and 0.69 fm), indicated as red, green, and black, respectively.

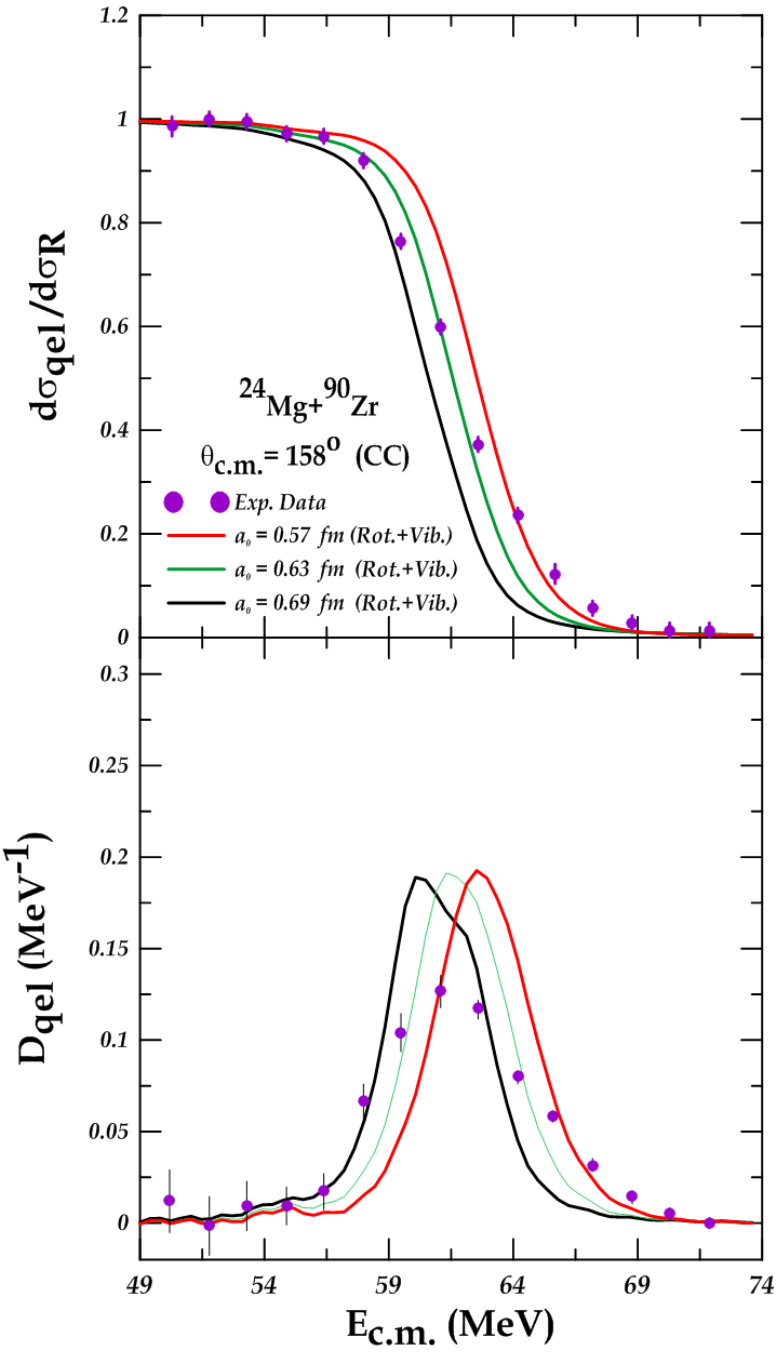

Fig. 4.2. The comparison of the calculated quasi-elastic scattering ratio to the Rutherford cross sections and the distribution at the sub-barrier energies with the corresponding experimental data for the system $^{25}Mg+^{90}Zr$ in the coupled channel (CC) calculations at a_0 = (0.57, 0.63, and 0.69 fm), indicated as red, green, and black, respectively.

The second part of result :In the $^{25}Mg+^{90}Zr$ system, In the single channel (SC) calculations, both the projectile and target nuclei were considered inert at three values of the real nuclear potential (potential depth V_0) (43.8, 58.8, and 73.8 MeV) table (4.2), and the diffusion parameter a_0 was considered to be 0.57 fm. It was previously determined in the first part from calculations by the χ^2 method as the best value for matching the experimental data with the theoretical data. In the coupled channel (CC), the target nucleus ^{90}Zr was vibrating and the projectile nucleus ^{25}Mg was rotating.

Table (4.2) : The fitted parameters of WS potential (the diffuseness parameters a_0, the depth potential V_0 ,and radius r_0), that is estimated from the SC and CC calculation, and the values of the χ^2 between experimental and theoretical data for the $^{24}Mg + ^{90}Zr$ system.

System	Channel	a_0 (fm)	r_0 (fm)	V_0 (MeV)	θ_{cm} $(deg.)$	χ^2	
						σ_{qel}/σ_R	D_{qel}
$^{24}Mg + ^{90}Zr$	SC	0.57	1.2	43.8	158	0.0433369	0.1141273
				58.8		0.2817738	0.0734226
				73.8		0.9258511	0.0731548
	CC	0.57	1.2	43.8	158	0.0268527	0.1034276
				58.8		0.0107140	0.0457186
				73.8		0.0127154	0.0199528

From table (4.2), The best-fit potential depth V_0 is 43.8 MeV obtained from a single-channel analysis in which the projectile ^{24}Mg nucleus and target ^{90}Zr nucleus are both inert, with a_0 is 0.57 fm. The chi squared χ^2 is 0.0433369. It represents the calculated ratio of the quasi-elastic scattering to the Rutherford cross sections. It was shown by the red line in Fig. 4.3. where D_{qel} = 0.0731548 is the best value for barrier distribution at potential depth V_0 = 73.8 MeV. It was shown by the black line in Fig. 4.3.

In a coupled-channels procedure, the best potential depth is 58.8 MeV. The obtained χ^2 value is 0.0107140, as shown by the green line in Fig. 4.4.It is the curve nearest to the curve of the experimental data. The best value of the barrier distribution D_{qel} is 0.0199528 at the depth potential V_0 = 73.8, represented by the black curve, Fig 4.4. By comparing the chi square calculations χ^2 values between SC and CC, the best-fit potential depth obtained through coupled channels. Through potential barrier calculations represented by distribution curves in the cases of single and coupled channels, The curve shifting to the right due to the value of the potential depth decreasing leads to a decrease in the value of the nuclear potential, and thus the height of the potential barrier will increase and the quasi-elastic scattering calculations will increase. On the contrary, if the potential depth increases, the nuclear potential also increases, so the potential barrier will decrease, leading to a decrease in quasi-elastic scattering calculations and a decrease in the height of the potential barrier distribution and its shift to the left.

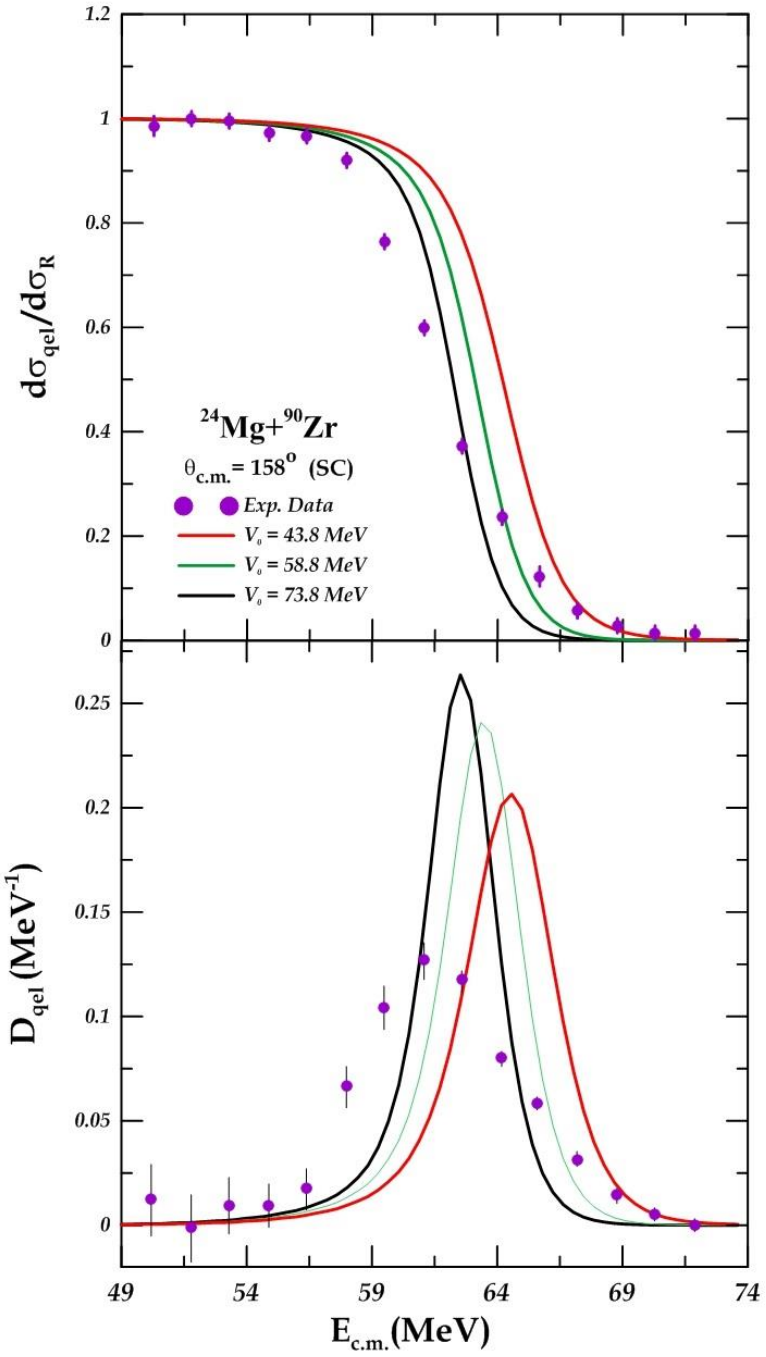

Fig.4.3. The comparison of the calculated quasi-elastic scattering ratio to the Rutherford cross sections and the distribution at the sub-barrier energies with the corresponding experimental data for the system $^{25}Mg+^{90}Zr$ in the single channel (SC) calculations at V_0 = (43.8, 58.8, and 73.8) MeV, indicated as red, green, and black, respectively.

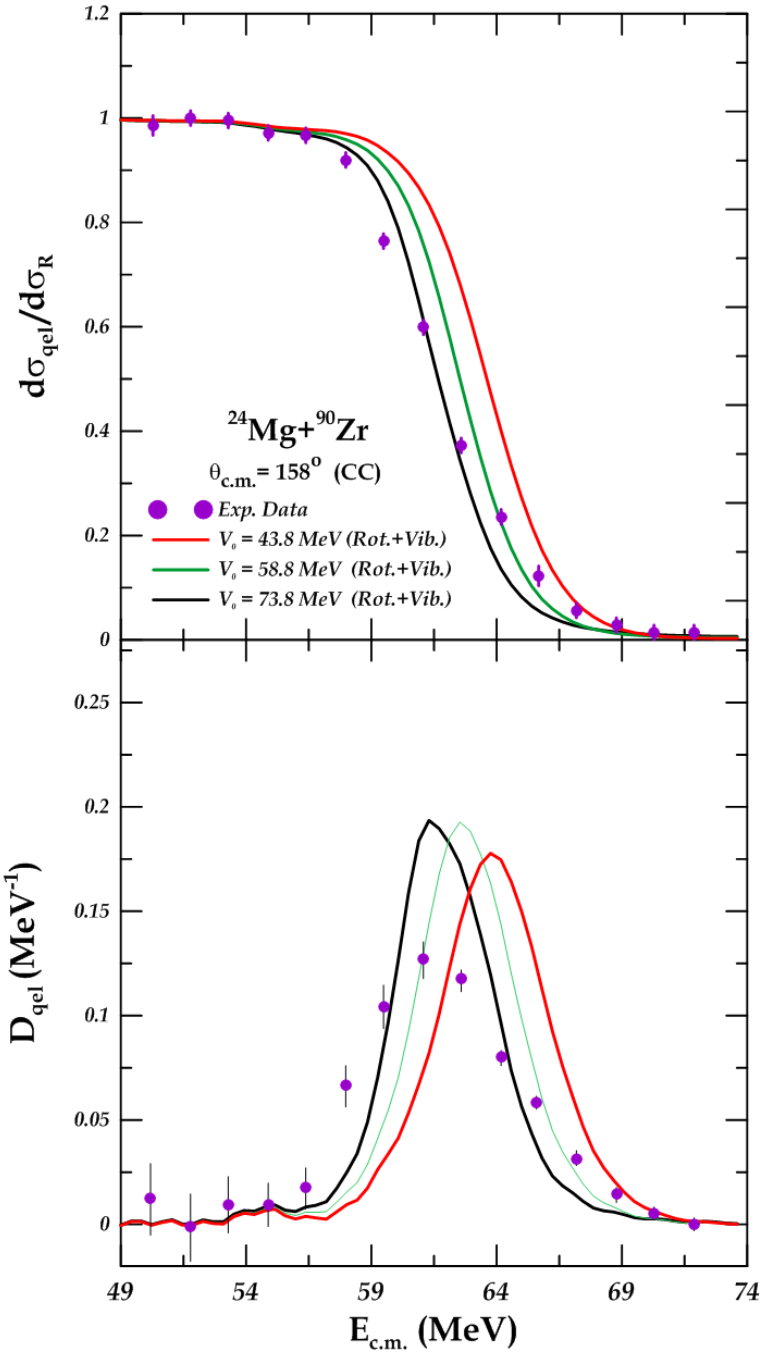

Fig.4.4. The comparison of the calculated quasi-elastic scattering ratio to the Rutherford cross sections and the distribution at the sub-barrier energies with the corresponding experimental data for the system $^{25}Mg+^{90}Zr$ in the coupled channel (CC) calculations at V_0 = (43.8, 58.8, and 73.8) MeV, indicated as red, green, and black, respectively.

4.2.2 ^{28}Si+^{120}Sn system

The first case in this part, the diffuseness parameter of 0.63 fm was the standard value [9] and that both the projectile and target nuclei were inert single channel (SC) at various values of a_0 is (0.60, 0.63, and 0.66) fm, respectively. In the second instance at coupled-channel (CC), the target nucleus ^{120}Sn was vibrating with a deformation coefficient of β_2 = 0.107 [68] to the state 2^+(1.171265 Mev), $E_{4^+}/E_{2^+} = 1.8$, whereas the projectile nucleus ^{28}Si was rotating with a deformation coefficient of β_2 = -0.478, β_4 = 0.250 [68] to the state 2^+(1.77903 Mev), where $E_{4^+}/E_{2^+} = 2.59$. the Woods-Saxon parameters were taken to be V_0 = 45.8 MeV, the radius parameter r_0 =1.2 fm , which is listed in Table 4.3. used the single phonon state of the quadruple excitation of the target nuclei were employed .

Table (4.3) : The fitted WS parameters (radius r_0, depth potential V_0, and the diffuseness parameters a_0), which were obtained from SC and CC calculation, and the values of the χ^2 between experimental and theoretical data for the ^{28}Si+^{120}Sn system

System	Channel	V_0 (MeV)	r_0 (fm)	a_0 (fm)	$\theta_{c.m.}$ $(deg.)$	χ^2	
						σ_{qel}/σ_R	D_{qel}
^{28}Si+^{120}Sn	SC	45.8	1.2	0.60	150.5	0.06072	0.03304
				0.63		0.10359	0.05258
				0.66		0.17721	0.08379
	CC	45.8	1.2	0.60	150.5	0.01259	0.01686
				0.63		0.00794	0.01954
				0.66		0.00475	0.02127

For a ^{28}Si+^{120}Sn system, from table (4.3), by using single-channel calculations, the best-fit diffuseness parameter is 0.60 fm. It is significantly lower than the standard value. χ^2 = 0.06072 is The calculated

ratio of the quasi-elastic to the Rutherford cross sections is represented by the red line in Fig. 4.5. It is the curve nearest to the curve of the experimental data, with V_0= 45.8 MeV. The best value for the distribution D_{qel} is 0.03304, as shown by the red line in Fig. 4.5, at the same diffuseness parameter value. When coupled-channel calculations were used, the best-fitting diffuseness parameter was 0.66 fm, with χ^2 = 0.00475 for a rotating projectile (P) and vibrating target (T), which was shown by the black line in Fig. 4.6, which is higher than the standard value. The best value of the distribution D_{qel} = 0.01686 at the diffuseness parameter 0.60 fm is denoted by the red line in Fig. 4.6. Furthermore, the resulting χ^2 values show that the best-fitting diffuseness parameter calculated using coupled channels fits the data better than the one calculated experimental using a single channel. The last part of the distribution curve fails to match the practical data because the theoretical calculations did not reach the correct coupling level for the practical data

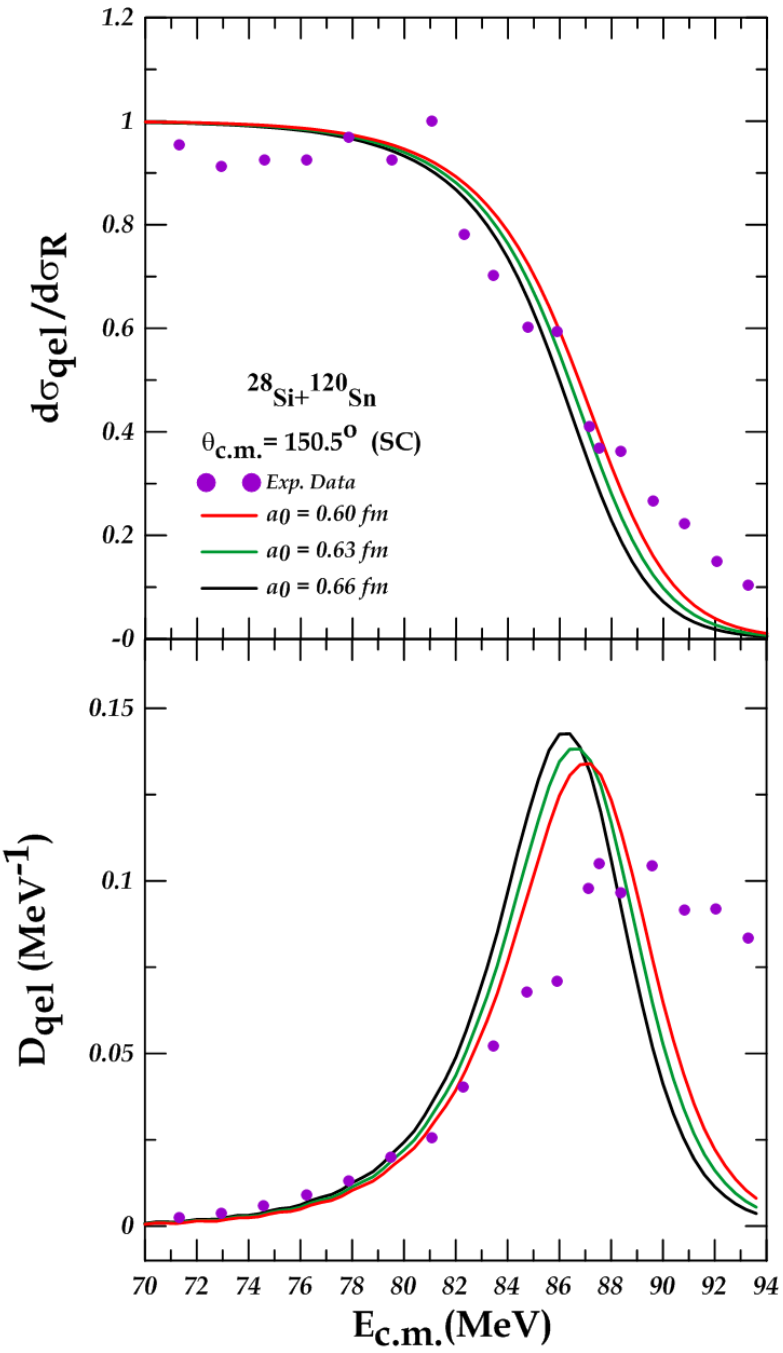

Fig.4.5. The comparison of the calculated quasi-elastic scattering ratio to the Rutherford cross sections and the distribution at the sub-barrier energies with the corresponding experimental data taken from [12] for the system ^{28}Si+^{120}Sn in the single channel (SC) calculations at a_0 = (0.60, 0.63,and 0.66 fm). indicated as red, green, and black, respectively.

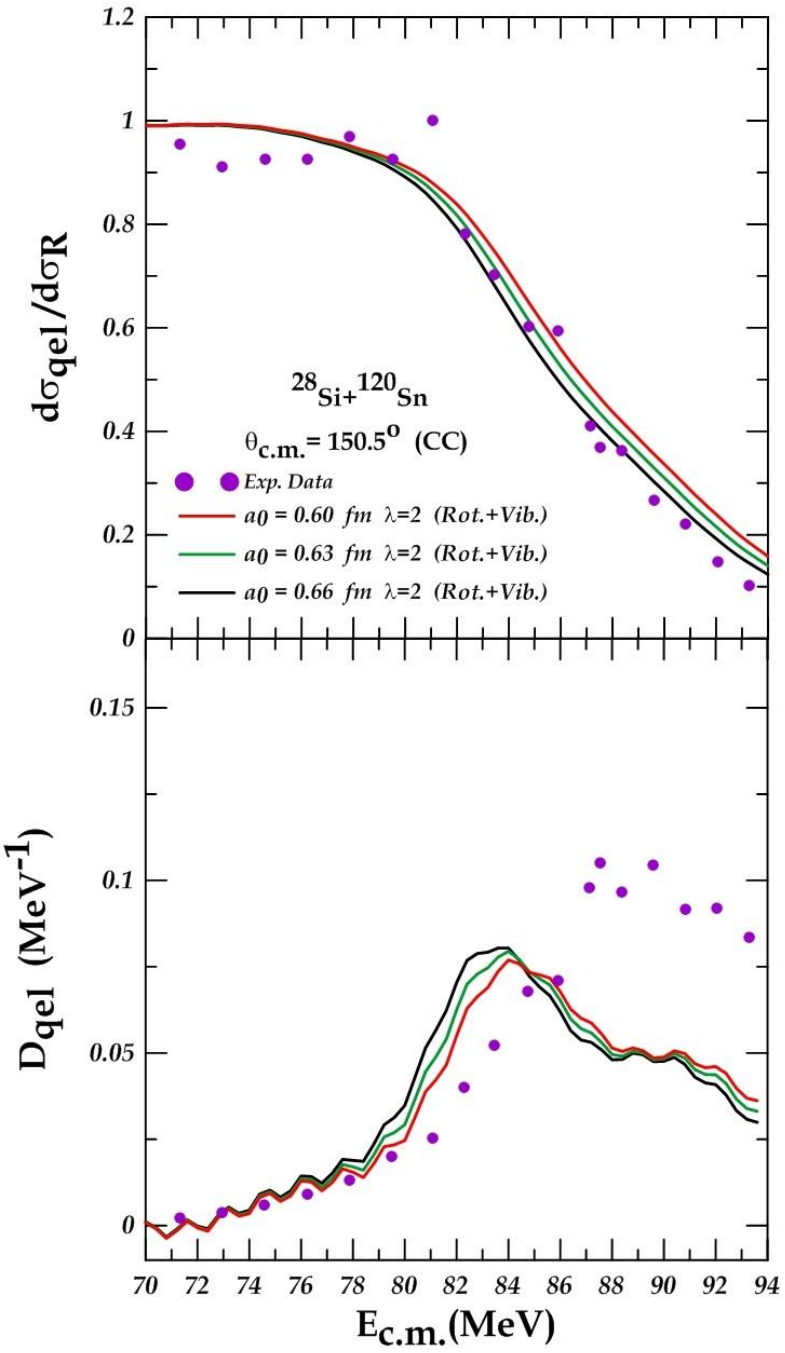

Fig.4.6. The comparison of the calculated quasi-elastic scattering ratio to the Rutherford cross sections and the distribution at the sub-barrier energies with the corresponding experimental data for the system $^{28}Si+^{120}Sn$ in the coupled channel (CC) calculations at a_0 = (0.60, 0.63,and 0.66 fm). indicated as red, green, and black, respectively.

The second part for the results , in the single channel (SC) calculations, where both the projectile and target nuclei were considered inert at three

values of the real nuclear potential (potential depth V_0) (38.8, 45.8, and 52.8 MeV), the diffusion parameter a_0 is 0.66 fm, which was previously determined by the χ^2 method as the best value for matching the experimental data with the theoretical data. By using the coupled-channel (CC) calculations, The target nucleus ^{120}Sn was vibrating, and the projectile nucleus ^{28}Si was rotating. and the radius parameter r_0 = 1.2 fm.

Table (4.4) : The fitted parameters of WS potential (the diffuseness parameters a_0, the depth potential V_0 ,and radius r_0), that is estimated from the SC and CC calculation, and the values of the χ^2 between experimental and theoretical data for the ^{28}Si+^{120}Sn system

System	Channel	a_0 (fm)	r_0 (fm)	V_0 (MeV)	$\theta_{c.m.}$ $(deg.)$	χ^2	
						σ_{qel}/σ_R	D_{qel}
^{28}Si+^{120}Sn	SC	0.66	1.2	38.8	150.5	0.0691344	0.0384049
				45.8		0.1772061	0.1183911
				52.8		0.4321193	0.1819151
	CC	0.66	1.2	38.8	150.5	0.0092564	0.0186956
				45.8		0.0051736	0.0250216
				52.8		0.0046239	0.0266695

From table (4.4), the best-fit potential depth V_0 is 38.8 MeV acquired through a single-channel analysis, with a_0 = 0.66 fm. The chi squared χ^2 value is 0.0691344. It represents the calculated ratio of the quasi-elastic scattering to the Rutherford cross sections, as shown by the red line in Fig. 4.7. The best value for barrier distribution D_{qel} is 0.0384049. It is shown by the red line in Fig. 4.7 at the same value as the potential depth. In a coupled-channel procedure, the best potential depth is 52.8 MeV. The obtained χ^2 value is 0.0046239, as shown by the black line in Fig. 4.8. The best value of the barrier distribution D_{qel} is 0.0186956 at the

potential depth V_0 of 38.8, as represented by the red line in Fig. 4.8, by comparing the χ^2 values between (SC) and (CC) . The best-fit potential depth obtained through the coupled channel calculations.

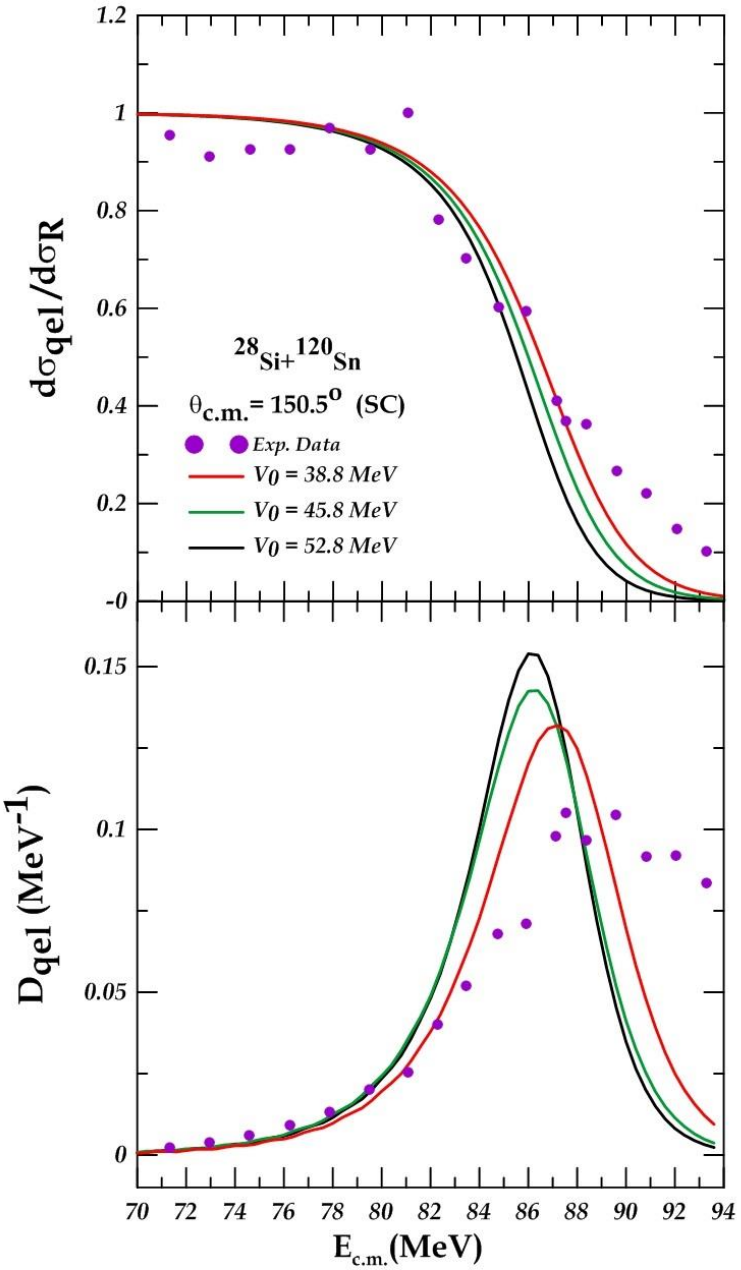

Fig.4.7. The comparison of the calculated quasi-elastic scattering ratio to the Rutherford cross sections and the distribution at the sub-barrier energies with the corresponding experimental data for the system **^{28}Si+^{120}Sn** in the single channel (SC) calculations at V_0 = (38.8, 45.8, and 52.8 MeV), indicated as red, green, and black, respectively.

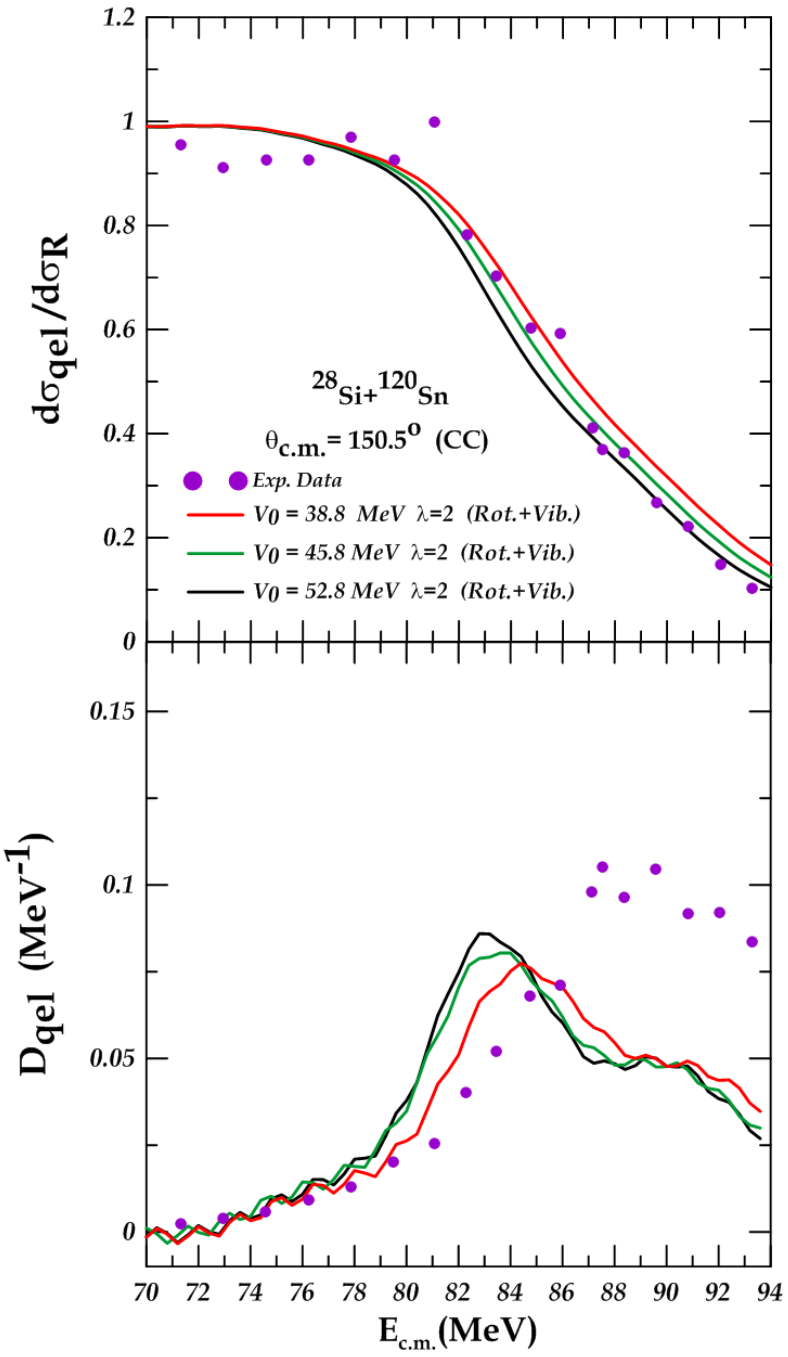

Fig.4.8. The comparison of the calculated quasi-elastic scattering ratio to the Rutherford cross sections and the distribution at the sub-barrier energies with the corresponding experimental data for the system **^{28}Si+^{120}Sn** in the coupled channel (CC) calculations at V_0 = (38.8, 45.8, and 52.8 MeV), indicated as red, green, and black, respectively.

4.2.3 ^{28}Si+^{150}Nd system

The first case where both the projectile and target nuclei are inert at three values for the diffuseness parameter a_0 (0.55, 0.63, and 0.71 fm). The diffuseness parameter of 0.63 fm was the standard value [9]. The second case, in the coupled-channel (CC) calculations, the projectile nucleus ^{28}Si was rotating with a deformation coefficient of β_2 = -0.478 and β_4 = 0.250 [68] to the state 2^+(1.77903 Mev), where $E_{4^+}/E_{2^+} =$ 2.59. while the target nucleus ^{150}Nd was rotating according to E_{4^+}/E_{2^+}= 2.9, But it was considered inert because the program does not respond to this case of coupling. The potential depth V_0 is 42.2 MeV, and the radius parameter r_0 is 1.2 fm.

Table(4.5) : The fitted **WS** parameters (radius r_0, depth potential V_0, and the diffuseness parameters a_0), which were obtained from SC and CC calculation, and the values of the χ^2 between experimental and theoretical data for the **^{28}Si+^{150}Nd** system

System	Channel	V_0 (MeV)	r_0 (fm)	a_0 (fm)	$\theta_{c.m.}$ $(deg.)$	χ^2	
						σ_{qel}/σ_R	D_{qel}
^{28}Si+^{150}Nd	SC	42.2	1.2	0.55	140	0.01936	0.03100
				0.63		0.05279	0.05130
				0.71		0.17076	0.10976
	CC	42.2	1.2	0.55	140	0.00843	0.00880
				0.63		0.00597	0.01078
				0.71		0.00828	0.01623

From table (4.5), by using single-channel (SC) calculations, the best-fitting diffuseness parameter a_o is 0.55 fm with χ^2 = 0.01936. It represents the calculated ratio of the quasi-elastic scattering to the Rutherford cross sections. This is shown by the red line in Fig. 4.9. The best-fit diffuseness parameter is rather low compared to the standard value. The optimum value for the distribution D_{qel} is 0.03100, as shown by the red line in Fig.

4.9, at the same diffuseness parameter value. On the other hand, coupling channels should be taken into account in the analysis of sub-barrier energies. By a coupled-channels procedure, the best-fit diffuseness parameter with a rotating projectile (P) and inert target (T) at diffuseness parameter a_0 = 0.63 fm with χ^2 = 0.00597 and V_0 = 42.2 MeV This is shown by the blue line in Fig. 4.10. The best-fitting diffuseness is in very good agreement with the standard value. The best value of the distribution D_{qel} is 0.00880 at the diffuseness parameter of 0.55 fm, as denoted by the red curve in Fig. 4.10. The results show that coupled-channel calculations produce a better fit to the experimental data than single-channel calculations.

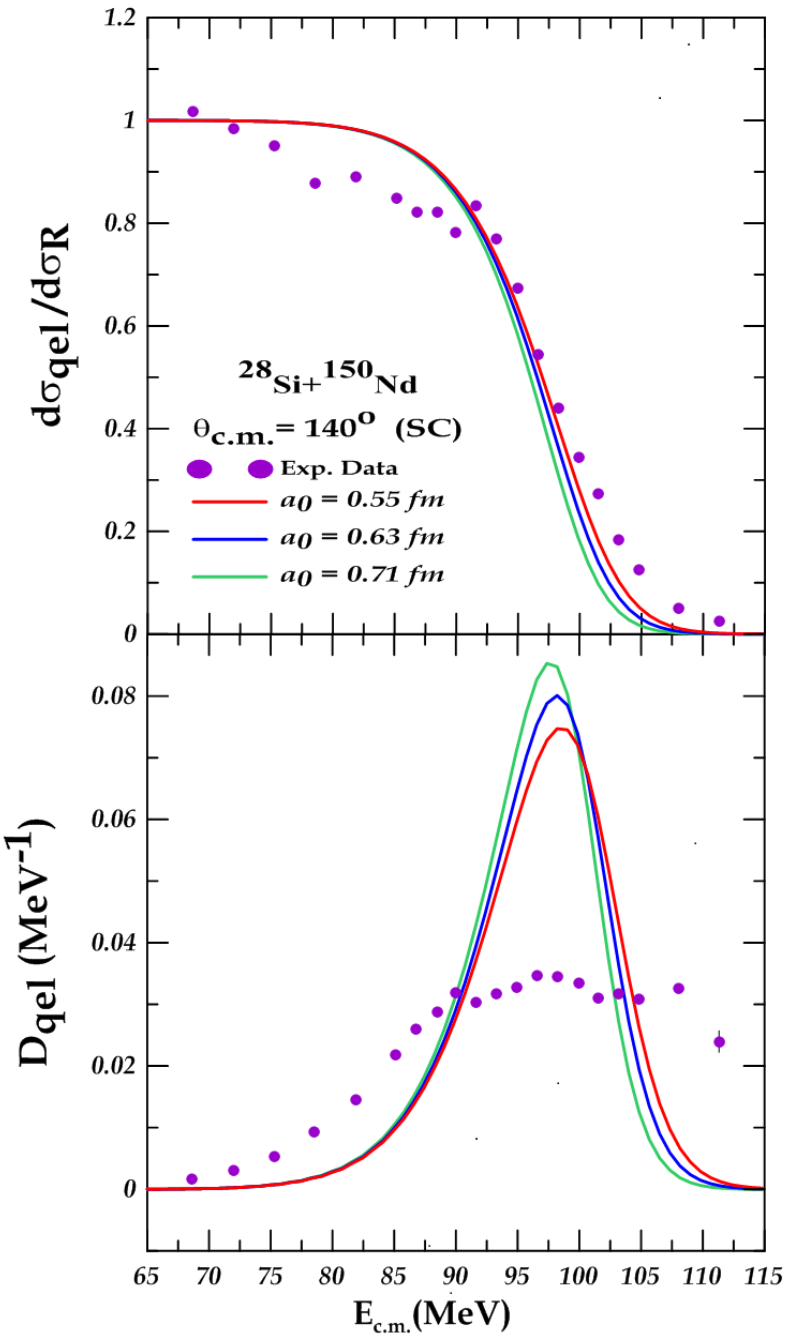

Fig. 4.9. The comparison of the calculated quasi-elastic scattering ratio to the Rutherford cross sections and the distribution at the sub-barrier energies with the corresponding experimental data taken from [23] for the system ^{28}Si+^{150}Nd in the single channel (SC) calculations at a_0 = (0.55, 0.63, and 0.71 fm). indicated as red, blue , and green, respectively.

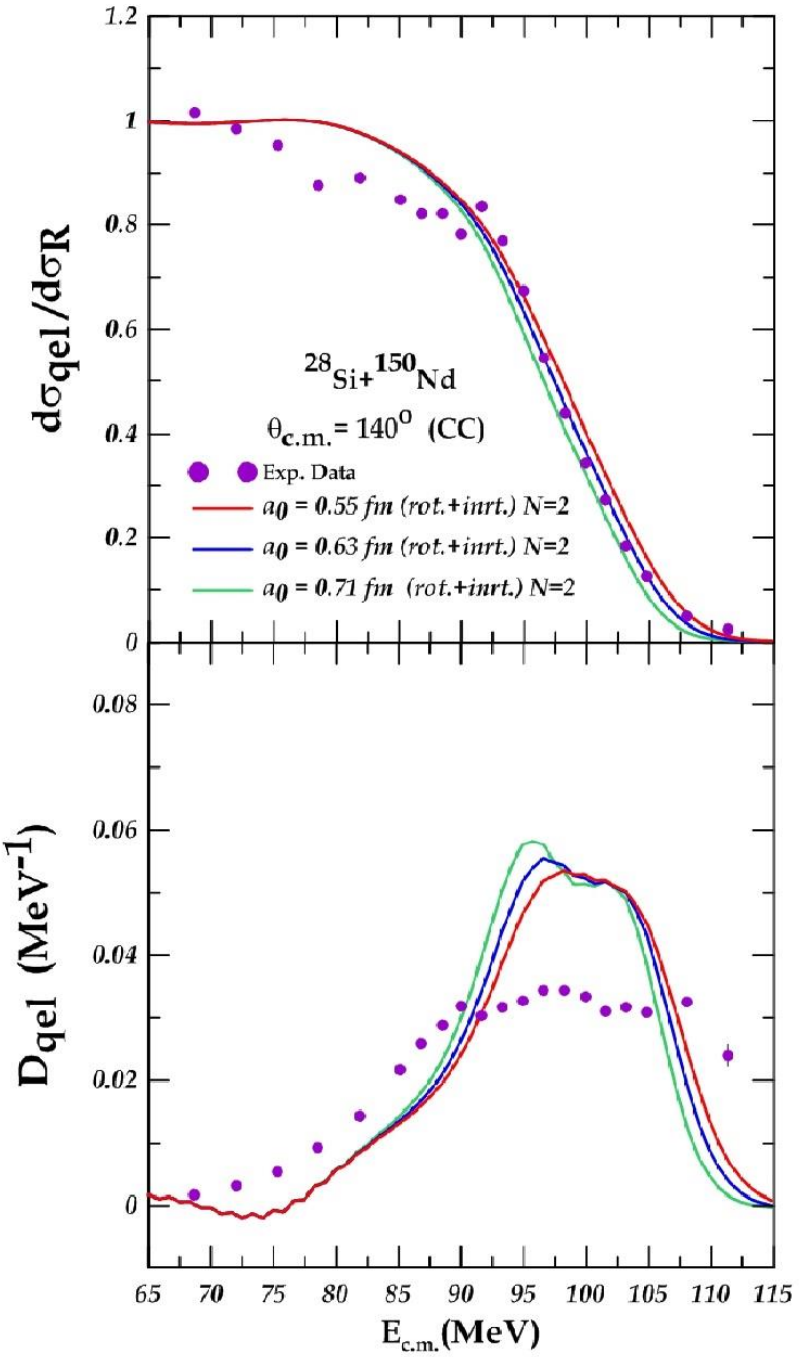

Fig. 4.10. The comparison of the calculated quasi-elastic scattering ratio to the Rutherford cross sections and the distribution at the sub-barrier energies with the corresponding experimental data for the system ^{28}Si+^{150}Nd in the coupled channel (CC) calculations at a_0 = (0.55, 0.63, and 0.71 fm). indicated as red, blue , and green, respectively.

The second part of the results shows that both the projectile and target nuclei were considered inert at three values of the real nuclear potential

(potential depth V_0) (22.2, 42.2, and 62.2 MeV). The diffuseness parameter a_0 = 0.63 fm was previously determined by using the χ^2 method as the best value for matching the experimental data with the theoretical data. In the coupled channel (CC) calculations, the projectile nucleus ^{28}Si was rotating, and the target nucleus ^{150}Nd was inert .The radius parameter r_0 is 1.2 fm.

Table (4.6) : The fitted parameters of WS potential (the diffuseness parameters a_0, the depth potential V_0 ,and radius r_0), that is estimated from the SC and CC calculation, and the values of the χ^2 between experimental and theoretical data for the **^{28}Si+^{150}Nd** system.

System	Channel	a_0 (fm)	r_0 (fm)	V_0 (MeV)	$\theta_{c.m}$ $(deg.)$	χ^2	
						σ_{qel}/σ_R	D_{qel}
^{28}Si+^{150}Nd	SC	0.63	1.2	22.2	140	0.0120001	0.0250845
				42.2		0.0527879	0.0512978
				62.2		0.1976138	0.1436154
	CC	0.63	1.2	22.2	140	0.0093331	0.0084162
				42.2		0.0059686	0.0107807
				62.2		0.0107800	0.0180037

From table (4.6), the best-fit potential depth V_0 is 22.2 MeV of the ^{28}Si+^{150}Nd system acquired through a single-channel analysis , with a_0 = 0.63 fm. The chi squared χ^2 value is 0.0120001. It represents the calculated ratio of the quasi-elastic scattering to the Rutherford cross sections. It was shown by the red line in Fig. 4.11. The best value for barrier distribution D_{qel} = 0.0250845 at the same value of the potential depth. It is denoted by the red-colored curve depicted in Fig. 4.11. In a coupled-channels procedure, the best potential depth is 42.2 MeV. The obtained χ^2 value is 0.0059686, as shown by the blue line in Fig. 4.12. The best value of the barrier distribution D_{qel} is 0.0084162 at the potential

depth V_0 of 22.2 MeV, represented by the red line in Fig. 4.12. by comparing the χ^2 values between SC and CC, the best-fitting potential depth is in very good agreement with the standard value.

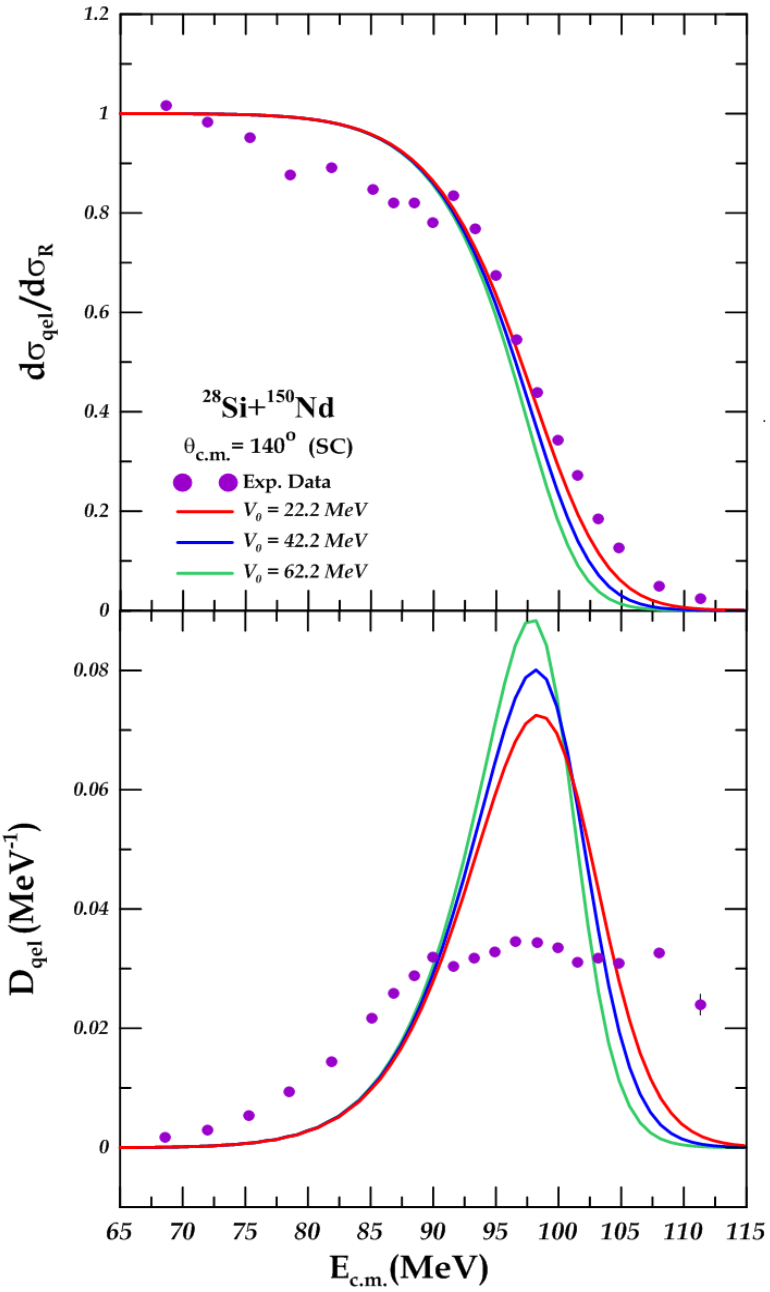

Fig.4.11. The comparison of the calculated quasi-elastic scattering ratio to the Rutherford cross sections and the distribution at the sub-barrier energies with the corresponding experimental data for the system $^{28}Si+^{150}Nd$ in the single channel (SC) calculations at V_0 = (22.2, 42.2, and 62.2 MeV), indicated as red, blue, and green, respectively.

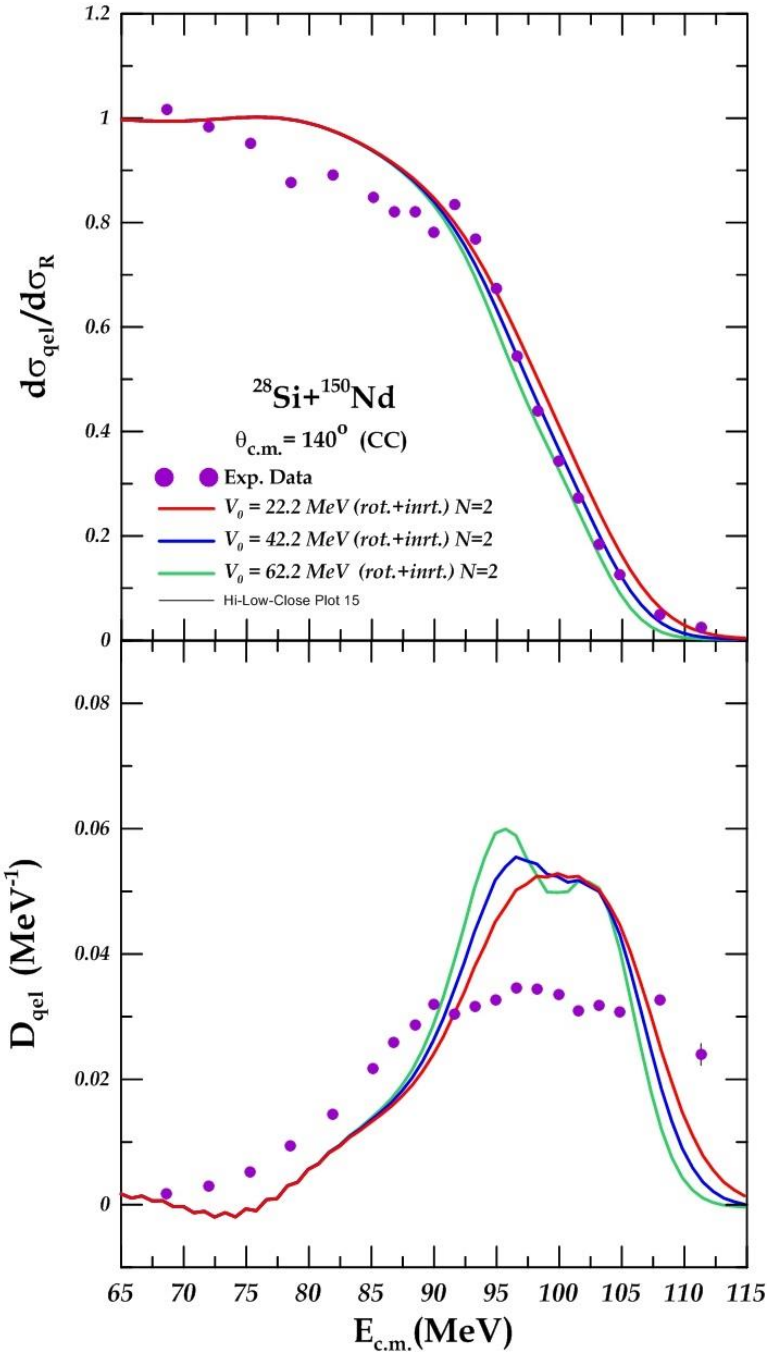

Fig.4.12. The comparison of the calculated quasi-elastic scattering ratio to the Rutherford cross sections and the distribution at the sub-barrier energies with the corresponding experimental data for the system ^{28}Si+^{150}Nd in the coupled channel (CC) calculations at V_0 = (22.2, 42.2, and 62.2 MeV), indicated as red, blue, and green, respectively.

4.2.4 ^{16}O+^{160}Gd System

In this system, the first case , where both the projectile and target nuclei were considered inert at three values of the diffusion parameter a_0 = (0.50, 0.54, and 0.63 fm) .In the second case at coupled channels (CC) calculation, the projectile nucleus ^{16}O was vibrating, this was deduced according to the ratio $E_{4^+}/E_{2^+} = 1.49$ with a deformation coefficient of β_2 = 0.364 [68] to the state 2^+ (6.9171 MeV). While the target nucleus ^{160}Gd was rotating, according to the ratio $E_{4^+}/E_{2^+} = 3.3$ with deformation coefficients of β_2= 0.280 and β_4= 0.065 [68], to the state 2^+(0.075263 MeV). But it was considered inert because the program does not respond to this case of coupling. The single phonon state of the quadruple excitation of the projectile nucleus was employed. The potential depth V_0 is 83.7 MeV, and the radius parameter r_0 is 1.2 fm.

Table(4.7) : The fitted **WS** parameters (radius r_0, depth potential V_0, and the diffuseness parameters a_0), which were obtained from SC and CC calculation, and the values of the χ^2 between experimental and theoretical data for the **^{16}O+^{160}Gd** system .

System	Channel	V_0 (MeV)	r_0 (fm)	a_0 (fm)	θ_{cm} $(deg.)$	χ^2	
						σ_{qel}/σ_R	D_{qel}
^{16}O+^{160}Gd	SC	83.7	1.2	0.50	170	0.1262659	0.0055259
				0.54		0.3379357	0.0079423
				0.63		3.8882560	0.0838409
	CC	83.7	1.2	0.50	170	0.0103542	0.0034493
				0.54		0.0341377	0.0071324
				0.63		0.2673588	0.0574917

From table 4.7 , according to single-channel calculations . The best-fitting diffuseness parameter a_0 is 0.50 fm. This value is a little compared to the standard value of 0.63 , The calculated ratio of the quasi-elastic to the

Rutherford cross sections is 0.1262659, which is the closest to the curve of the experimental data. It is shown by the red line in Fig. 4.13. The optimum value for the distribution D_{qel} is 0.0055259, as shown by the red line in Fig. 4.13. at the same value of the diffuseness parameter ,with V_0 = 83.7 MeV . According to the coupled-channel calculations with a vibration projectile (P) and inert target (T), the best-fit diffuseness parameter a_0 is 0.50 fm, χ^2 = 0.0103542. It is represented by the red line in Fig. 4.14. the best value for the distribution D_{qel} is 0.0034493 at the same diffuseness parameter value and denoted by the red-colored curve in Fig. 4.14. The results show that coupled-channel calculations produce a better fit to the experimental data than single-channel calculations.

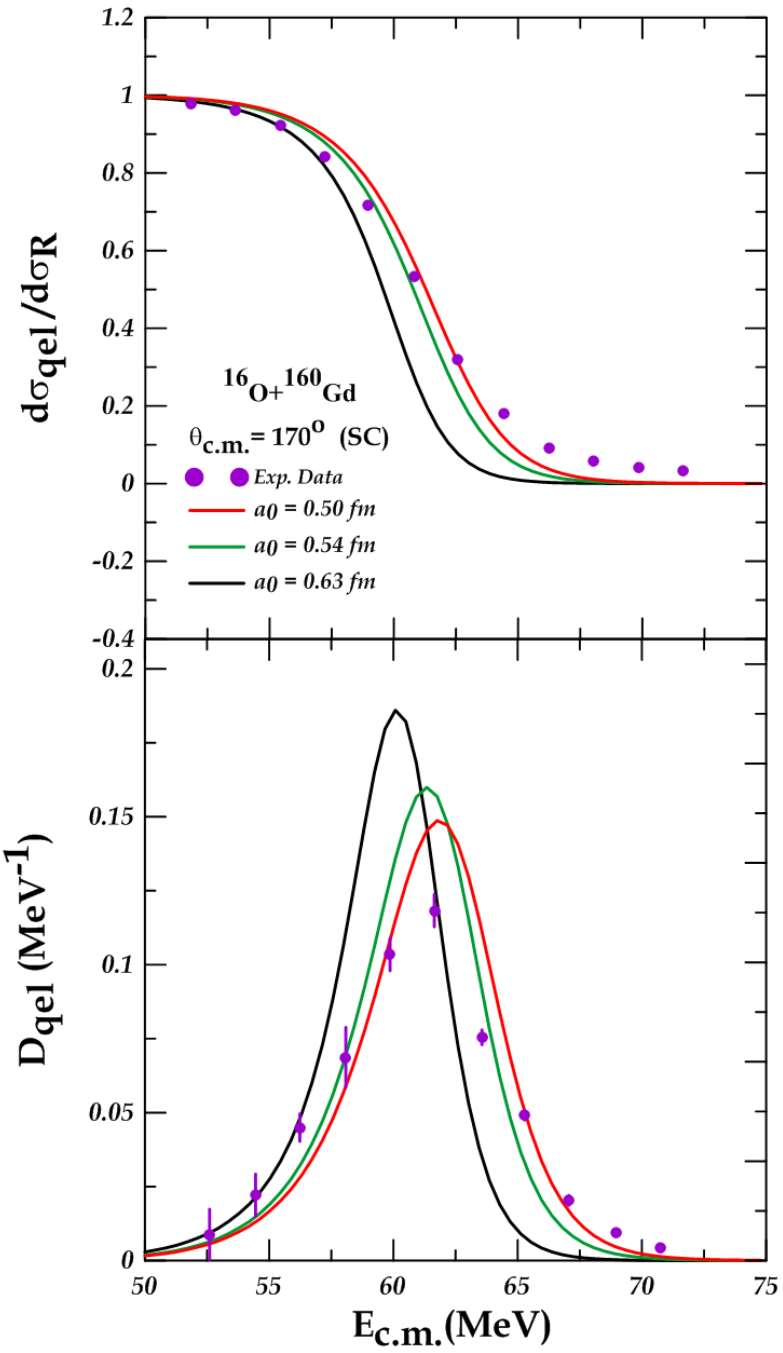

Fig. 4.13. The comparison of the calculated quasi-elastic scattering ratio to the Rutherford cross sections and the distribution at the sub-barrier energies with the corresponding experimental data taken from [69] for the system $^{16}O+^{160}Gd$ in the single channel (SC) calculations at a_0 = (0.50, 0.54, and 0.63fm), indicated as red, green , and black, respectively.

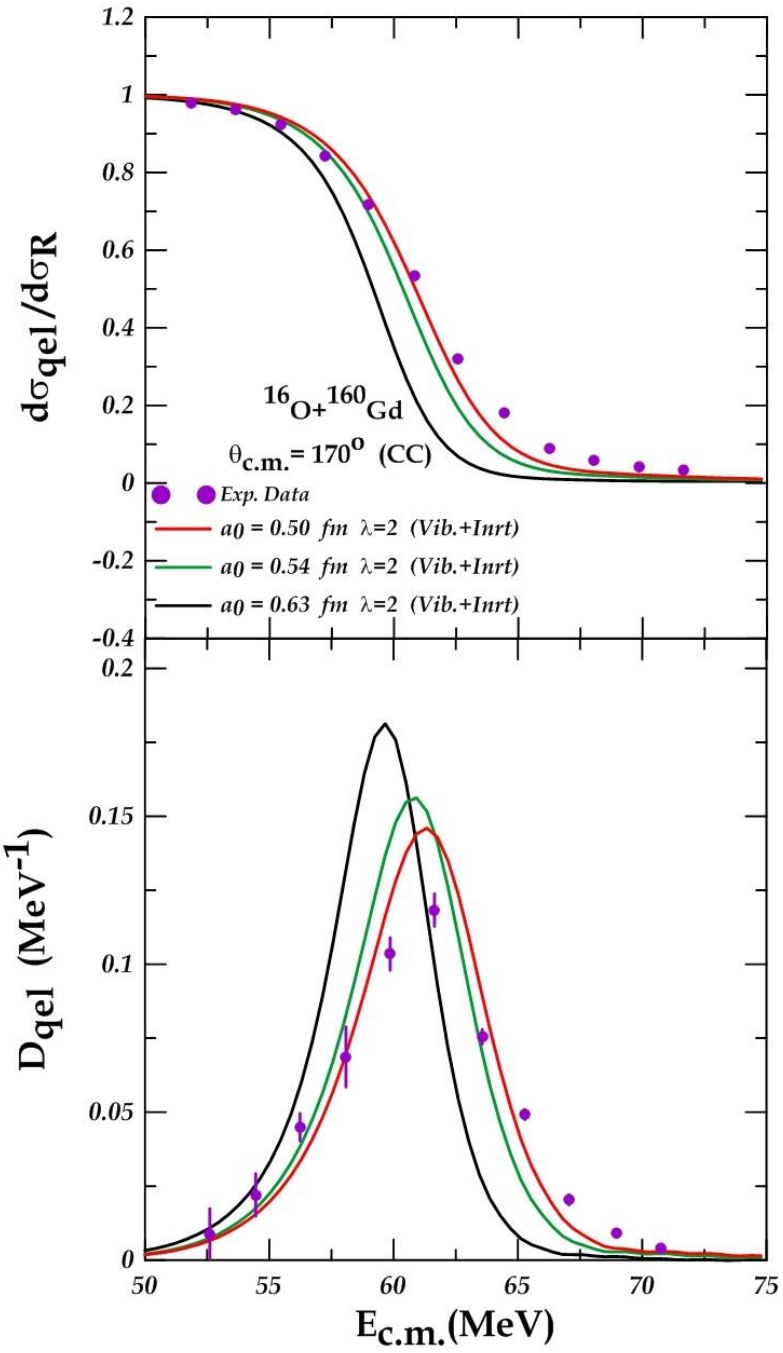

Fig. 4.14. The comparison of the calculated quasi-elastic scattering ratio to the Rutherford cross sections and the distribution at the sub-barrier energies with the corresponding experimental data for the system $^{16}O+^{160}Gd$ in the coupled channel (CC) calculations at a_0 = (0.50, 0.54, and 0.63fm). indicated as red, green , and black, respectively.

The Second part of the results, according to the single channel (SC) calculations, at three values of the real nuclear potential (potential depth

V_0) (58.7, 83.7, and 108.7 MeV) and the diffusion parameter a_0 = 0.50 fm were considered, was previously determined by the χ^2 method as the best value for matching the experimental data with the theoretical data. In coupled-channels (CC) calculations. The projectile nucleus ^{16}O was vibrating, the target nucleus ^{160}Gd was inert . The radius parameter r_0 = 1.2 fm.

Table (4.8) : The fitted parameters of WS potential (the diffuseness parameters a_0, the depth potential V_0 ,and radius r_0), that is estimated from the SC and CC calculation, and the values of the χ^2 between experimental and theoretical data for the **^{16}O+^{160}Gd** system.

System	Channel	a_0 (fm)	r_0 (fm)	V_0 (MeV)	θ_{cm} $(deg.)$	χ^2	
						σ_{qel}/σ_R	D_{qel}
^{16}O+^{160}Gd	SC	0.50	1.2	58.7	170	0.04873	0.0072179
				83.7		0.12627	0.0055259
				108.7		0.27427	0.0074302
	CC	0.50	1.2	58.7	170	0.00522	0.0034521
				83.7		0.01035	0.0034493
				108.7		0.02409	0.0057510

In table (4.8), the best-fit potential depth V_0 of the ^{16}O+^{160}Gd system acquired through a single-channel analysis is 58.7 MeV, with a_0 = 0.50 fm. the chi square χ^2 = 0.04873, It was shown by the red line in Fig. 4.15. The best value for barrier distribution D_{qel} is 0.0055259 at the potential depth V_0 = 83.7 MeV. It was shown by the green line in Fig. 4.15. In a coupled-channels calculations , the best potential depth is 58.7 MeV. The obtained χ^2 value is 0.00522, as shown by the red line in Fig. 4.16. The best value of the barrier distribution D_{qel} is 0.0034493 at the potential depth V_0 = 83.7MeV is represented by the green curve Fig. 4.16.

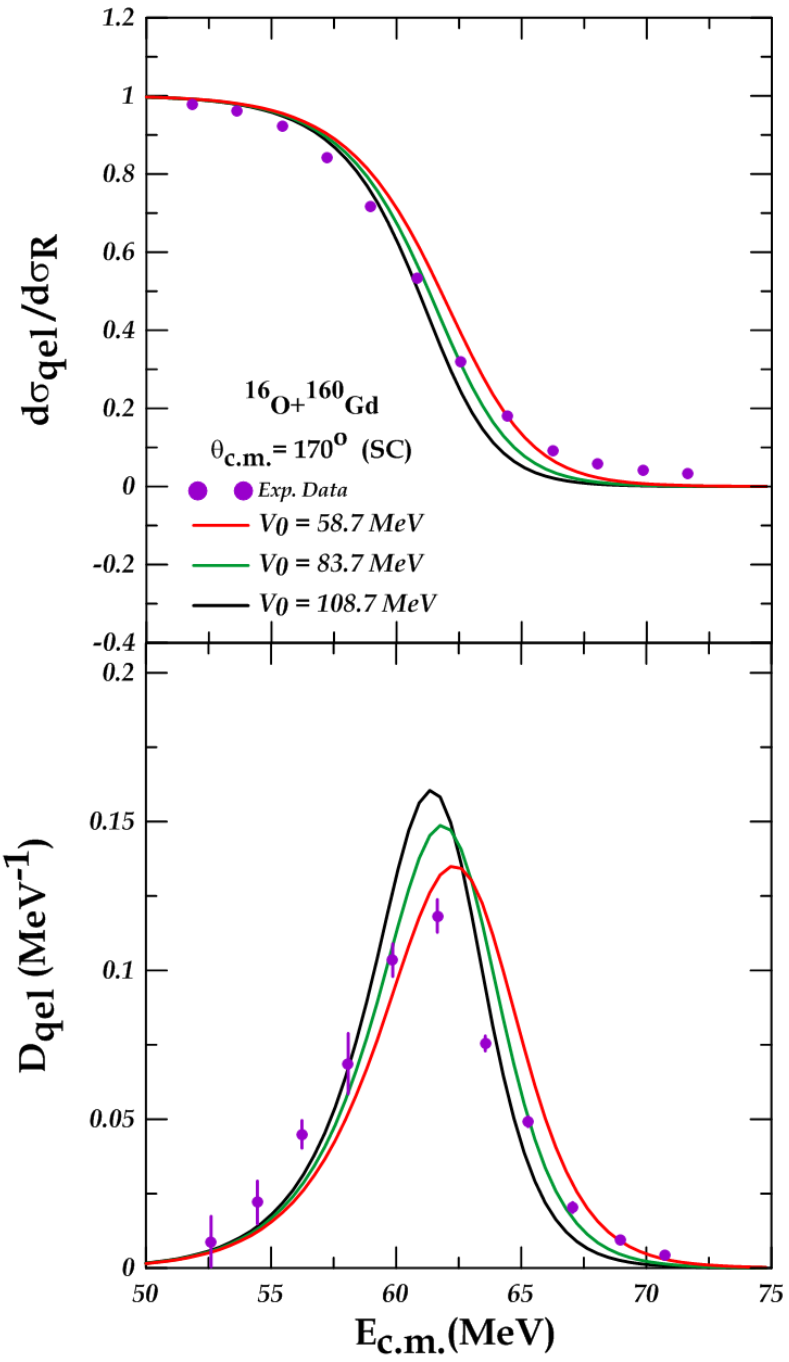

Fig.4.15 The comparison of the calculated quasi-elastic scattering ratio to the Rutherford cross sections and the distribution at the sub-barrier energies with the corresponding experimental data for the system $^{16}O+^{160}Gd$ in the single channel (SC) calculations at V_0 = (58.7, 83.7, and 108.7 MeV), indicated as red, green, and black, respectively.

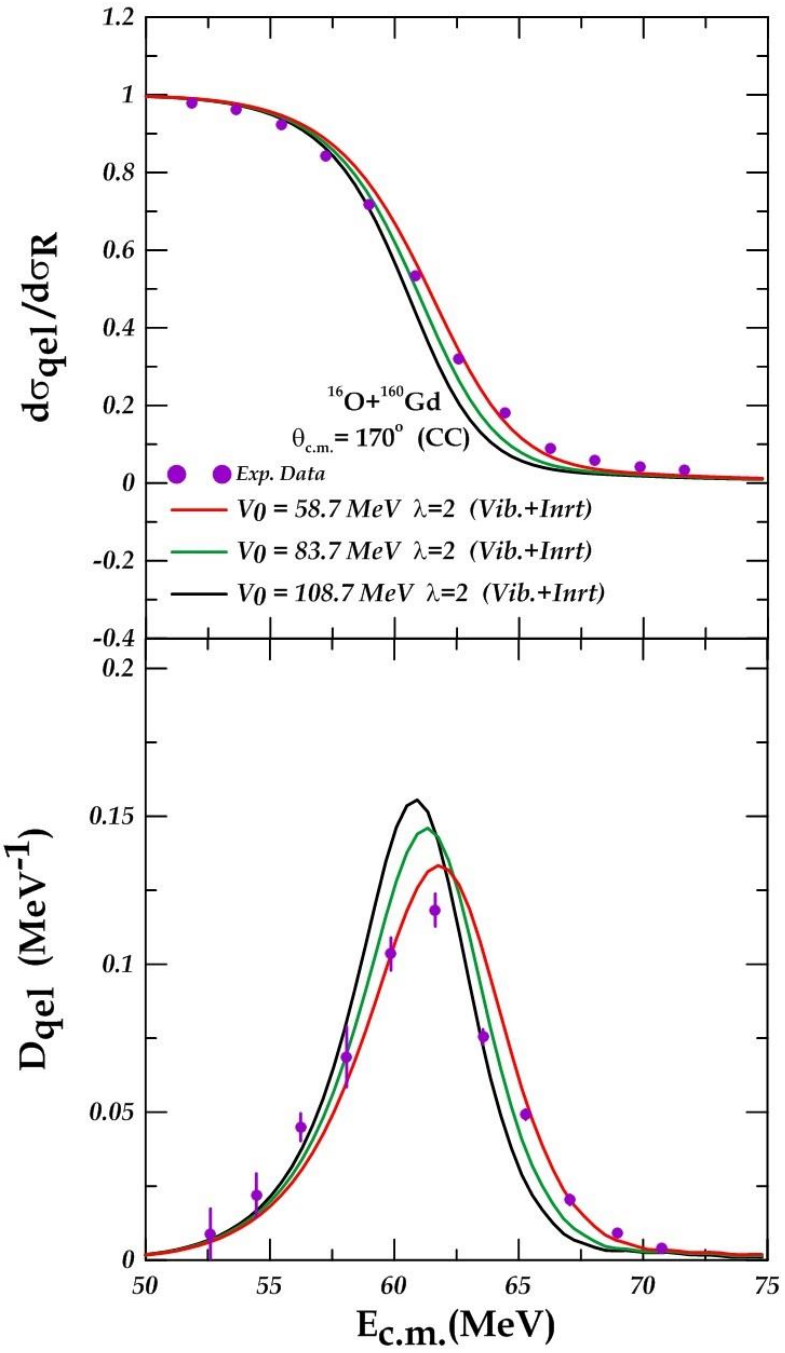

Fig.4.16 The comparison of the calculated quasi-elastic scattering ratio to the Rutherford cross sections and the distribution at the sub-barrier energies with the corresponding experimental data for the system $^{16}O+^{160}Gd$ in the coupled channel (CC) calculations at V_0 = (58.7, 83.7, and 108.7 MeV), indicated as red, green, and black, respectively.

4.2.5 ^{12}C+^{197}Au system

In the first case, both the projectile and target nuclei were considered inert (SC) at three values of the diffusion parameter (0.59, 0.63, and 0.67) fm, with 0.63 fm being the standard value [9]. In the second case, at coupled channel (CC) calculations, the projectile nucleus was ^{12}C was rotational, where E_{4^+}/E_{2^+}= 2.9 with a deformation coefficient of β_2 = 0.582 [68] to the state 2^+ (4.43982 MeV), while the target nucleus was ^{197}Au, In the rotational state, this was deduced according to the ratio $E_{5/2^+}/E_{1/2^+}$ = 3.6 with a deformation coefficient of β_2 = -0.131 , β_4= -0.031[68]. To the state 2^+ (0.077351 MeV). The radius parameter r_0 is equal to 1.2 fm.

Table (4.9) : The fitted **WS** parameters (radius r_0, depth potential V_0, and the diffuseness parameters a_0), which were obtained from SC and CC calculation, and the values of the χ^2 between experimental and theoretical data for the **^{12}C+^{197}Au** system.

System	Channel	V_0 (MeV)	r_0 (fm)	a_0 (fm)	θ_{cm} $(deg.)$	χ^2	
						σ_{qel}/σ_R	D_{qel}
^{12}C+^{197}Au	SC	58.8	1.2	0.59	180	0.0542071	0.0104545
				0.63		0.1054816	0.0149919
				0.67		0.2654193	0.0398066
	CC	58.8	1.2	0.59	180	0.0141393	0.0235719
				0.63		0.0059362	0.0350599
				0.67		0.0077787	0.0552774

According to the results for the ^{12}C+^{197}Au system shown in Table (4.9), when a single-channel SC calculations, the best fitted diffuseness parameter a_0 is 0.59, which is less than the standard value. The potential depth V_0 is 58.8 MeV. χ^2 is 0.0542071, as shown by the red line in Fig. 4.17. The best value for the barrier distribution D_{qel} is 0.0104545 at the

same value of the diffuseness parameter, and it is represented by the red curve in Fig. 4.17. By using coupled channel (CC) calculations, the best-fit diffuseness parameter with a rotating projectile (P) and rotating target (T) is 0.63. It is considerably in agreement with the standard value, The value of chi-squared χ^2 is 0.0059362, as shown by the green line in Fig. 4.18. The best value of the distribution D_{qel} is 0.0235719 at the diffuseness parameter of 0.59 fm, represented by the red curve in Fig. 4.18. The resulting $\chi 2$ values show that the best-fitting diffuseness parameter calculated using coupled channels fits the experimental data better than the one calculated using a single channel.

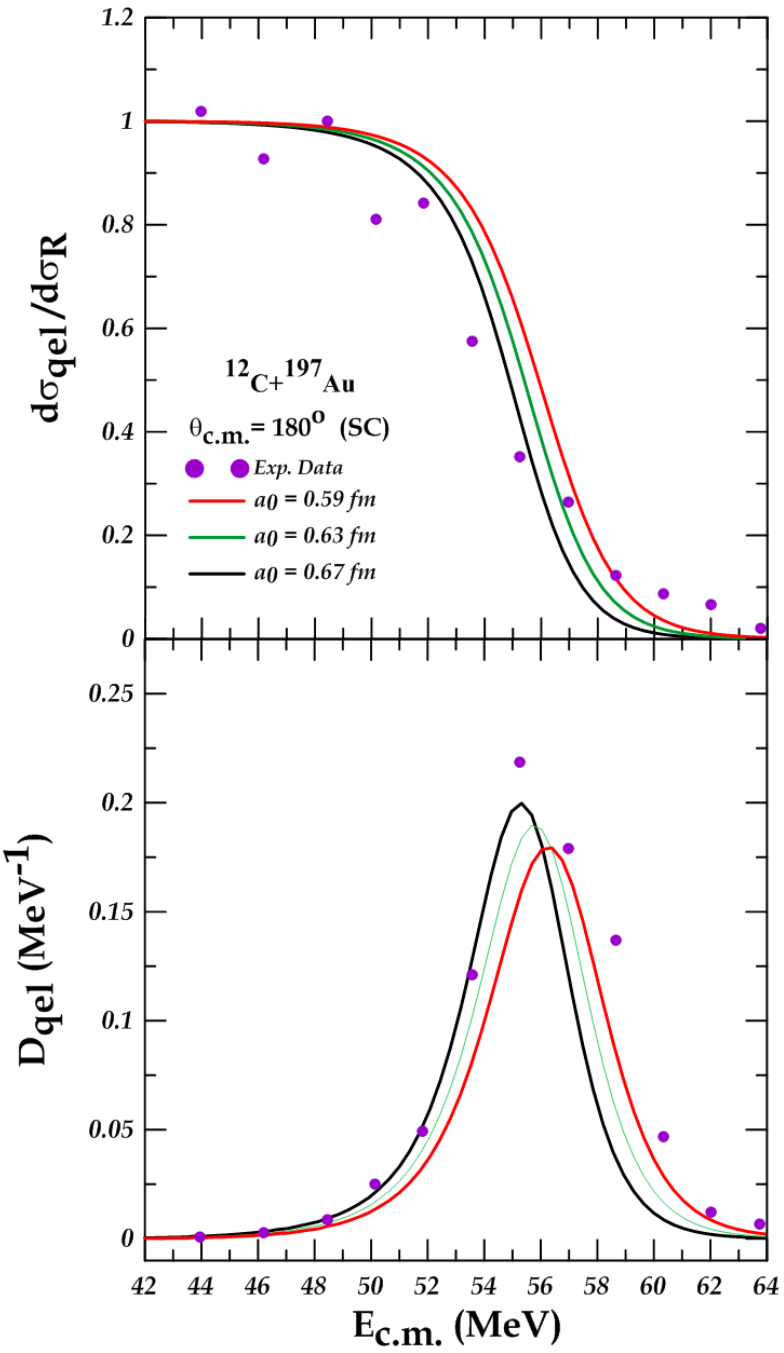

Fig.4.17. The comparison of the calculated quasi-elastic scattering ratio to the Rutherford cross sections and the distribution at the sub-barrier energies with the corresponding experimental data taken from [70] for the system $^{12}C+^{197}Au$ in the single channel (SC) calculations at a_0 = (0.59, 0.63, and 0.67 fm). indicated as red, green , and black, respectively.

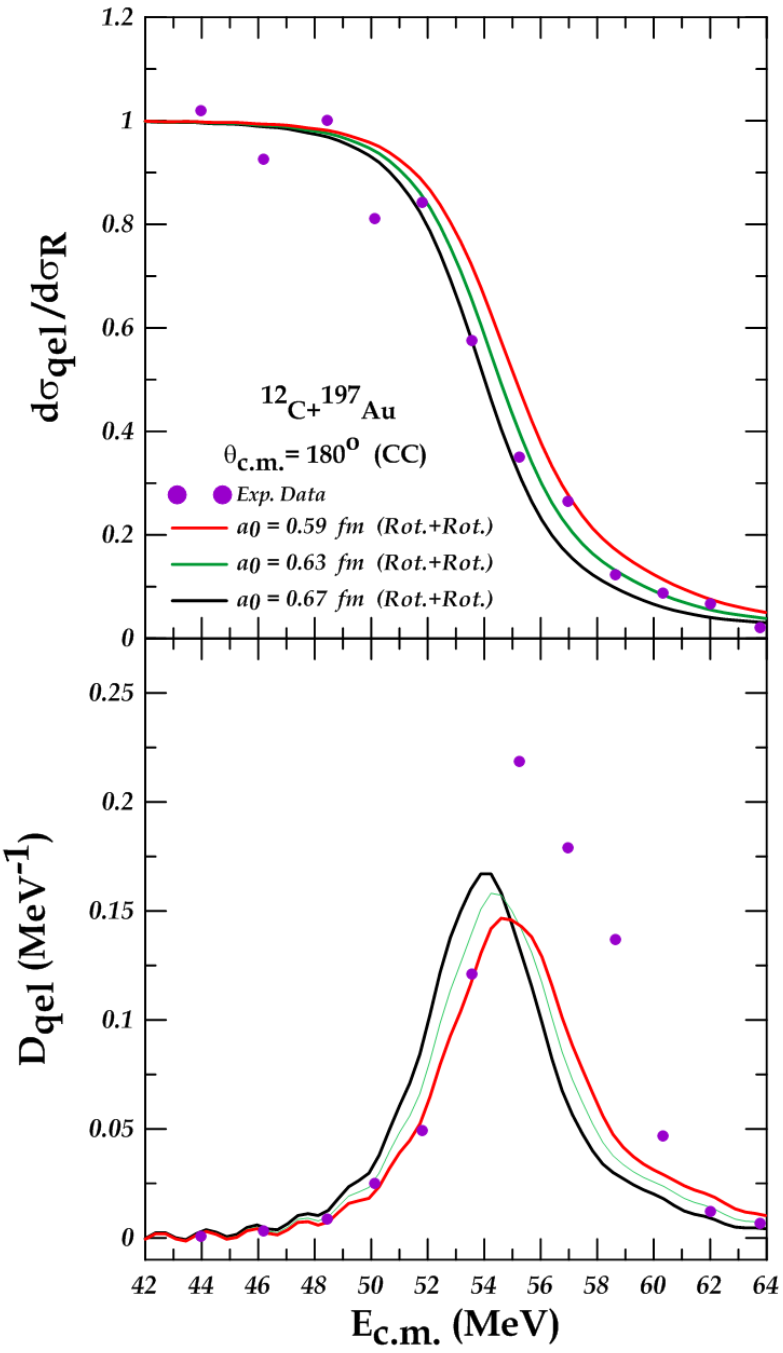

Fig.4.18. The comparison of the calculated quasi-elastic scattering ratio to the Rutherford cross sections and the distribution at the sub-barrier energies with the corresponding experimental data for the system $^{12}C+^{197}Au$ in the coupled channel (CC) calculations at a_0 = (0.59, 0.63, and 0.67 fm). indicated as red, green , and black, respectively.

The second part of the results includes two cases: the first case where both the projectile and target nuclei were considered inert (SC) at three

values of the real nuclear potential (potential depth V_0) (48.8, 53.8, and 68.8) MeV, and we considered the diffusion parameter a_0 = 0.63 fm. It was previously determined by the χ^2 method as the best value for matching the experimental data with the theoretical data. In the second case, at the coupled channel (CC), The target nucleus ^{12}C was rotating, the projectile nucleus ^{197}Au was rotating . The radius parameter r_0 was 1.2 fm.

Table (4.10) : The fitted parameters of WS potential (the diffuseness parameters a_0, the depth potential V_0 ,and radius r_0), that is estimated from the SC and CC calculation, and the values of the χ^2 between experimental and theoretical data for the **$^{12}C+^{197}Au$** system

System	Channel	a_0 (fm)	r_0 (fm)	V_0 (MeV)	θ_{cm} $(deg.)$	χ^2	
						σ_{qel}/σ_R	D_{qel}
$^{12}C+^{197}Au$	SC	0.63	1.2	48.8	180	0.0508598	0.0099349
				58.8		0.1054816	0.0149919
				68.8		0.2342481	0.0349948
	CC	0.63	1.2	48.8	180	0.0133151	0.0230850
				58.8		0.0059362	0.0350599
				68.8		0.0063233	0.0522743

From table (4.10) The best-fit potential depth V_0 is 48.8 MeV of the $^{12}C+^{197}Au$ system acquired through a single-channel analysis . with a_0 = 0.63 fm. The chi square χ^2 is 0.0508598, which is the curve that is closest to the experimental data curve as shown by the red line in Fig. 4.19. The best value for barrier distribution D_{qel} is 0.0099349 at the same potential depth. It was shown by the red line in Fig. 4.19. In coupled-channels calculations, the best potential depth is 58.8 MeV, with target (T) and projectile (P) rotating. The obtained χ^2 value is 0.0059362, as shown by the green line in Fig.4.20.It is in complete agreement with the

experimental data curve. The best value of the barrier distribution D_{qel} is 0.0230850 at the depth potential V_0= 48.8 MeV ,represented by the red curve in Fig.4.20.

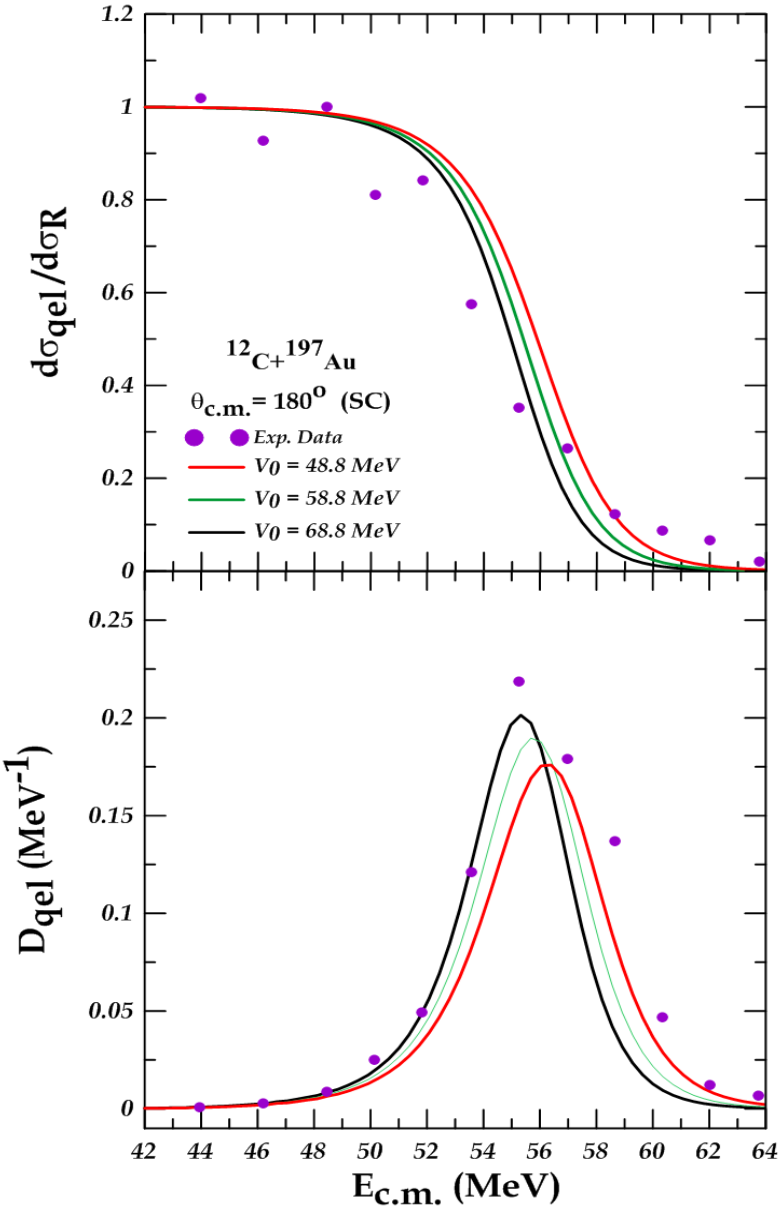

Fig. 4.19. The comparison of the calculated quasi-elastic scattering ratio to the Rutherford cross sections and the distribution at the sub-barrier energies with the corresponding experimental data for the system $^{12}C+^{197}Au$ in the single channel (SC) calculations at V_0 = (48.8, 58.8, and 68.8 MeV), indicated as red, green, and black, respectively.

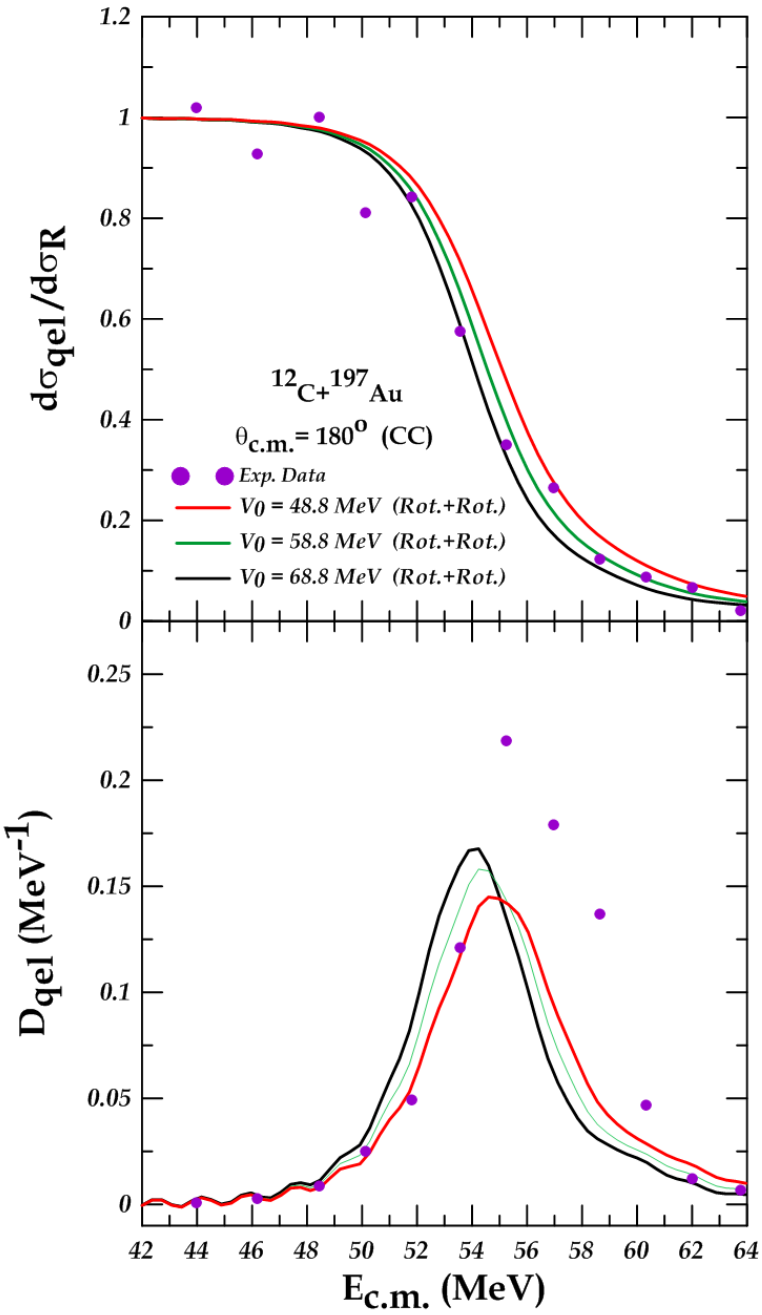

Fig. 4.20. The comparison of the calculated quasi-elastic scattering ratio to the Rutherford cross sections and the distribution at the sub-barrier energies with the corresponding experimental data for the system $^{12}C+^{197}Au$ in the coupled channel (CC) calculations at V_0 = (48.8, 58.8, and 68.8 MeV), indicated as red, green, and black, respectively.

4.2.6 ^{6}Li+^{144}Sm System

The first case In this system, where both the projectile ^{6}Li and target nuclei^{144}Sm were considered inert ,single channel calculations (SC) at different values of the diffusion parameter a_0 is (0.59, 0.63, and 0.67) fm, respectively and we considered the diffusion parameter 0.63 fm is the standard value[9].In the second case, at coupled-channel (CC) ,the projectile nucleus ^{6}Li does not have a deformation coefficient, so it is considered an inert nucleus . The target nucleus ^{144}Sm was vibrating with a deformation coefficient of $\beta_3 = 0.151$ [68] to the state 2^{+}(1.660027 MeV), where $E_{4^+}/E_{2^+} = 1.32$.The single phonon state of the octupole excitation of the target nuclei, the potential depth V_0= 50 MeV, and the radius parameter r_0 = 1.2 fm.

Table (4.11) : The fitted **WS** parameters (radius r_0, depth potential V_0, and the diffuseness parameters a_0), which were obtained from SC and CC calculation, and the values of the χ^2 between experimental and theoretical data for the **^{6}Li+^{144}Sm** system.

System	Channel	V_0 (MeV)	r_0 (fm)	a_0 (fm)	$\theta_{.c.m}$ $(deg.)$	χ^2	
						σ_{qel}/σ_R	D_{qel}
^{6}Li+^{144}Sm	SC	50	1.2	0.59	170	0.0045772	0.5392147
				0.63		0.0012624	0.4655860
				0.67		0.0054699	0.3775857
	CC	50	1.2	0.59	170	0.0050365	0.4407188
				0.63		0.0007709	0.4049674
				0.67		0.0025455	0.0147660

Table (4.11) shows the results of a single channel (SC) data analysis. The χ^2 is 0.0012624. It represents the calculated ratio of the quasi-elastic scattering to the Rutherford cross sections at the diffuseness parameter 0.63 fm, as shown by the green line in Fig. 4.21. It is the curve closest to

the curve of the experimental data. The best value of the distribution D is 0.37758577 at the diffuseness parameter a_0 = 0.67, illustrated by the black curve in Fig. 4.21. At The coupled-channel calculation with inert projectile (P) and a vibrating target (T) that the best fit of χ^2 is 0.0007709 at the diffuseness parameter a_0 = 0.63 fm, which is represented by the green line in Fig.4.22. where V_0 = 50 MeV. The best value of the distribution D_{qel} represented by the black curve in Fig. 4.22. is 0.0147660 at the diffuseness parameter of 0.67 fm. From those results, we note that there was a good agreement between the experimental data and theoretical calculations in both cases, single and coupled channels.

.

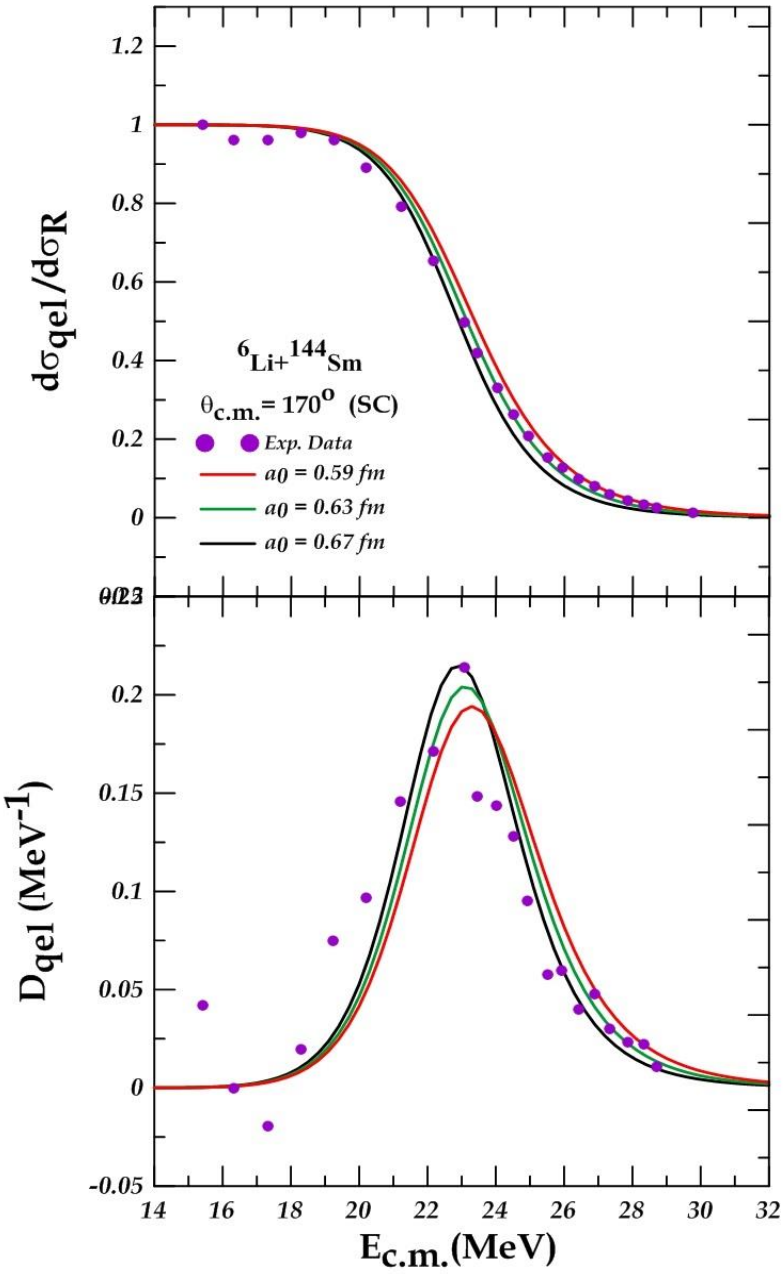

Fig. 4.21. The comparison of the calculated quasi-elastic scattering ratio to the Rutherford cross sections and the distribution at the sub-barrier energies with the corresponding experimental data taken from [71] for the system ^{6}Li+^{144}Sm in the single channel (SC) calculations at a_0 = (0.59, 0.63, and 0.67 fm). indicated as red, green , and black, respectively.

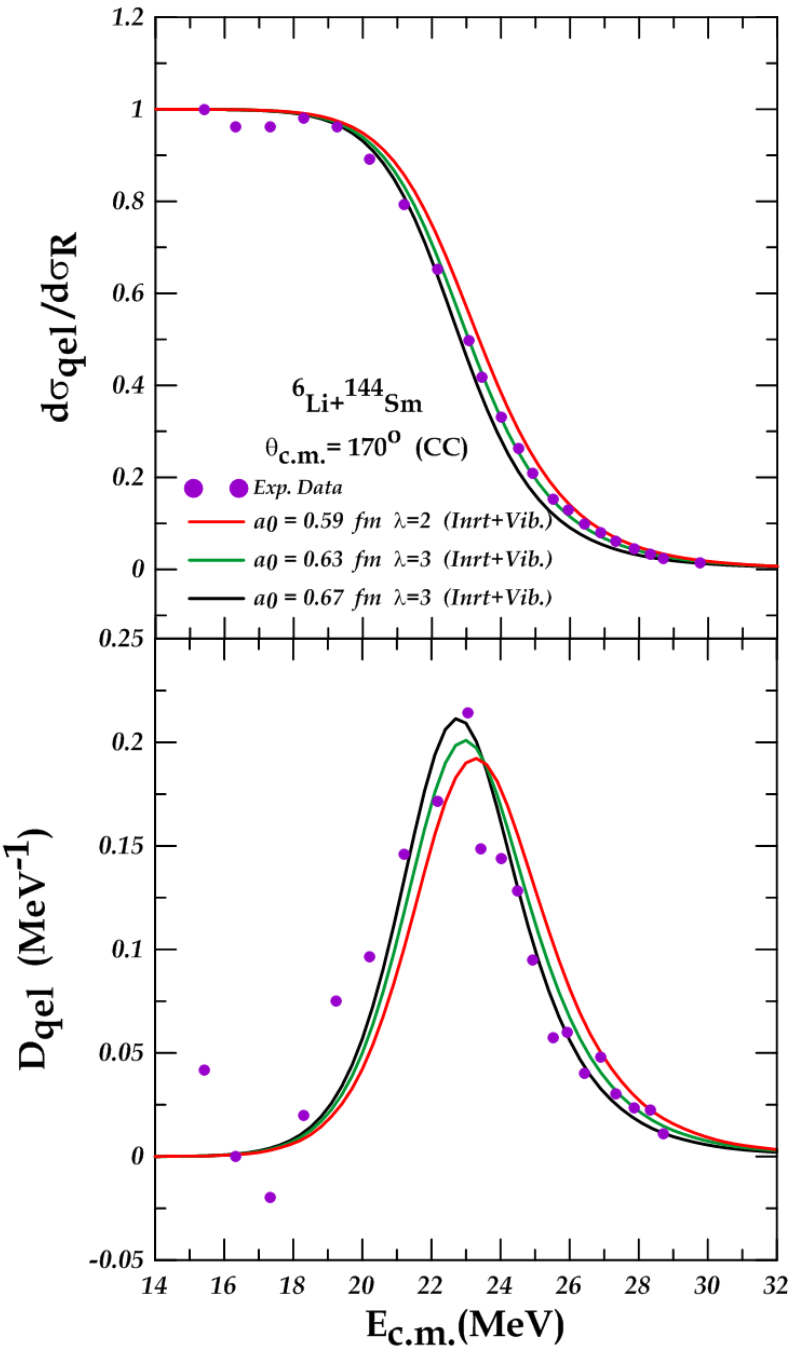

Fig. 4.22. The comparison of the calculated quasi-elastic scattering ratio to the Rutherford cross sections and the distribution at the sub-barrier energies with the corresponding experimental data for the system ^{6}Li+^{144}Sm in the coupled channel (CC) calculations at a_0 = (0.59, 0.63, and 0.67 fm). indicated as red, green , and black, respectively.

The second part of the results , the first case where both the projectile and target nuclei were considered inert (SC) at three values of the real nuclear potential (potential depth V_0) (30.0, 50.0, and 70.0) MeV, and we considered the diffusion parameter a_0 = 0.63 fm. It was previously determined by the χ^2 method as the best value for matching the experimental data with the theoretical data. In the second case, at the coupled channel (CC), the projectile nucleus ^{6}Li was inert and the target nucleus ^{144}Sm was vibrating. The radius parameter r_0 = 1.2 fm.

Table (4.12) : The fitted parameters of WS potential (the diffuseness parameters a_0, the depth potential V_0 ,and radius r_0), that is estimated from the SC and CC calculation, and the values of the χ^2 between experimental and theoretical data for the **^{6}Li+^{144}Sm** system.

System	Channel	a_0 (fm)	r_0 (fm)	V_0 (MeV)	θ_{cm} $(deg.)$	χ^2	
						σ_{qel}/σ_R	D_{qel}
^{6}Li+^{144}Sm	SC	0.63	1.2	30.0	170	0.0108333	0.5277192
				50.0		0.0012624	0.4655860
				70.0		0.0086471	0.4177707
	CC	0.63	1.2	30.0	170	0.0134418	0.2853361
				50.0		0.0007709	0.4049674
				70.0		0.0044709	0.0146228

From Table 4.12, the best fit for the chi-square χ^2 is 0.0012624 at the potential depth V_0 = 50.0 MeV, which was acquired from SC data analysis. It was shown by the green line in Fig. 4.23. This is the curve that is closest to the curve of the experimental data. The best fit value of the distribution D_{qel} is 0.4177707 at the depth potential V_0 = 70.0 MeV, as shown by the green line in Fig. 4.23. According to the coupled-channel calculations with an inert projectile (P) and a vibrating target (T), the χ^2 is 0.0007709 at the potential depth V_0 = 50.0 MeV, as shown by the green

line in Fig. 4.24. It is the curve nearest to the curve of the experimental data, while the best fit value of the distribution D_{qel} is 0.0146228 at the depth potential V_0 = 70.0 MeV, represented by the black curve in Fig 4.24.

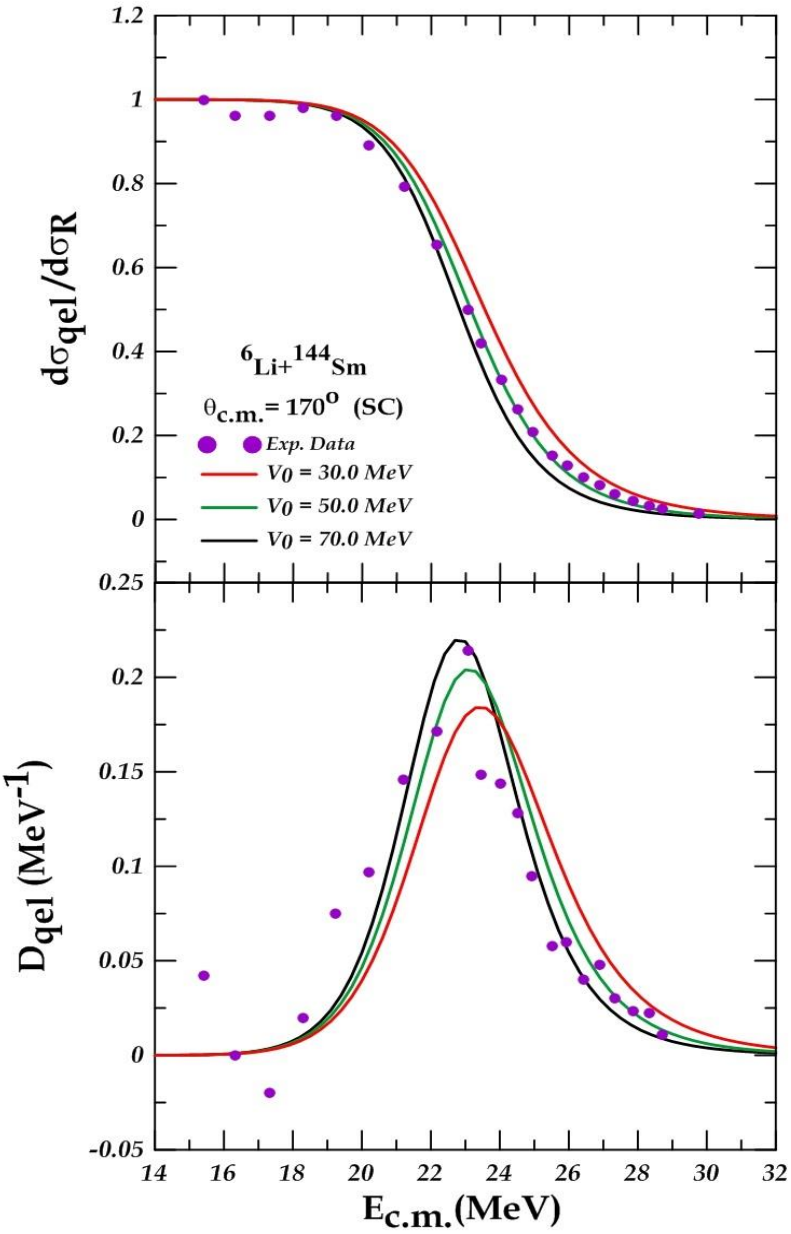

Fig. 4.23. The comparison of the calculated quasi-elastic scattering ratio to the Rutherford cross sections and the distribution at the sub-barrier energies with the corresponding experimental data for the system ^{6}Li+^{144}Sm in the single channel (SC) calculations at V_0 = (30.0, 50.0, and 70.0MeV), indicated as red, green, and black, respectively.

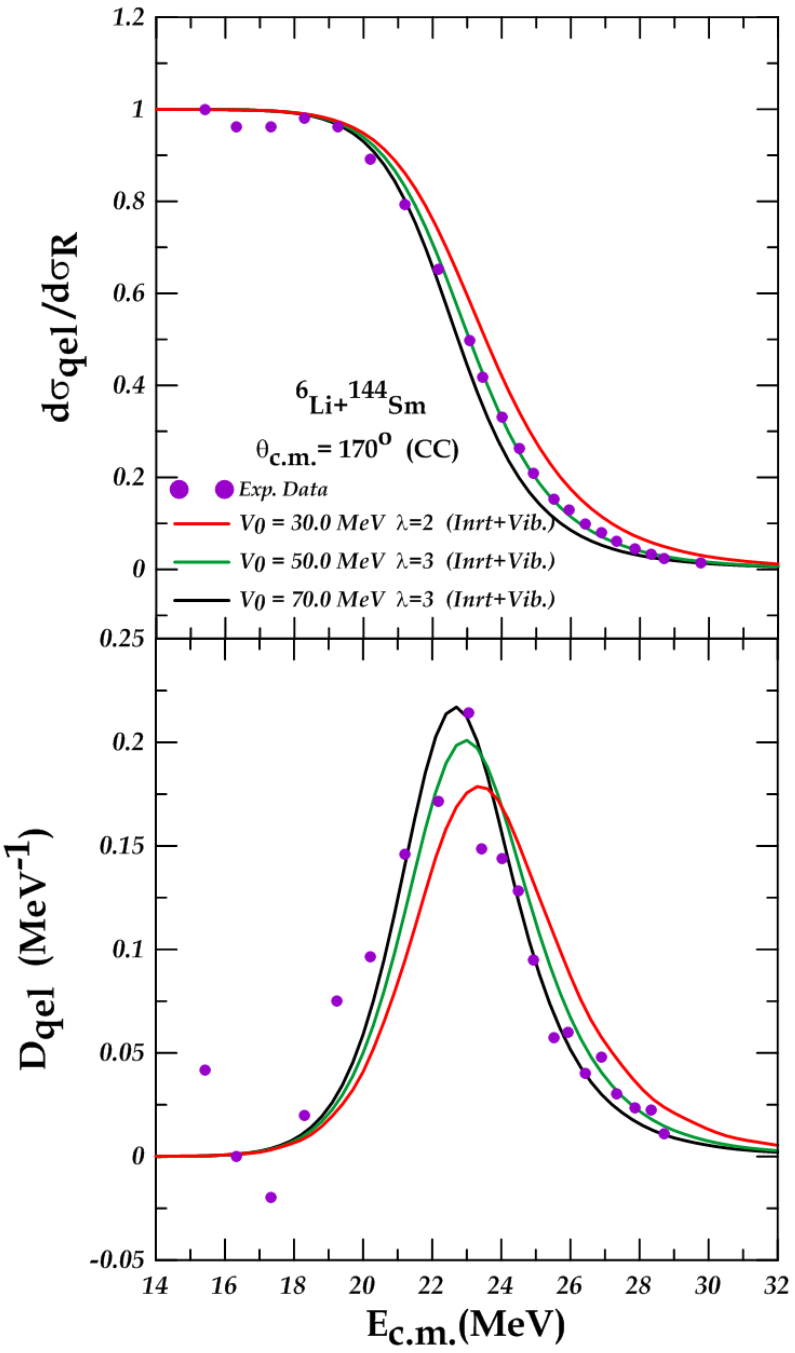

Fig. 4.24. The comparison of the calculated quasi-elastic scattering ratio to the Rutherford cross sections and the distribution at the sub-barrier energies with the corresponding experimental data for the system ^{6}Li+^{144}Sm in the coupled channel (CC) calculations at V_0 = (30.0, 50.0, and 70.0MeV), indicated as red, green, and black, respectively.

4.2.7 ^{28}Si + ^{124}Sn system

In this system, in single-channel calculations (SC), where the projectile and target nuclei are inert, various values of the diffuseness parameter a_0 (0.59, 0.63, and 0.67) fm The diffusion parameter of 0.63 fm was the standard value [9]. In the second instance, at the coupled channel (CC), the projectile nucleus ^{28}Si was rotating with deformation coefficients of β_2 = -0.478 and β_4 = 0.250 [68] to the state 2^+(1.77903 Mev), whereas the target nucleus ^{124}Sn was vibrating with a deformation coefficient of β_2 = 0.095 [68] to the state 2^+(1131.739 Mev). Used the single phonon state of the quadruple excitation for the target nuclei, V_0 = 57.8 MeV, and the radius parameter r_0 is 1.2 fm, which are listed in Table 4.13.

Table (4.13) : The fitted **WS** parameters (radius r_0, depth potential V_0, and the diffuseness parameters a_0), which were obtained from SC and CC calculation, and the values of the χ^2 between experimental and theoretical data for the **^{28}Si+^{124}Sn** system.

System	Channel	V_0 (MeV)	r_0 (fm)	a_0 (fm)	θ_{cm} $(deg.)$	χ^2	
						σ_{qel}/σ_R	D_{qel}
^{28}Si+^{124}Sn	SC	57.8	1.2	0.59	150.5	0.0564366	0.0830102
				0.63		0.1500343	0.0646768
				0.67		0.3891832	0.0531651
	CC	57.8	1.2	0.59	150.5	0.0161496	0.0456320
				0.63		0.0082924	0.0650904
				0.67		0.0054746	0.0123133

For a ^{28}Si+^{124}Sn system, from table 4.13, the best-fitting diffuseness parameter obtained using a single-channel calculation is 0.59 fm, with χ^2 of 0.0564366, V_0 = 45.8 MeV. The best-fit diffuseness parameter is significantly lower than the standard value. The calculated ratio of the quasi-elastic to the Rutherford cross sections is shown by the red line in Fig. 4.25 The best value for the distribution D_{qel} is 0.0531651. It is

represented in Fig. 4.25. at the diffuseness parameter of 0.67 fm. When a coupled-channel calculation is used, the best-fitting diffuseness parameter is 0.67 fm, with χ^2 = 0.0054746 for a rotating projectile (P) and vibrating target (T). The best-fit diffuseness parameter, which is shown by the black line in Fig. 4.26, is higher than the standard value. Furthermore, the resulting χ^2 values show that the best-fitting diffuseness parameter calculated using coupled channels fits the experimental data better than the one calculated using a single channel. The best value of the distribution D_{qel} is 0.0123133 at the same diffuseness parameter value, denoted by the black line in Fig. 4.26. (D_{qel}).

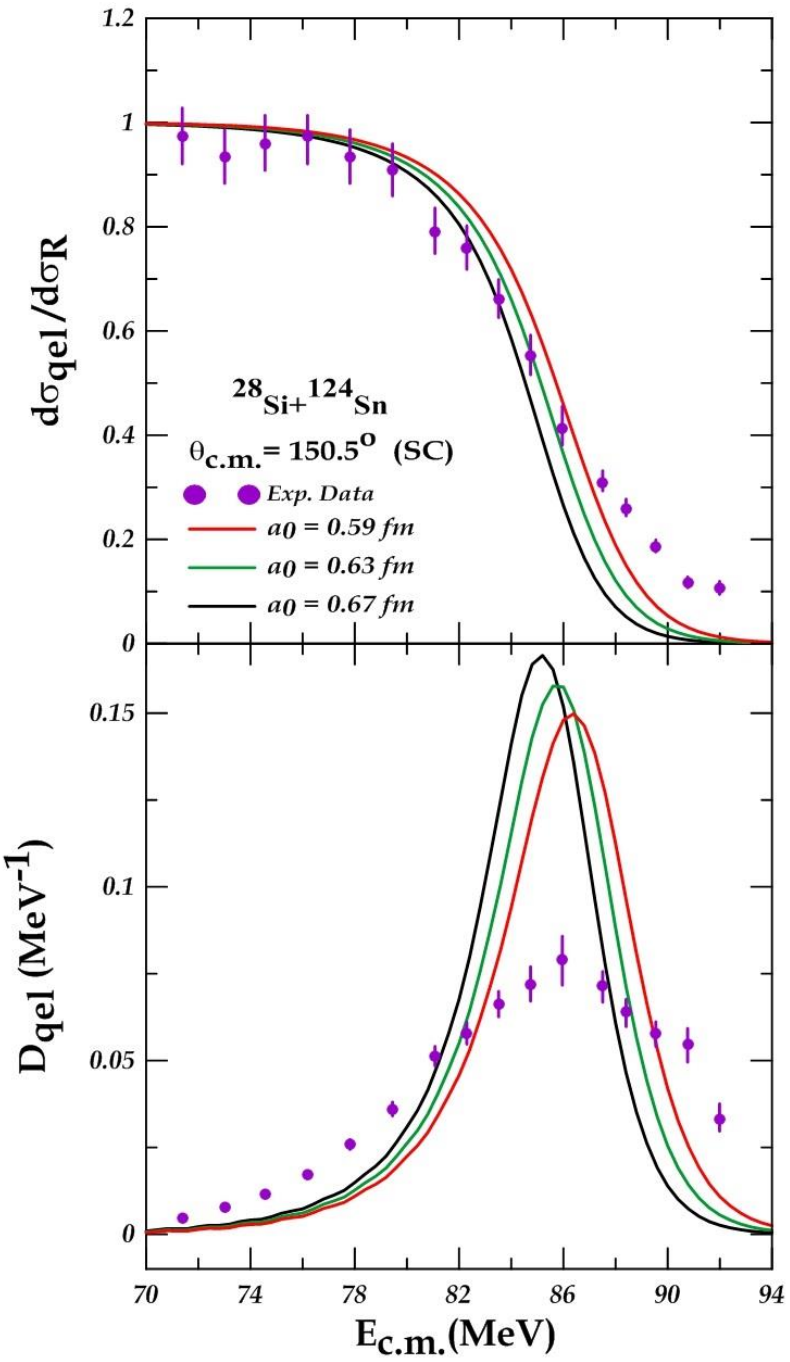

Fig. 4.25. The comparison of the calculated quasi-elastic scattering ratio to the Rutherford cross sections and the distribution at the sub-barrier energies with the corresponding experimental data taken from [12] for the system $^{28}Si+^{124}Sn$ in the single channel (SC) calculations at a_0 = (0.59, 0.63, and 0.67 fm). indicated as red, green , and black, respectively.

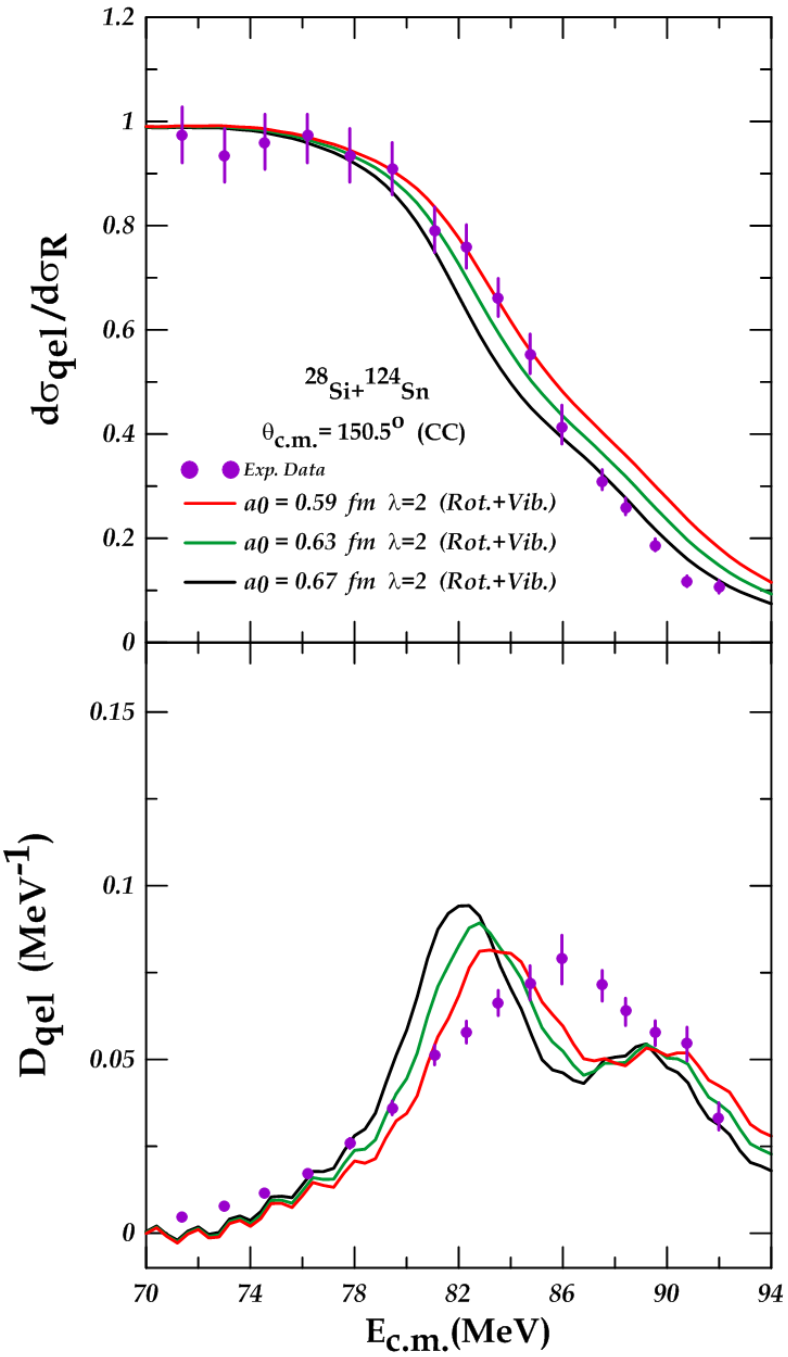

Fig. 4.26. The comparison of the calculated quasi-elastic scattering ratio to the Rutherford cross sections and the distribution at the sub-barrier energies with the corresponding experimental data for the system ^{28}Si+^{124}Sn in the coupled channel (CC) calculations at a_0 = (0.59, 0.63, and 0.67 fm). indicated as red, green , and black, respectively.

The second part of the results ,In the single-channel calculation (SC), at three values of the real nuclear potential (potential depth V_0) (39.8, 57.8, and 75.8) MeV, the diffusion parameter a_0 is 0.67 fm, which was determined by the χ^2 method as the best value for matching the experimental data with the theoretical data. In the coupled channel calculation (CC), the target nucleus ^{124}Sn was vibrating, the projectile nucleus ^{28}Si was rotating, and the radius parameter r_0 was 1.2 fm.

Table (4.14) : The fitted parameters of WS potential (the diffuseness parameters a_0, the depth potential V_0 ,and radius r_0), that is estimated from the SC and CC calculation, and the values of the χ^2 between experimental and theoretical data for the **^{28}Si+^{124}Sn** system.

System	Channel	a_0 (fm)	r_0 (fm)	V_0 (MeV)	θ_{cm} $(deg.)$	χ^2	
						σ_{qel}/σ_R	D_{qel}
^{28}Si+^{124}Sn	SC	0.67	1.2	39.8	150.5	0.0306459	0.0680265
				57.8		0.3891832	0.0531651
				75.8		3.1410810	0.0850578
	CC	0.67	1.2	39.8	150.5	0.0162533	0.0611206
				57.8		0.0056777	0.1233548
				75.8		0.0190049	0.0203015

From table 4.14, the best-fit potential depth V_0 is 39.8 MeV of the ^{28}Si+^{124}Sn system acquired through a single-channel SC data analysis with a_0 = 0.67 fm. The chi squared χ^2 value is 0.0306459. It represents the calculated ratio of the quasi-elastic scattering to the Rutherford cross sections. It was shown by the red line in Fig. 4.27. At the potential depth V_0 = 39.8 MeV, the best value for barrier distribution D_{qel} is 0.0531651, as expressed by the green line in Fig. 4.27. In a coupled-channels procedure, the best potential depth is 57.8 MeV. The obtained χ^2 value is

0.0056777, as shown by the green line in Fig. 4.28. It represents the calculated ratio of the quasi-elastic to the Rutherford cross sections from chi-square calculations. The best value of the barrier distribution D_{qel} is 0.0203015 at the depth potential V_0 of 75.8, as represented by the black line in Fig. 4.28.can see the best-fit potential depth obtained through coupling channels.

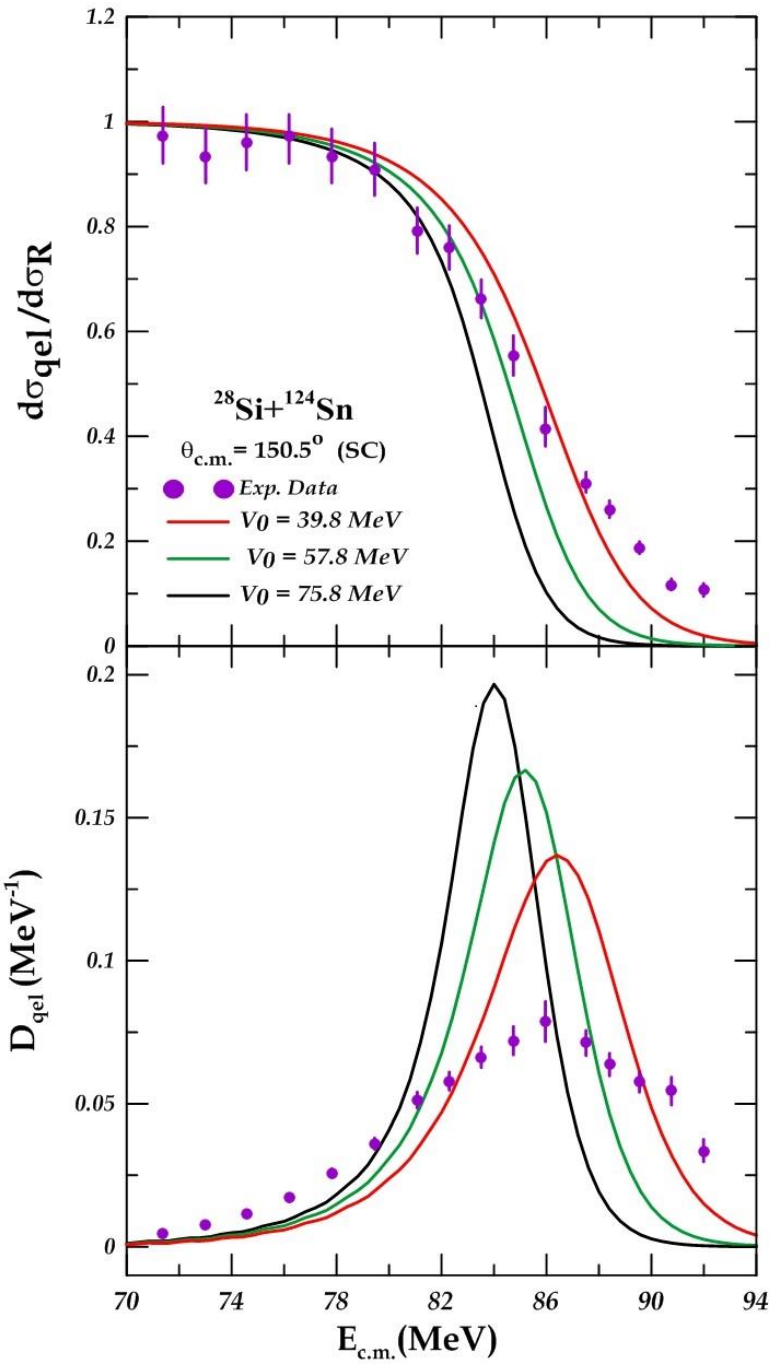

Fig 4.27. The comparison of the calculated quasi-elastic scattering ratio to the Rutherford cross sections and the distribution at the sub-barrier energies with the corresponding experimental data for the system $^{28}Si+^{124}Sn$ in the single channel (SC) calculations at V_0 = (39.8, 57.8, and 75.8 MeV), indicated as red, green, and black, respectively.

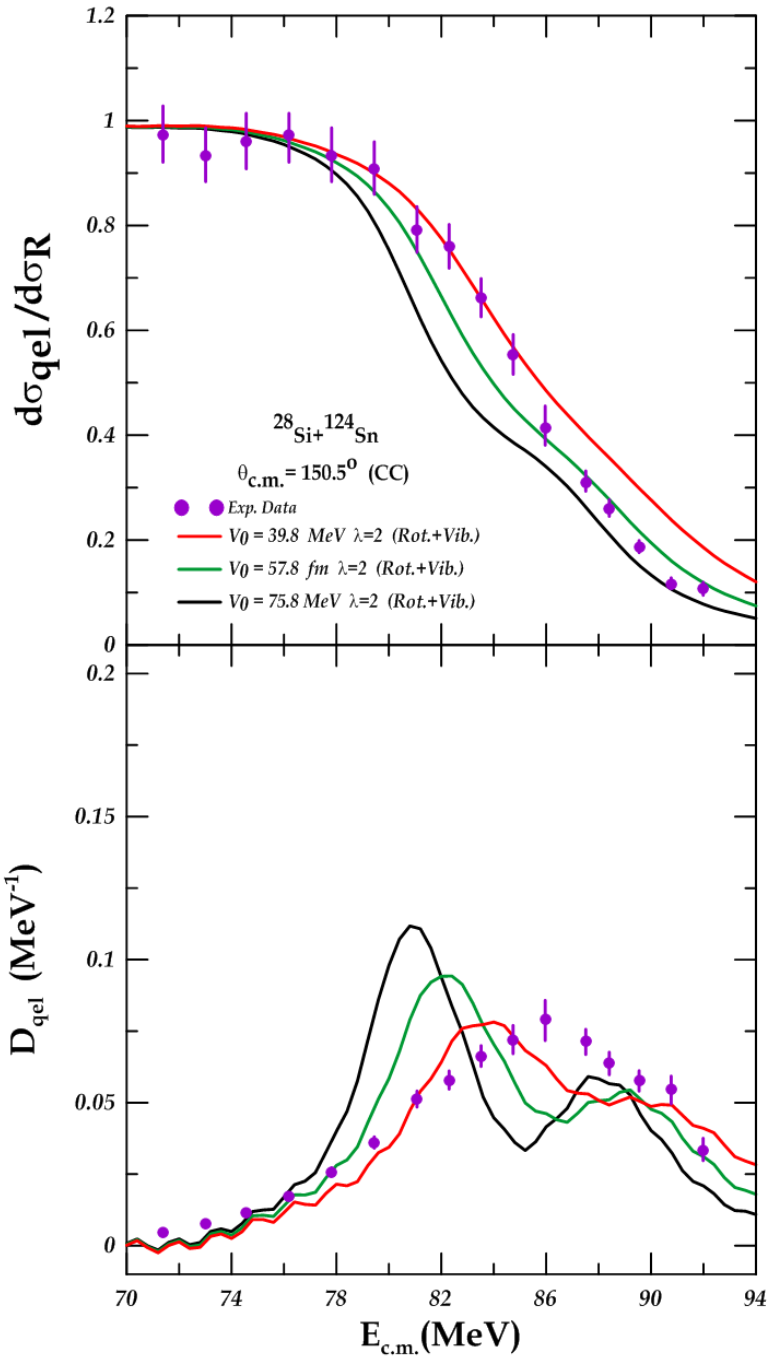

Fig 4.28. The comparison of the calculated quasi-elastic scattering ratio to the Rutherford cross sections and the distribution at the sub-barrier energies with the corresponding experimental data for the system $^{28}Si+^{124}Sn$ in the coupled channel (CC) calculations at V_0 = (39.8, 57.8, and 75.8 MeV), indicated as red, green, and black, respectively.

4.2.8 ^{6}Li +^{159}Tb system

The first case in this system in which the projectile and target nuclei were both to be inert (SC) at three different values of the diffuseness parameter a_0=(0.49, 0.56, and 0.63 fm). In the second case, from the coupled-channel (CC) calculations, the projectile nucleus was a ^{6}Li nucleus that does not have a deformation coefficient, so it is considered an inert nucleus. While the target nucleus ^{159}Tb was rotating, this was deduced according to the ratio $E^{+7/2}/E^{+5/2}$ = 2.37 with a deformation coefficient β_2 = 0.271and β_4= 0.062 [68] to the state $E^{+5/2}$ = (0.0579964 MeV). the radius parameter r_0 = 1.2 fm, and V_0 = 150 MeV.

Table (4.15) : The fitted WS parameters (radius r_0, depth potential V_0, and the diffuseness parameters a_0), which were obtained from SC and CC calculation, and the values of the χ^2 between experimental and theoretical data for the **^{6}Li+^{159}Tb** system.

System	Channel	V_0 (MeV)	r_0 (fm)	a_0 (fm)	θ_{cm} $(deg.)$	χ^2	
						σ_{qel}/σ_R	D_{qel}
^{6}Li+^{159}Tb	SC	150	1.2	0.49	170	0.0041861	0.0059974
				0.56		0.0071479	0.0067585
				0.63		0.0731850	0.0313004
	CC	150	1.2	0.49	170	0.0237944	0.1220439
				0.56		0.0045601	0.0029612
				0.63		0.0254165	0.0183521

Table (4.15) illustrates the results of a single channel calculations analysis. The χ^2 is **0.0041861**. It represents the calculated ratio of the quasi-elastic scattering to the Rutherford cross sections at the diffuseness parameter a_0 of 0.49 fm, as shown by the red line in Fig. 4.29. It is the curve closest to the curve of the experimental data. The best value of the distribution D_{qel} is 0.0059974 at the same value of the diffuseness parameter, as shown by the red line in Fig. 4.29. In the coupled-channel

calculations with the inert projectile (P) and a rotating target (T), the best fit of χ^2 is 0.0045601 at the diffuseness parameter a_0 = 0.56 fm, which is represented by the green line in Fig. 4.30, where V_0 = 150 MeV. The best value of the distribution D_{qel} is **0.0029612** at the same value of the diffuseness parameter, represented by the black curve in Fig. 4.30. It is closest to the experimental data curve.

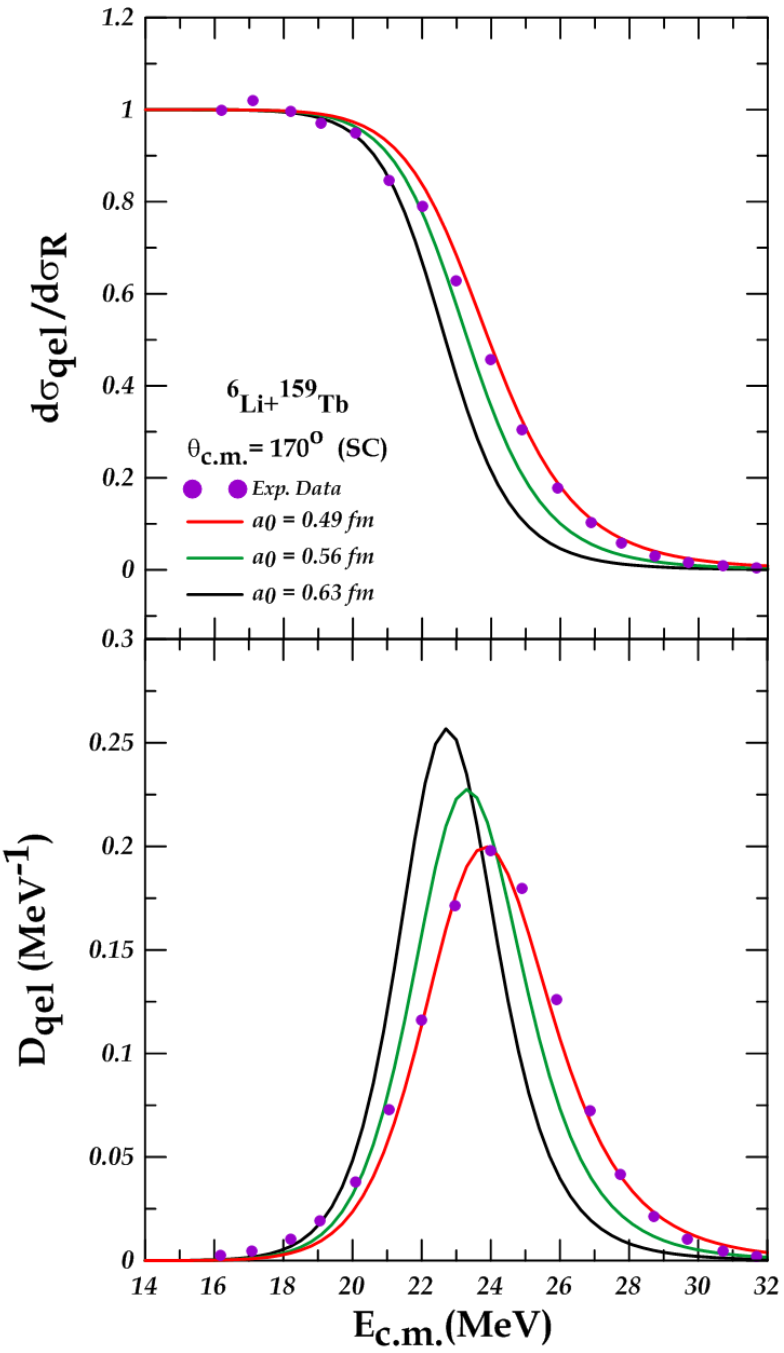

Fig. 4.29. The comparison of the calculated quasi-elastic scattering ratio to the Rutherford cross sections and the distribution at the sub-barrier energies with the corresponding experimental data taken from [72] for the system ^{6}Li+^{159}Tb in the single channel (SC) calculations at a_0 = (0.49, 0.56, and 0.63 fm). indicated as red, green , and black, respectively.

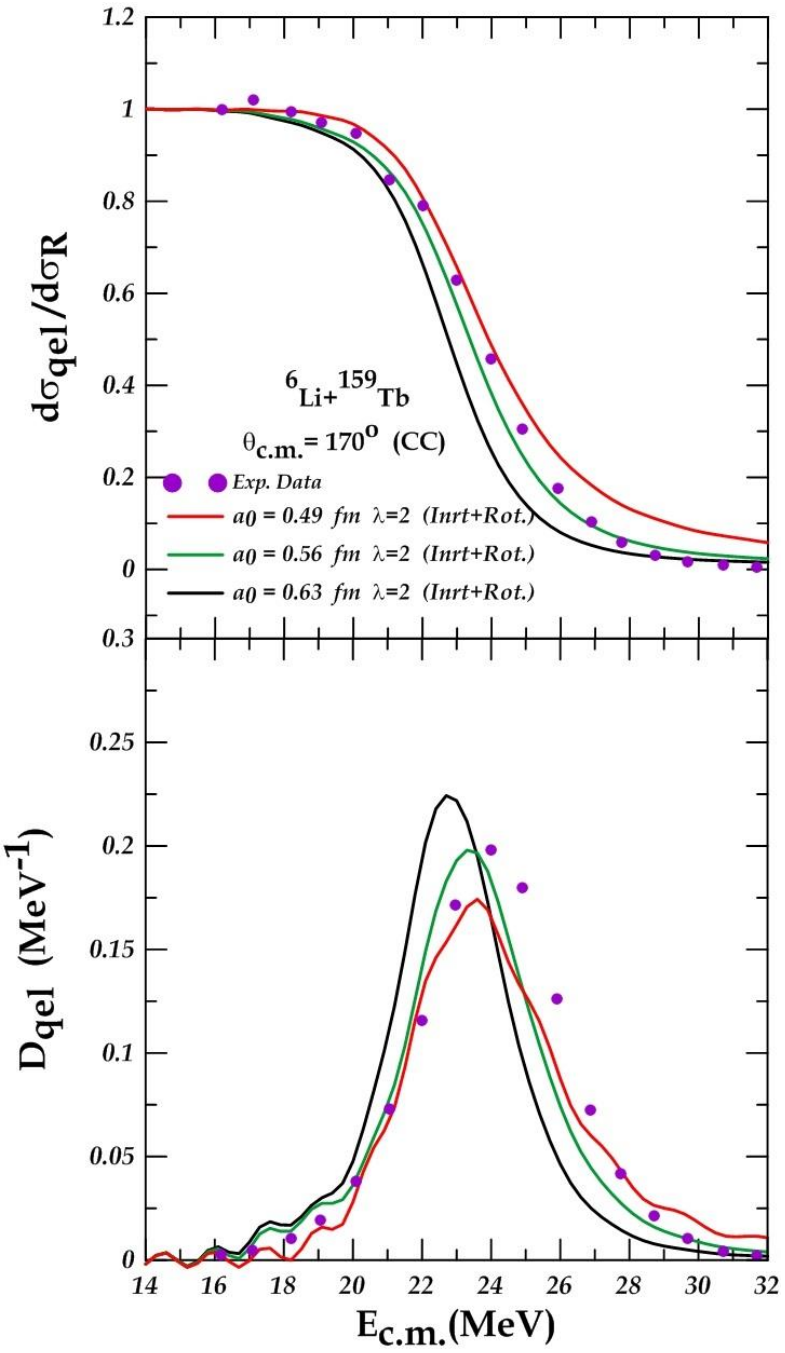

Fig. 4.30. The comparison of the calculated quasi-elastic scattering ratio to the Rutherford cross sections and the distribution at the sub-barrier energies with the corresponding experimental data for the system ^{6}Li+^{159}Tb in the coupled channel (CC) calculations at a_0 = (0.49, 0.56, and 0.63 fm). indicated as red, green , and black, respectively.

The results in the second part, in single-channel calculations at three different values of the real nuclear potential (potential depth V_0) (100, 150, and 200 MeV), the diffusion parameter a_0 was 0.56 fm . It was

previously determined by the χ^2 method as the best value for matching the experimental data with the theoretical data. by using the coupled channel calculations, where the projectile nucleus ^{6}Li was inert and the target nucleus ^{159}Tb was rotating, the radius parameter r_0 is 1.2 fm.

Table (4.16) : The fitted parameters of WS potential (the diffuseness parameters a_0, the depth potential V_0 ,and radius r_0), that is estimated from the SC and CC calculation, and the values of the χ^2 between experimental and theoretical data for the **^{6}Li+^{159}Tb** system.

System	Channel	a_0 (fm)	r_0 (fm)	V_0 (MeV)	θ_{cm} $(deg.)$	χ^2	
						σ_{qel}/σ_R	D_{qel}
^{6}Li+^{159}Tb	SC	0.56	1.2	100	170	0.0012967	0.0044234
				150		0.0071479	0.0067585
				200		0.0247474	0.0132033
	CC	0.56	1.2	100	170	0.0039023	0.0013463
				150		0.0045601	0.0029612
				200		0.0069025	0.0058359

From table (4.16) ,the best-fit potential depth V_0 is 100 MeV obtained from a single-channel (SC) analysis, with a_0 = 0.56 fm. The chi squared χ^2 is 0.0012967. It represents the calculated ratio of the quasi-elastic scattering to the Rutherford cross sections. As shown by the red line in Fig. 4.31. the best value for barrier distribution D_{qel} is 0.0044234 at the same value of the potential depth . It was shown by the red line in Fig. 4.31.In a coupled-channels (CC)calculation, the best potential depth is 100 MeV. The obtained χ^2 value is 0.0039023, as shown by the red line in Fig. 4.32. It is the curve nearest to the curve of the experimental data. the best value of the barrier distribution D_{qel} is 0.0013463 at the same value of potential depth, represented by the red curve. Fig. 4.32.

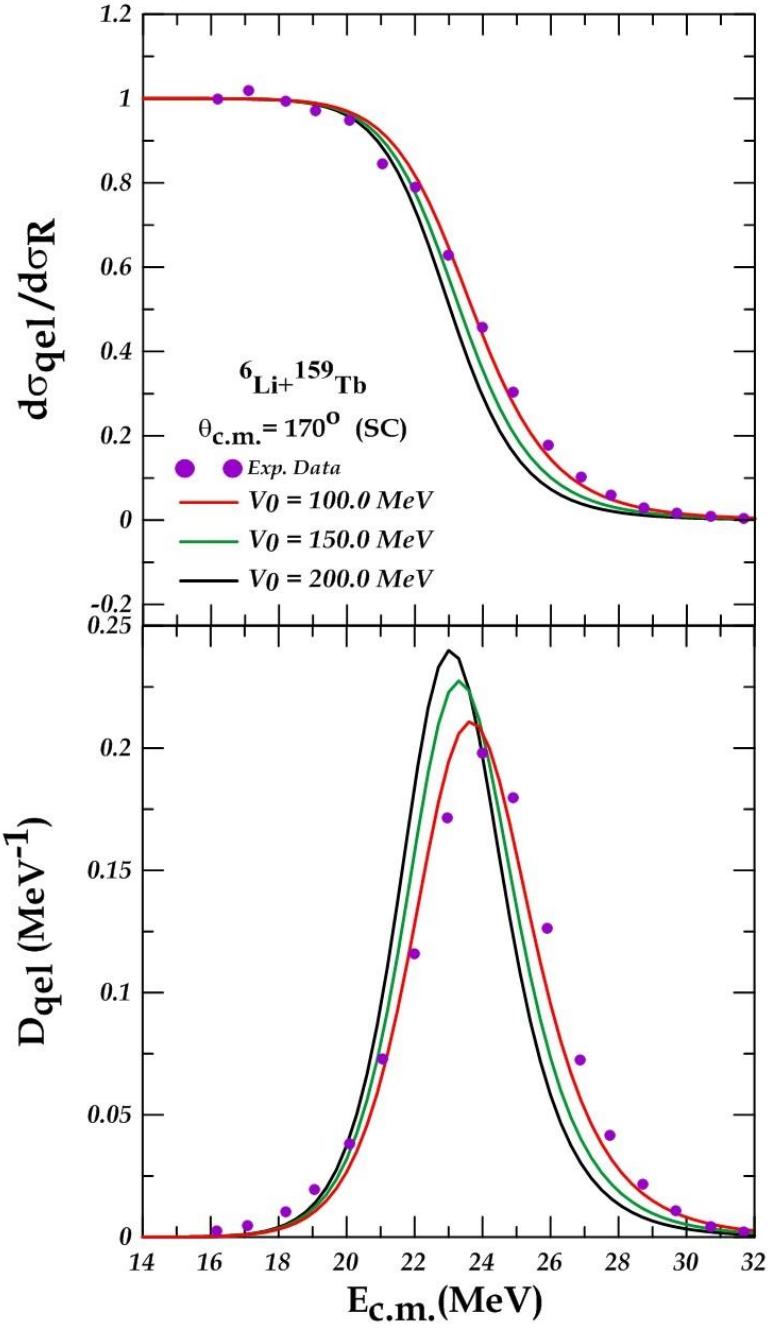

Fig 4.31. The comparison of the calculated quasi-elastic scattering ratio to the Rutherford cross sections and the distribution at the sub-barrier energies with the corresponding experimental data for the system ^{6}Li+^{159}Tb in the single channel (SC) calculations at V_0 = (100, 150, and 200MeV), indicated as red, green, and black, respectively.

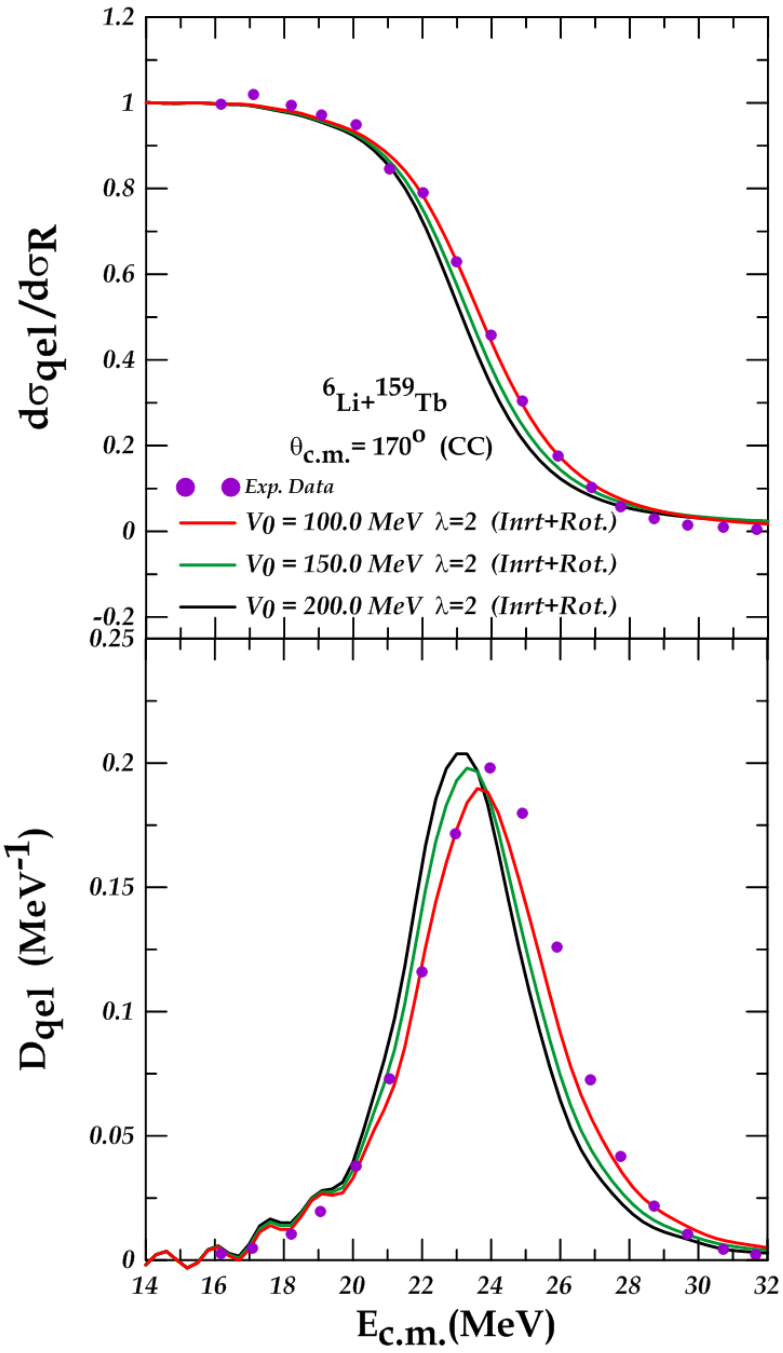

Fig 4.32. The comparison of the calculated quasi-elastic scattering ratio to the Rutherford cross sections and the distribution at the sub-barrier energies with the corresponding experimental data for the system ^{6}Li+^{159}Tb in the coupled channel (CC) calculations at V_0 = (100, 150, and 200MeV), indicated as red, green, and black, respectively.

4.2.9 ^{22}Ne+^{248}Cm system

The single channel (SC) calculations at three different values of the diffuseness parameter a_0 (0.37, 0.41, and 0.45) fm. We have not taken the diffuseness parameter a_0 = 0.63 fm as a standard value, where a much lower value was taken from it . In the second case, at coupled-channel (CC) calculations, the projectile nucleus was^{22}Ne rotates, this was deduced according to the ratio $E_{4^+}/E_{2^+} = 2.6$ with a deformation coefficients of $\beta_2 = 0.326, \beta_4 = 0.225$ [68] to the state 2^+(1.274537 MeV) ,and the target nucleus ^{248}Cm was rotating with a deformation coefficients of $\beta_2 = 0.235$, $\beta_4 = 0.040$ [68] to the state 2^+(0.043403 MeV),where $E_{4^+}/E_{2^+} = 3.3$. the radius parameter r_0 is 1.2 fm and V_0 = 250 MeV.

Table (4.17): The fitted WS parameters (radius r_0, depth potential V_0, and the diffuseness parameters a_0), which were obtained from SC and CC calculation, and the values of the χ^2 between experimental and theoretical data for the **^{22}Ne+^{248}Cm** system.

System	Channel	V_0 (MeV)	r_0 (fm)	a_0 (fm)	θ_{cm} $(deg.)$	χ^2	
						σ_{qel}/σ_R	D_{qel}
^{22}Ne+^{248}Cm	SC	250	1.2	0.37	170	0.2017372	0.1126973
				0.41		1.1328630	0.1077053
				0.45		6.1290560	0.3180656
	CC	250	1.2	0.37	170	0.0145340	0.0269347
				0.41		0.0801992	0.0189638
				0.45		0.3336833	0.0256196

From table (4.17), by using a single-channel(SC)calculation, The best-fitting diffuseness parameter obtained is 0.37 fm, with χ^2 being 0.2017372. It represents the calculated ratio of the quasi-elastic scattering

to the Rutherford cross sections, as shown by the red line in Fig. 4.33. The best-fit diffuseness parameter is significantly lower than the standard value of 0.63fm . The best value for the distribution D_{qel} is 0.1077053. It is represented by the green line in Fig. 4.33. at the diffuseness parameter a_0 of 0.41 fm, ,V_0 is 250 MeV. When a coupled-channel calculation is used, the best-fitting diffuseness parameter a_0 is 0.37 fm, with χ^2 = 0.0145340, where the projectile P and the target T were rotating . which is shown by the red line in Fig. 4.34. The best value of the distribution D_{qel} is 0.0123133 at diffuseness parameter a_0 =0.41, denoted by the green line in Fig. 4.34.

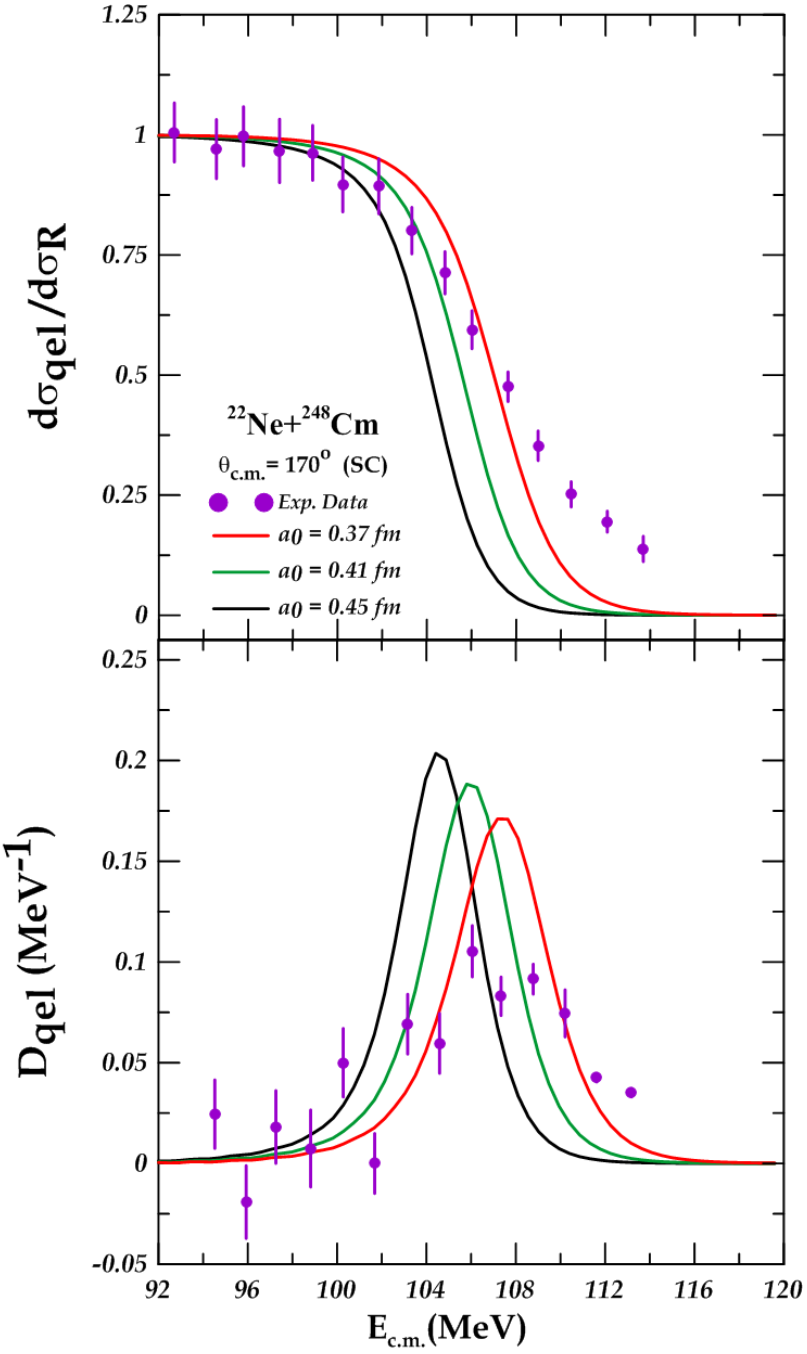

Fig. 4.33. The comparison of the calculated quasi-elastic scattering ratio to the Rutherford cross sections and the distribution at the sub-barrier energies with the corresponding experimental data taken from [73] for the system $^{22}Ne+^{248}Cm$ in the single channel (SC) calculations at a_0 = (0.37, 0.41, and 0.45 fm). indicated as red, green , and black, respectively.

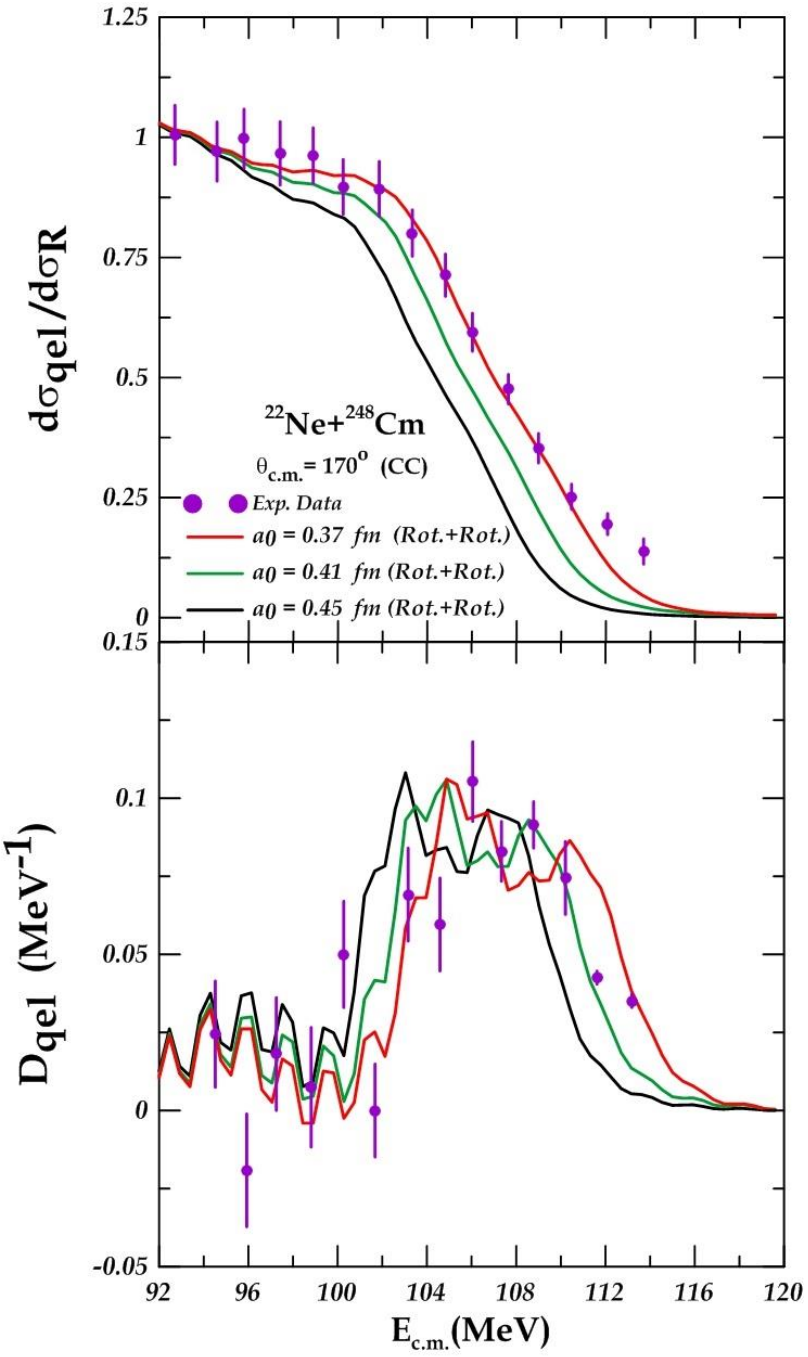

Fig. 4.34. The comparison of the calculated quasi-elastic scattering ratio to the Rutherford cross sections and the distribution at the sub-barrier energies with the corresponding experimental data for the system ^{22}Ne+^{248}Cm in the coupled channel (SC) calculations at a_0 = (0.37, 0.41, and 0.45 fm). indicated as red, green , and black, respectively.

The results in the second part, In the single-channel (SC) calculations at three values of the real nuclear potential (potential depth V_0) (180, 250,

and 320 MeV), the diffuseness parameter a_0 was considered to be 0.37 fm. In the coupled channel (CC) calculations, the projectile nucleus ^{22}Ne and the target nucleus ^{248}Cm were rotating. At the same values of potential depth V_0, the radius parameter r_0 =1.2 fm.

Table (4.18): The fitted parameters of WS potential (the diffuseness parameters a_0, the depth potential V_0 ,and radius r_0), that is estimated from the SC and CC calculation, and the values of the χ^2 between experimental and theoretical data for the **^{22}Ne+^{248}Cm** system.

System	Channel	a_0 (fm)	r_0 (fm)	V_0 (MeV)	θ_{cm} $(deg.)$	χ^2	
						σ_{qel}/σ_R	D_{qel}
^{22}Ne+^{248}Cm	SC	0.37	1.2	180	170	0.0708295	0.1370306
				250		0.2017372	0.1126973
				320		0.4320837	0.1045710
	CC	0.37	1.2	180	170	0.0064500	0.0668203
				250		0.0145340	0.0269347
				320		0.0232961	0.0338822

From table (4.18) that the best-fit potential depth V_0 is 180 MeV acquired through a single-channel analysis at the diffuseness parameter a_0 is 0.37 fm. The chi square χ^2 is 0.0708295, This is the curve that is closest to the experimental data curve, as shown by the red line in Fig. 4.35. The best value for barrier distribution D_{qel} is 0.1045710 at potential depth V_0 = 320 MeV. It was shown by the black line in Fig. 4.35. In a coupled-channel (CC) calculations, the best potential depth is 180 MeV, with the target (T) and projectile (P) rotating. The obtained χ^2 value is 0.0064500, shown by the red line in Fig.4.36.The best value of the barrier distribution D_{qel} is 0.0269347 at the depth potential V_0= 250 MeV represented by the green curve Fig.4.36.

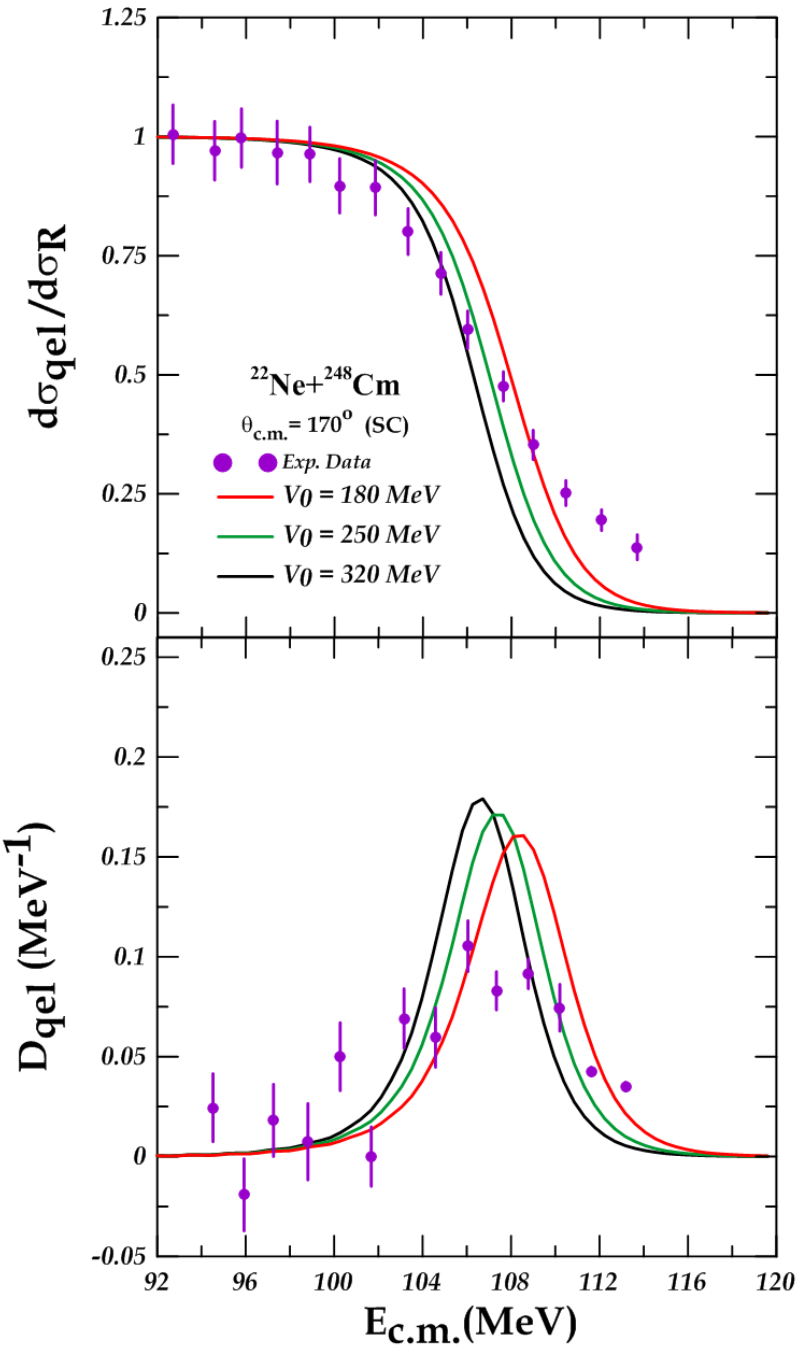

Fig 4.35. The comparison of the calculated quasi-elastic scattering ratio to the Rutherford cross sections and the distribution at the sub-barrier energies with the corresponding experimental data for the system $^{22}Ne+^{248}Cm$ in the single channel (SC) calculations at V_0 = (180, 250, and 320 MeV), indicated as red, green, and black, respectively.

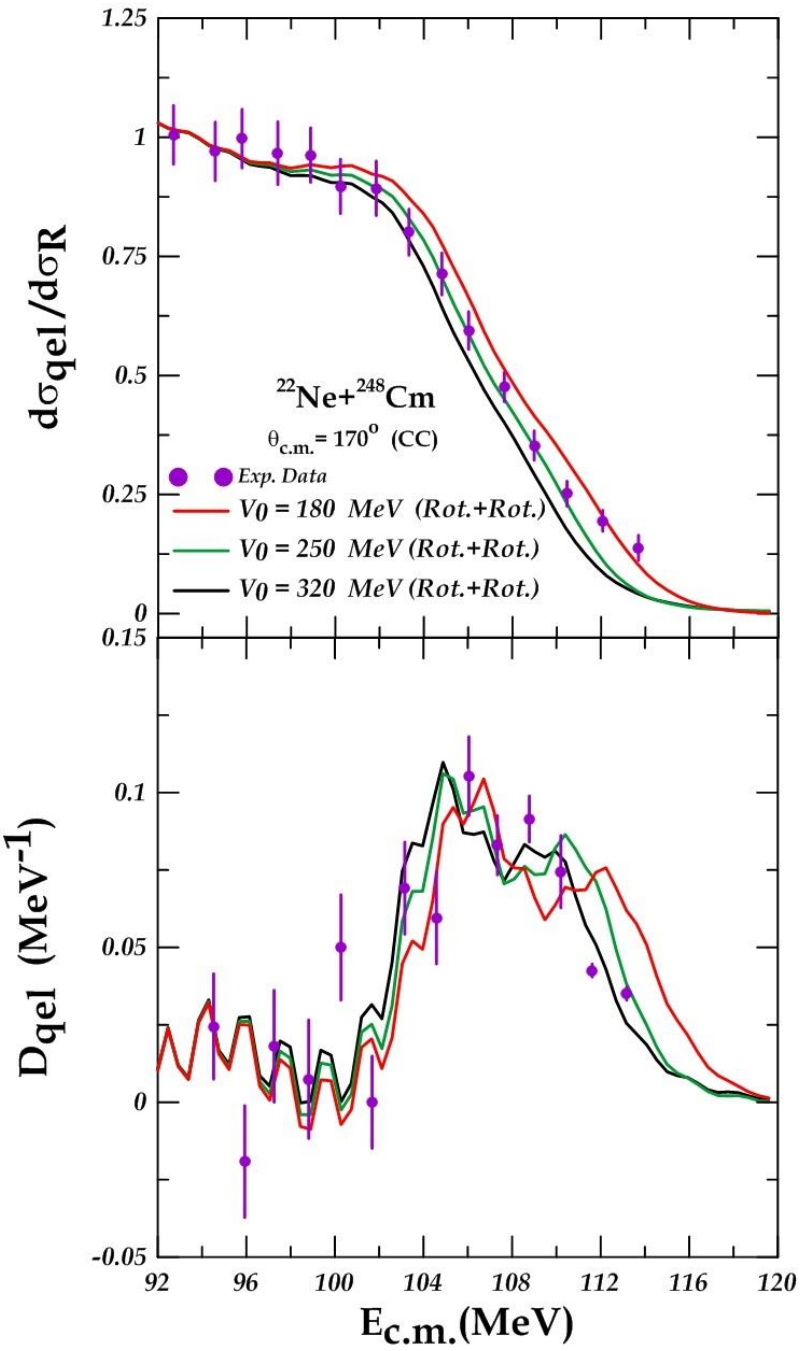

Fig 4.36. The comparison of the calculated quasi-elastic scattering ratio to the Rutherford cross sections and the distribution at the sub-barrier energies with the corresponding experimental data for the system $^{22}Ne+^{248}Cm$ in the coupled channel (CC) calculations at V_0 = (180, 250, and 320 MeV), indicated as red, green, and black, respectively.

4.2.10 ^{10}B + ^{232}Th system

In this system were processed in two cases. The single channel (SC) calculations, at three different values of the diffuseness parameter a_0,it is (0.43, 0.63, and 0.83) fm. The diffuseness parameter of 0.63 fm is the standard value [9]. In coupled-channel (CC) calculations, the projectile nucleus was ^{10}B inert to the state 2^+(3.58713 MeV), and the target nucleus ^{232}Th was rotating with deformation coefficients of $\beta_2 = 0.207, \beta_4 = 0.108$[68]to the state 2^+(0.049369MeV), where $E_{4^+}/E_{2^+} = 3.2$ .the radius parameter r_0 = 1.2 fm and V_0 = 15.8 MeV.

Table (4.19): The fitted parameters of WS potential (the diffuseness parameters a_0, the depth potential V_0 ,and radius r_0), that is estimated from the SC and CC calculations, and the values of the χ^2 between experimental and theoretical data for the **^{10}B+^{232}Th** system.

System	Channel	V_0 (MeV)	r_0 (fm)	a_0 (fm)	θ_{cm} $(deg.)$	χ^2	
						σ_{qel}/σ_R	D_{qel}
^{10}B+^{232}Th	SC	15.8	1.2	0.43	161	0.0060353	0.0075599
				0.63		0.0178566	0.0056552
				0.83		0.0636182	0.0056455
	CC	15.8	1.2	0.43	161	0.0057186	0.0077472
				0.63		0.0157265	0.0083779
				0.83		0.0681547	0.0023579

In the first case, from table (4.19),by using a single-channel (SC)calculations , The best-fitting diffuseness parameter obtained 0.43 fm, with χ^2 being 0.0060353. It represents the calculated ratio of the quasi-elastic scattering to the Rutherford cross section as a function of energy, as shown by the red line in Fig. 4.37.The best-fit diffuseness parameter is lower than the standard value of 0.63fm . V_0 is 15.8 MeV.

The best value for the distribution D_{qel} is 0.0056455. It is represented by the blue line in Fig. 4.37. at the diffuseness parameter a_0 of 0.83 fm. When a coupled-channel calculations is used, the best-fitting diffuseness parameter a_0 is 0.43 fm, with χ^2 = 0.0057186, where the projectile ^{10}B inert and the target ^{232}Th was rotating. which is shown by the red line in Fig. 4.38.Furthermore, the resulting χ^2 values show that the best-fitting diffuseness parameter calculated using coupled channels fits the experimental data better than the one calculated using a single channel. The best value of the distribution D_{qel} is 0.0023579 at the diffuseness parameter a_0= 0.83, denoted by the blue line in Fig. 4.38.

.

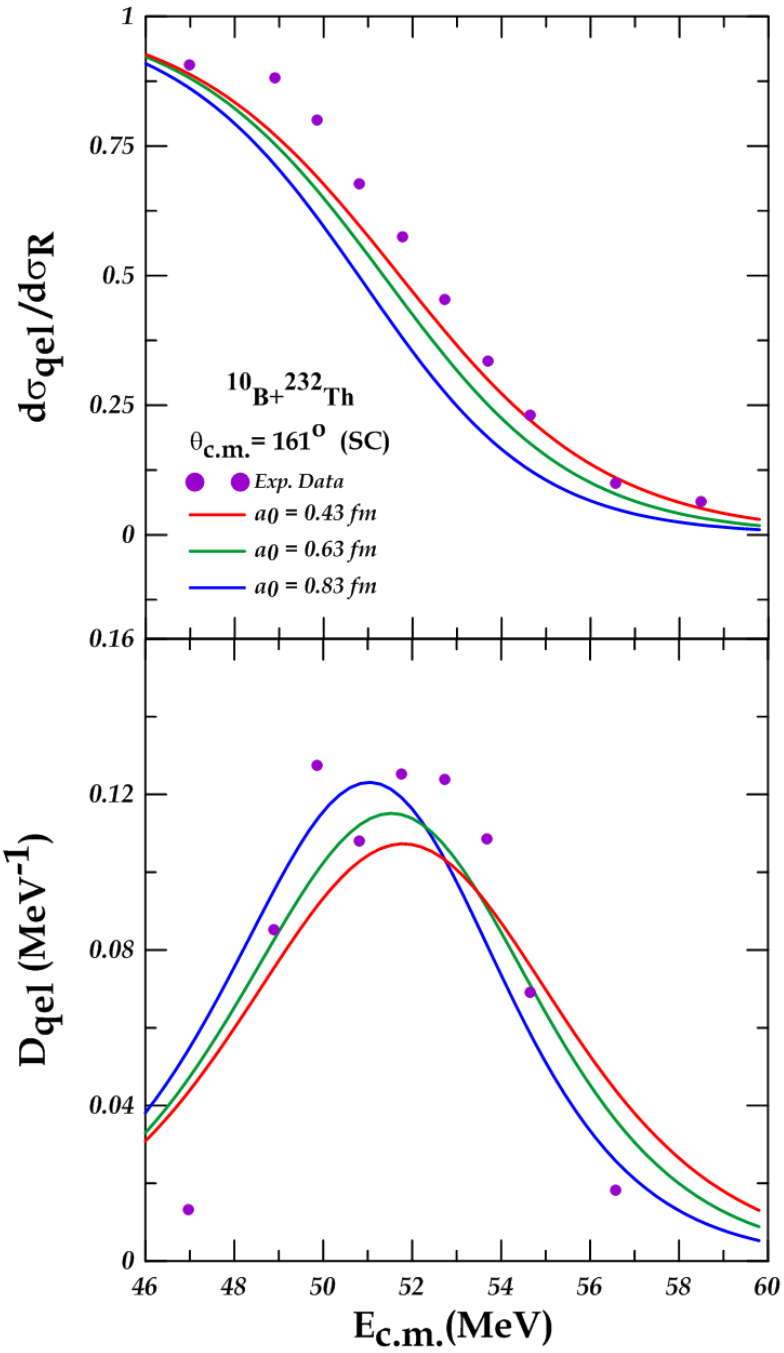

Fig. 4.37 The comparison of the calculated quasi-elastic scattering ratio to the Rutherford cross section and the distribution at the sub-barrier energies with the corresponding experimental data taken from [74] for the system $^{10}B+^{232}Th$ in the single channel (SC) calculations at a_0 = (0.43, 0.63, and 0.83 fm). indicated as red, green , and blue, respectively.

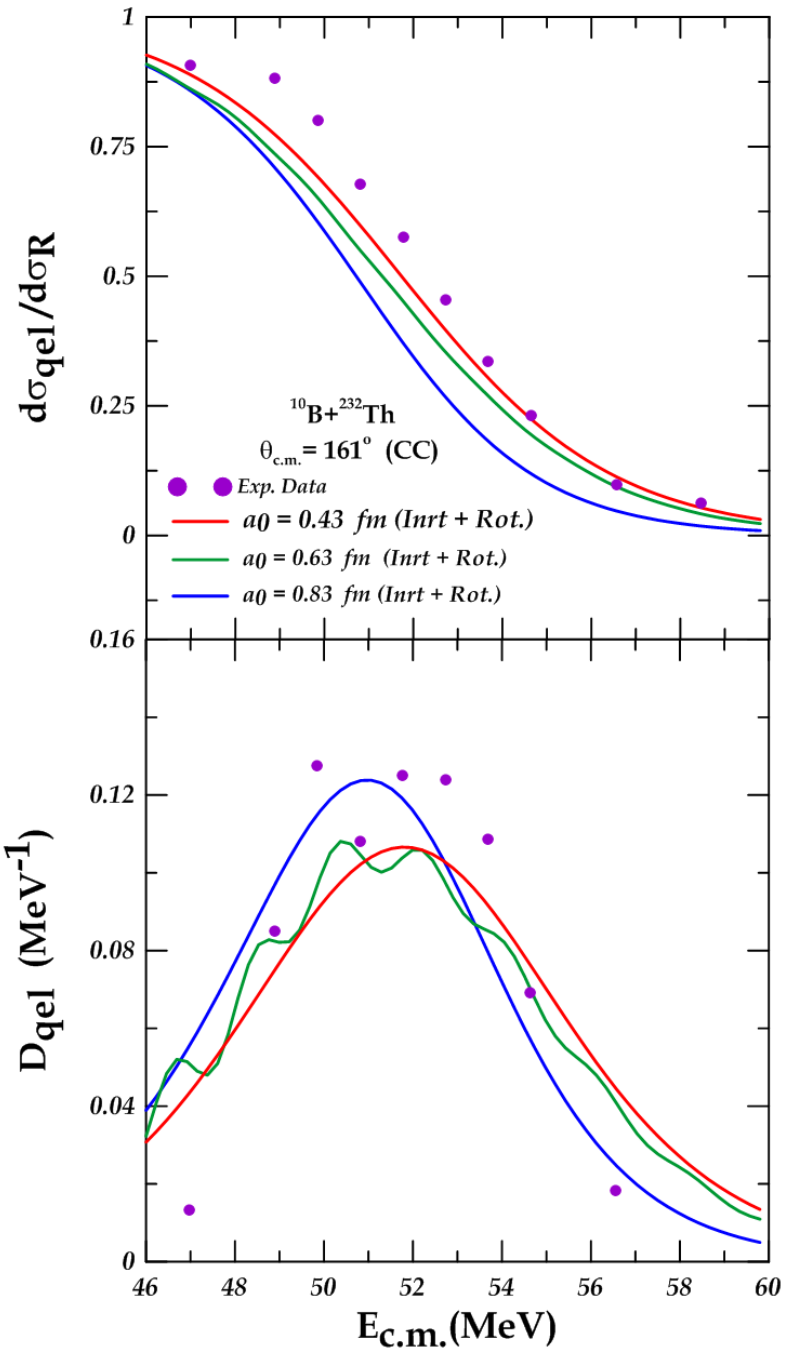

Fig. 4.38 Shows the comparison of the calculated quasi-elastic scattering ratio to the Rutherford cross section and the distribution at the sub-barrier energies with the corresponding experimental data for the system $^{10}B+^{232}Th$ in the coupled channel (CC) calculations at a_0 = (0.43, 0.63, and 0.83 fm). indicated as red, green , and blue, respectively.

In The second case , from single-channel (SC) calculations at three values of the real nuclear potential (potential depth V_0) (8.8, 15.8, and 22.8 MeV), considered the diffusion parameter a_0 to be 0.83 fm. It was previously determined by the χ^2 method as the best value for matching the experimental data with the theoretical calculations, in the coupled channel (CC) calculations, the projectile nucleus ^{10}B was inert, and the target nucleus ^{232}Th was rotating. the radius parameter r_0 is 1.2 fm.

Table (4.20): The fitted parameters of WS potential (the diffuseness parameters a_0, the depth potential V_0 ,and radius r_0), that is estimated from the SC and CC calculations, and the values of the χ^2 between experimental and theoretical data for the **$^{10}B+^{232}Th$** system.

System	Channel	a_0 (fm)	r_0 (fm)	V_0 (MeV)	θ_{cm} $(deg.)$	χ^2	
						σ_{qel}/σ_R	D_{qel}
$^{10}B+^{232}Th$	SC	0.83	1.2	8.8	161	0.0233270	0.0058398
				15.8		0.0060353	0.0075599
				22.8		0.0206442	0.0092680
	CC	0.83	1.2	8.8	161	0.0206442	0.0085781
				15.8		0.0057186	0.0077472
				22.8		0.1253349	0.0042818

From table (4.22) , the best-fit potential depth V_0 is 15.8 MeV obtained from a single-channel analysis calculations, with a_0 = 0.83 fm. The chi squared χ^2 is 0.0060353. It represents the calculated ratio of the quasi-elastic scattering to the Rutherford cross section as function of energy . As shown by the green line in Fig. 4.39. The best value for barrier distribution D_{qel} is 0.0058398,at the V_0= 8.8MeV. It was shown by the red line in Fig. 4.39. In a coupled-channels calculations, the best potential depth is 15.8 MeV. The obtained χ^2 value is 0.0057186, as shown by the

green line in Fig.4.40.It is the curve nearest to the curve of the experimental data. the best value of the barrier distribution D_{qel} is 0.0042818 at the depth potential V_0 = 22.8MeV, represented by the blue curve. Fig. 4.40. the best-fit potential depth obtained through a coupled channel.

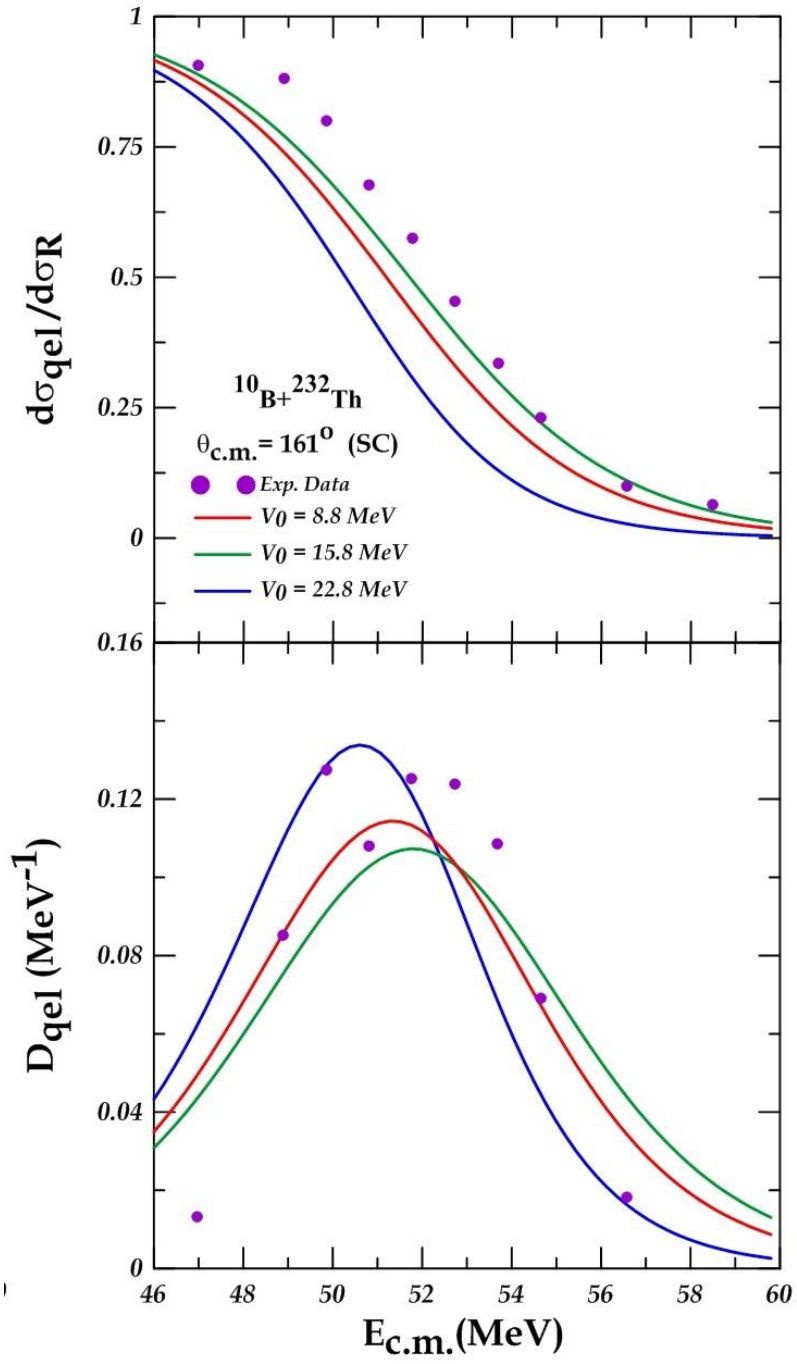

Fig 4.39. Shows the comparison of the calculated quasi-elastic scattering ratio to the Rutherford cross section and the distribution at the sub-barrier energies depending on the angle(θ) with the corresponding experimental data for the system $^{10}B+^{232}Th$. in a single channel (SC) calculations at V_0 = (8.8, 15.8, and 22.8 MeV), indicated as red, green, and blue, respectively.

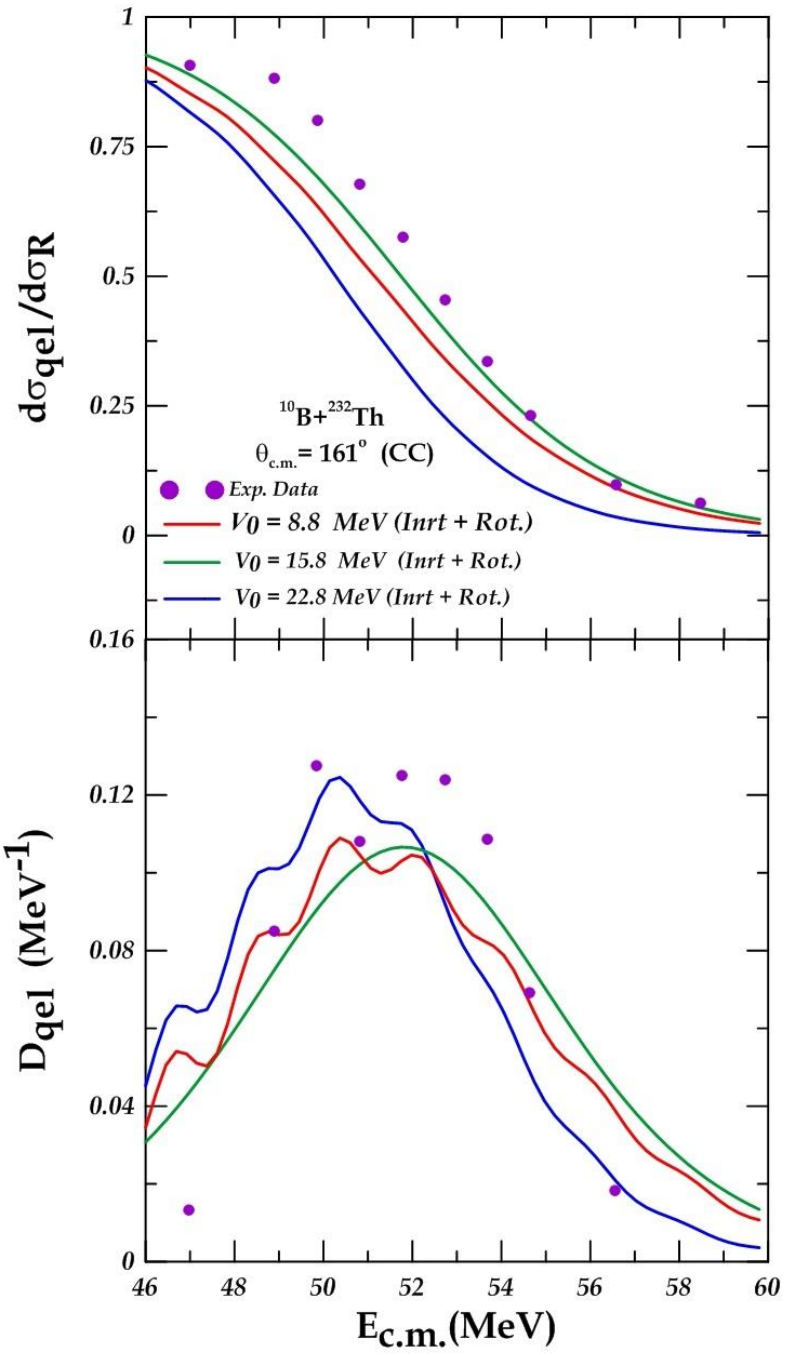

Fig 4.40. Shows the comparison of the calculated quasi-elastic scattering ratio to the Rutherford cross section and the distribution at the sub-barrier energies as a function of energy with the corresponding experimental data for the system $^{10}B+^{232}Th$. in coupled channel (SC) calculations at V_0 = (8.8, 15.8, and 22.8 MeV), indicated as red, green, and blue, respectively.

Chapter 5
Conclusions and Future work

Chapter 5

Conclusions and Future work

5.1 Conclusions

1. The diffuseness parameter a_0 for most systems fully consistent with the standard value (0.63) fm in the coupled channel calculations.

2. In the calculations of single channel (SC) The theoretical calculations for some systems coincide with the practical values at the value less of the standard value for diffusivity parameter a_0 = (0.63) fm, while in coupled channel (CC) calculations, the match occurred at a_0 = 0.63.

3. In these systems (^{22}Ne+^{248}Cm, ^{10}B+^{232}Th), the diffuseness parameter a_0 of 0.63 was not taken as a standard value. Where a much lower diffusion parameter a_0 was taken from it because the nucleus of the projectile was a stable nucleus, the diffuseness parameter has a low value, and the target nucleus is a heavy nucleus. Its diffuseness parameter is low, so the result of the reaction is a low diffusion parameter, less than the standard value.
4. In this study, we found that the effect of coupling is very important to be included in the calculations because the coupling in more systems studied made the theoretical calculations closer to the experimental data compared to the single channel calculations.
5. Through potential barrier calculations represented by distribution curves in the cases of single and coupled channels. We note the potential barrier distribution curve shifting to the right due to the value of the potential depth decreasing; this leads to a decrease in the value of the nuclear potential, and thus the height of the potential barrier will increase and the quasi-elastic scattering calculations will increase. On

the contrary, if the potential depth increases, the nuclear potential also increases, so the potential barrier will decrease, leading to a decrease in quasi-elastic scattering calculations and a decrease in the height of the potential barrier distribution and its shift to the left.

5.2 Suggestions for future work

provide the following proposals since it is well recognized that further research is necessary to pinpoint many of the features that significantly affect mathematical calculations:

1. Developing the study of quasi-elastic scattering and calculating the ratio of quasi-elastic to the Rutherford differential cross section $(d\sigma_{qel})/(d\sigma_R)$ and quasi-elastic barrier distribution (D_{qel}) and quasi-elastic scattering probability as functions of the energy center of mass $(E_{c.m.})$ for all nuclei by using the semiclassical treatment.

2. Comparison Procedure between the diffuseness parameters that have been obtained from large-angle quasi-elastic scattering and fusion cross sections.

3. study the surface diffuseness parameters with quasi-elastic scattering for another inter-nucleus potential such as realistic interaction (M3Y).

4. This work can be repeated but instead of using CCFULL one can use more realistic coupled channel (CC) calculations by employing the computer code XFRESCO , which is the graphical interface for FRESCO code written by Thompson which needs Linux operating system to run it. FRESCO has more advantage over CCFULL to include the realistic coupled-channels calculation with more parameters.

References

References

[1] M. L. I. Ibrahim, M. Zamrun, and H. A. Kassim, “Analysis of the nuclear potential for heavy-ion systems through large-angle quasi-elastic scattering,” Phys. Rev. C, vol. 87, no. 2, p. 24611, 2013.

[2] B. Nigussie, “Complete and incomplete fusion studies in some ^{14}N+ ^{59}Co systems.” M.SC.Thesis,Addis Ababa University, 2012.

[3] R. Stock, “Encyclopedia of applied high energy and particle physics” , vol .40,no.45,2009.

[4] K. E. Rehm, “Quasi-elastic heavy-ion collisions,” Annu. Rev. Nucl. Part. Sci., vol. 41, no. 1, pp. 429–468, 1991.

[5] G. Kaur, B. Behera, P. Sharma, M. Thakur, and R. Mahajan, in Proceedings of the DAE Symp. on Nucl. Phys, p. 530, 2014.

[6] S. S. Ntshangase, "Measurement of the fusion barrier distribution for the ^{86}Kr+ ^{208}Pb reaction." M.SC.Thesis University of Zululand, 2005.

[7] S. Landowne and C. H. Dasso, “On the distribution of angular momentum absorbed by compound nuclei in heavy-ion fusion reactions,” Phys. Lett. B, vol. 138, no. 1–3, pp. 32–34, 1984.

[8] K. Hagino, N. Rowley, and A. T. Kruppa, “A program for coupled-channels calculations with all order couplings for heavy-ion fusion reactions,” ., Phys. Rev., vol 123, no.1,pp.143-1521999.

[9] K. Washiyama, K. Hagino, and M. Dasgupta, “Probing surface diffuseness of nucleus-nucleus potential with quasielastic scattering at deep sub-barrier energies”., vol 73,no.2,pp.034607, 2006.

[10] K. Hagino and N. Rowley, “Large-angle scattering and quasi-elastic barrier distributions,” Phys. Rev ,vol.69,no.5,pp.054610, 2004.

[11] F. A. Majeed, K. S. Jassim, and N. H. Abbas, “Role of Coupled-Channels in Heavy Ions Reactions at the Coulomb Barrier,”,

vol.3,no.2,pp.2319-7064, 2014.

[12] M. Sharma, A. Rani , S. Mandal , S. Nath , N. Madhavan , J. Gehlot , K. Chakraborty , R. Gupta , C.V Ahmad , A. Parihari , R. Biswas , S. Noor , D. Vishwakarma , P. Khandelwal , C.Kumar, P. S. Rawat , P. Sherpa , and S. Kumar., "Quasi-Elastic Scattering Measurements for ^{28}Si+ ^{116,120,124} Sn systems near the Coulomb barrier," in Proceedings of the DAE Symp. on Nucl. Phys, vol. 65, p. 433, 2021.

[13] N. Wang and W. Scheid, "Quasi-elastic scattering and fusion with a modified Woods-Saxon potential," Phys. Rev. C, vol. 78, no. 1, p. 14607, 2008.

[14] K. Hagino, T. Takehi, A. B. Balantekin, and N. Takigawa, "Surface diffuseness anomaly in heavy-ion potentials for large-angle quasielastic scattering," Phys. Rev. C, vol. 71, no.4, p. 44612, 2005.

[15] K. Washiyama, K. Hagino, and M. Dasgupta, "Probing surface diffuseness of nucleus-nucleus potential with quasielastic scattering at deep sub-barrier energies," Phys. Rev. C, vol. 73, no. 3, p. 34607, 2006.

[16] L. R. Gasques,M. Evers, D. J. Hinde, M. Dasgupta, P. R. S. Gomes, R. M. Anjos, M. L. Brown, M. D. Rodríguez, R. G. Thomas, and K. Hagino.,"Systematic study of the nuclear potential through high precision back-angle quasi-elastic scattering measurements," Phys. Rev. C, vol. 76, no. 2, p. 24612, 2007.

[17] M. Zamrun F, K. Hagino, S. Mitsuoka, and H. Ikezoe, "Coupled-channels analyses for large-angle quasi-elastic scattering in massive systems," Phys. Rev. C - Nucl. Phys., vol. 77, no. 3, 2008.

[18] C. J. Lin, H. M. Jia, H. Q. Zhang, F. Yang, X. X. Xu, F. Jia, Z. H. Liu, and K. Hagino., "Systematic study of the surface properties of

the nuclear potential with high precision large-angle quasi-elastic scatterings," Phys. Rev. C, vol. 79, no. 6, p. 64603, 2009.

[19] C. J. Lin, H. M. Jia, H. Q. Zhang, F. Yang, X. X. Xu, Z. H. Liu, and S. T. Zhang., "Nuclear reactions studied by quasi-elastic measurements with high precision at backward angles,".,vol. 17,no.6, 2011.

[20] K. S. Jassim, F. A. Mageed, G. S. Jassim, "Diffuseness parameters of Woods–Saxon potential for heavy-ion systems through large-angle quasi-elastic scattering,". ,vol.3,no. 2319-7064 , 2014.

[21] K. S. Jassim , Q. J. Tarbool, "A Study of the surface diffuseness of inter-nucleus potential with quasi-elastic scattering for the $^{32,\ 34}$S+ ^{208}Pb," Albahir J., vol. 1, no. 1, p.125-140, 2015.

[22] Q. J. Tarbool, K. S. Jassim, and A. A. Abojassim, "Surface diffuseness parameter with quasi-elastic scattering for some heavy-ion systems," Int. J. Nucl. Energy Sci. Technol., vol. 13, no. 2, pp. 110–119, 2019.

[23] S. Biswas, , A.Chakraborty, , A.Jhingan, D.Arora, B.R.Behera, RohanBiswas , NabenduKumarDeb, S.S.Ghugre, PankajK.Giri , K.S.Golda,G.Kaur, A.Kumar, M.Kumar, B.Mukherjee , B.K.Nayak, A.Parihari, N.K.Rai, S.Rai R.Raut, RudraN.Sahoo , andA.K.Sinha. ,"Quasielastic scattering measurements in the ^{28}Si+^{142,150}Nd systems," Phys. Rev. C, vol. 102, no. 1, p. 14613, 2020.

[24] A. J. Hassan , K. S. Jassim, "Effect of surface diffuseness parameter on quasi-elastic scattering calculations for ^{6}He+^{64}Zn, ^{7}Li+^{64}Zn and ^{8}Li+^{90}Zr systems," NeuroQuantology, vol. 18, no. 9, pp. 40–44,. 2020.

[25] P. Biswas,A.Mukherjee1, D.Chattopadhyay,SaikatBhattacharjee, M.K.Pradhan,Md.MoinShaikh,SubinitRoy,A.Goswami,P.Basu1,S.S antra,S.K.Pandit,K.Mahata , A.Shrivastava., "Large back-angle

quasielastic scattering for ^{7}Li + ^{159}Tb," Phys. Rev. C, vol. 103, no. 1, pp.14606, 2021.

[26] N. H. Hayef , K. S. Jassim, "Coupled channels for quasi-elastic scattering of determining diffuseness parameters in Woods-Saxon potential for nuclear reaction Coupled Channels for Quasi-elastic Scattering of Determining Diffuseness Parameters in Woods-Saxon Potential for Nuclear Reaction,"., vol. 2414,pp. 030012 ,2023.

[27] J. R. Taylor,"Scattering theory"the quantum theory of nonrelativistic collisions., Canada, published simultaneously ,1972.

[28] D. A. Bromley, "Treatise on Heavy-Ion Science: Nuclei Far From Stability". New York,Plenum publishing Corporation 1985.

[29] C. J. Joachain, "Quantum collision theory," North-Holland; Amsterdam, The Netherlands,1975.

[30] J. Toke and W. U. Schroder,"Excitation energy division in dissipative heavy-ion collisions," Annu. Rev. Nucl. Part. Sci., vol. 42, no. 1, pp. 401–446, 1992.

[31] F. A. Majeed, R. S. Hamodi, and F. M. Hussian, "Semiclassical coupled channels calculations in heavy-ion fusion reaction," Adv. Stud. Theor. Phys., vol. 11, no. 9, pp. 415–427, 2017.

[32] E. Merzbacher, Quantum mechanics. John Wiley and Sons, 1998.

[33] R. D. Woods and D. S. Saxon, "Diffuse surface optical model for nucleon-nuclei scattering," Phys. Rev., vol. 95, no. 2, p. 577, 1954.

[34] K. Hagino and N. Takigawa, "Subbarrier fusion reactions and many-particle quantum tunneling," Prog. Theor. Phys., vol. 128, no. 6, pp. 1061–1106, 2012.

[35] B. A. Brown, "Lecture notes in nuclear structure physics," Natl. Super Conduct. Cyclotr. Lab., vol. 11, 2005.

[36] L. Gan, Z. H. Li, H. B. Sun, S. P. Hu, E. T. Li, and J. Zhong, "Systematic study of the Woods-Saxon potential

parametersbetween heavy-ions," Chinese Phys. C, vol. 45, no. 5, p. 54105, 2021.

[37] N. K. Glendenning, "Interplay of classical and quantal descriptions of heavy-ion interactions," Rev. Mod. Phys., vol. 47, no. 3, p. 659, 1975.

[38] A. Messiah, "Quantum mechanics", New York, Mineola, 2014.

[39] J. D. Walecka, "Theoretical nuclear and subnuclear physics". World Scientific, 2004.

[40] H.Timmers, " Expressions of Inner Freedom", Ph.D. thesis, Australian National University , 1996.

[41] Q. J. Tarbool. ALKraawi, "Probing Surface Diffuseness Parameters of Inter-Nucleus Potential Quasi- Elastic Scattering in some Heavy-Ion Systems," thesis, Babylon University,2015.

[42] F. M. Hussain, "Semiclassical Approach for Nuclear Fusion Reactions of Some Medium and Heavy Nuclei," Ph.D. thesis,Al-Mustansiriya University , 2017.

[43] K. Desalegn, "Complete and Incomplete Fusion Reactions in ^{16}O+ ^{93}Nb Systems at Various Projectile Energies." thesis, Addis Ababa University, 2013.

[44] H. Paetz gen. Schieck and H. Paetz gen. Schieck, "Nuclear Reactions of Particles with Spin," *Nucl. React. An Introd.*, pp. 105–123, 2014.

[45] W. Nörenberg, H. A. Weidenmüller, W. Nörenberg, and H. A. Weidenmüller, "Coulomb excitation," *Introd. to Theory Heavy-Ion Collisions*, pp. 152–177, 1976.

[46] M. Weber and C. Herlitzius, "Heavy Ion Scattering at the Tandem Accelerator," Technical report, Technische Universität München page 30), 2010.

[47] J. Lilley ,John Wiley and Sons" Nuclear physics principles and

applications"., 2013.

[48] E. Krane ,S. Kenneth," Introduction Nuclear Physics".,New York, John Wiley and Sons,1988.

[49] S. S. M. Wong, "Introductory nuclear physics".Germany, John Wiley and Sons ,1998.

[50] H. Paar, "An Introduction to Advanced Quantum Physics"., New York ,John Wiley and Sons, 2010.

[51] G. Esposito, G. Marmo, G. Miele, and G. Sudarshan, "Advanced concepts in quantum mechanics". Cambridge, University Press, 2014.

[52] G. B. Arfken and H. J. Weber, "Mathematical methods for physicis." American Association of physics teachers, 1999.

[53] E. D. A. H. Kazim, "Effect of Coupled Channels in Elastic and Inelastic Scattering of Weakly Bound Nuclei for some Selected Systems," thesis, 2014.

[54] Y.K.Gupta, B.K.Nayak, U.Gargc, K.Hagino, K.B.Howard, N.Sensharmac, M.¸Senyigite, W.P.Tanc, P.D.OMalleyc, M.Smithc, RamandeepGandhi,T.Anderson,R.J.deBoer,B.Frentzc,A.Gyurjinyan , O.Hall, M.R.Hall, J.Huc, E.Lamere, Q.Liu, A.Lo, "Determination of hexadecapole (β4) deformation of the light-mass nucleus ^{24}Mg using quasi-elastic scattering measurements," Phys. Lett. B, vol. 806, p. 135473, 2020.

[55] A. R. Edmonds, "Angular momentum in quantum mechanics",. Princeton university press, vol. 4,p.146,1996.

[56] K. Hagino, N. Takigawa, A. B. Balantekin, and J. R. Bennett, "Path integral approach to no-Coriolis approximation in heavy-ion collisions," Phys. Rev. C, vol. 52, no. 1, p. 286, 1995.

[57] A. T. Kruppa, P. Romain, M. A. Nagarajan, and N. Rowley, "Effect of multiphonon coupling on heavy-ion fusion," Nucl. Phys. A, vol.

560, no. 3, pp. 845–862, 1993.

[58] K. Hagino and N. Rowley, “Large-angle scattering and quasielastic barrier distributions,” Phys. Rev. C, vol. 69, no. 5, p. 54610, 2004.

[59] A. Bohr, I. Hamamoto, and B. R. Mottelson, “Pseudo spin in rotating nuclear potentials,” Phys. Scr., vol. 26, no. 4, p. 267, 1982.

[60] M. Dasgupta, D. J. Hinde, N. Rowley, and A. M. Stefanini, "Measuring Barriers to Fusion," vol. 48, p.401-461, 1998.

[61] J. de Boer and J. Eichler, “The reorientation effect,” Adv. Nucl. Phys. vol. 1, pp. 1–65, 1968.

[62] M. Zamrun, K. Hagino, S. Mitsuoka, and H. Ikezoe, “Coupled-channels analyses for large-angle quasi-elastic scattering in massive systems,” Phys. Rev. C, vol. 77, no. 3, p. 34604, 2008.

[63] K. Hagino, S. Kuyucak, and N. Takigawa, “Excitation of nuclear anharmonic vibrations in heavy-ion fusion reactions,” *Phys. Rev. C*, vol. 57, no. 3, p. 1349, 1998.

[64] L. R. Gasques et al., "Systematic study of the nuclear potential through high precision back-angle quasi-elastic scattering measurements," Phys. Rev. C, vol. 76, no. 2, p. 24612, 2007.

[65] F.LachelloandA.Arima,"PhaseCoexistenceinTransitionalNucle iandtheInteracting-BosonModel." Cambridge University Press, Cambridge, vol.81,p.1191-1194 , 1987.

[66] N. Rowley, G. R. Satchler, and P. H. Stelson, "distribution of barriers’ interpretation of heavy-ion fusion,"Phys. Lett. B, vol. 254, no. 1–2, pp. 25–29, 1991.

[67] S. Biswas, A. Chakraborty , A. Jhingan , D. Arora , B.R. Behera , Rohan Biswas , N. Kumar , S.S. Ghugre , P. K. Giri , K.S. Golda , G. Kaur , A. Kumar , M. Kumar , B. Mukherjee , B.K. Nayak, A. Parihari , N.K. Rai , S. Rai , R. Raut , Rudra N. Sahoo , and A.K. Sinha., "Barrier distribution for the ^{28}Si+ ^{150}Nd system through

quasi-elastic excitation function measurement," in Proceedings of the DAE Symp. on Nucl. Phys, vol. 64, p. 439,2019.

[68] S. Raman, C. W. Nestor Jr, and P. Tikkanen, "Transition probability from the ground to the first-excited 2+ state of even–even nuclides,"At. Data Nucl. Data Tables, vol. 78, no. 1, pp. 1–128, 2001.

[69] B.K. Nayak , A. Saxena1 Sukanya, G. Mohanto, A. Parihari, E.T. Mirgule, B. Srinivasan, P.C. Rout, 1 M. Kushwaha, S. Arora, C. Joshi, A. Sharma, "Determination of hexadecapole deformation for ^{160}Gd nucleus using quasi-elastic scattering," in Proceedings of the DAE Symp. on Nucl. Phys, vol. 62, p. 398, 2017.

[70] A. K. S. N K Ghosh1, S .Chatterjee1, R. Raut1, S .S. Ghugre, A. Rani, S. Mandal, D. Kaur, B. R. Behera, A .Vinayak, M. M. Hosamani, C. Bhattacharya, A. Roy, I. Mazumdar, R. Biswas, A. Parihari, J. Gehlot, S. Nath, N. Madhavan, "Back angle quasi-elastic scattering and Fusion Excitation function and studies for the ^{12,13}C+^{197}Au reaction.," in Proceedings of the DAE Symp. on Nucl. Phys, , vol. 64, p 557,2019 .

[71] R. Fereidonnejad and H. Sadeghi, "Heavy-Ion Fusion and Quasi-Elastic Scattering Of ^{6,7}Li+ ^{144}Sm and ^{6,7}Li+ ^{152}Sm Reactions Using Coupled-Channel Calculation Around the Coulomb Barrier,"J. Res. Many-body Syst., vol. 11, no. 2, pp. 84–97, 2021.

[72] P. Biswas , P. Biswas, A. Mukherjee, D. Chattopadhyay, S.Bhattacharjee, M. K. Pradhan, M. Moin Shaikh, S. Roy, A. Goswami, P. Basu, S. Santra, S. K. Pandit, K. Mahata, and A. Shrivastava., "Quasielastic backscattering and barrier distribution for the weakly bound projectile ^{6}Li on ^{159}Tb,." *Phys. Rev. C*, vol. 104, no. 3, p. 34620, 2021.

[73] T. Tanaka, K. Morita, K. Morimoto, D. Kaji, H. Haba, R. A. Boll, N. T. Brewer, S. Van Cleve, D. J. Dean, S. Ishizawa, Y. Komori,K. Nishio, T. Niwase, B. C. Rasco, J. B. Roberto, K. P. Rykaczewski, H. Sakai, D. W. Stracener, and K. Hagino , "Study of quasielastic barrier distributions as a step towards the synthesis of superheavy elements with hot fusion reactions," Phys. Rev. Lett., vol. 124, no. 5, p. 52502, 2020.

[74] S. Dubey, D. C. Biswas, S. Mukherjee, D. Patel, Y. K. Gupta, G. K. Prajapati, B. N. Joshi, L. S. Danu, S. Mukhopadhyay, B. V. John, S. V. Suryanarayana, and R. P. Vind ., "Quasi-elastic scattering and transfer angular distribution for $^{10,\ 11}$B+ ^{232}Th systems at near-barrier energies," Phys. Rev. C, vol. 94, no. 6, p. 64610, 2016.

الخلاصة

في هذا الدراسة ، أحد المكونات الأساسية لفهم التصادم بين نواتين هو معرفة الجهد النووي بين تلك النواتين المتصادمتين ، والذي يحدث عندما تكون قريبة بما يكفي للتصادم ، من أجل تحليل الجهد النووي. لقد ثبت أن التشتت شبه المرن بزاوية كبيرة هو أسلوب فعال لفحص الجهود النووية. تم وصف الجهود التي تصف التفاعلات بين النوى ، والتي تتكون جهد كولوم والجهد النووي ، باستخدام إمكانات Woods-Saxon (WS). تم إجراء حسابات القناة المفردة (SC) والقناة المقترنة (CC) للتحقيق في الحركة النسبية للنواة المتصادمة وحركاتها الداخلية وتأثيرها على حساب نسبة المقاطع العرضية شبه المرنة إلى المقاطع العرضية المتناثرة في رذرفورد ، وكذلك التحقيق في طريقة الانتشار السطحي للعثور على أفضل قيمة مناسبة لمعلمات الانتشار مقارنة بالبيانات التجريبية. في هذه الأطروحة ، تم اجراء دراسة وتحليل منهجي للجهد النووي (معلمات انتشار السطح ، العمق المحتمل) لأنظمة الأيونات الثقيلة التالية: $^{24}Mg+^{90}Zr$,$^{28}Si+^{120}Sn$,$^{28}Si+^{150}Nd$,$^{16}O+^{160}Gd$, $^{12}C+^{197}Au$, $^{6}Li+^{144}Sm$,$^{28}Si + ^{124}Sn$, ^{6}Li . $^{22}Ne+^{248}Cm$,$^{10}B+^{232}Th$,^{159}Tb+. تم استخدام برنامج الكمبيوتر CQEL ، والذي يعتبر أحدث إصدار من برنامج الكمبيوتر CCFUL. تمت برمجته بواسطة هاجينو وزملاؤه من العلماء اليابانيين. تم استخدام طريقة مربع كاي χ^2 للعثور على أفضل القيم المناسبة لـ (معلمات الانتشار a_0 والعمق المحتمل V_0) بناءً على مقارنة الحسابات النظرية والبيانات التجريبية .

في هذه الأنظمة ($^{6}Li + ^{144}Sm$, $^{6}Li +^{159}Tb$, and $^{10}B+^{232}Th$) ، وجد أن أفضل قيمة لمعلمة الانتشار تم تحديدها باستخدام حساب القنوات المقترنة باستخدام مقذوف خامل وهدف مثار ، باستثناء النظام $^{28}Si+^{150}Nd$ ، حيث ان الهدف خامل والقذيفة مثارة ، ونفس الشيء بالنسبة للأنظمة ($^{28}Si+^{120}Sn$, $^{24}Mg+^{90}Zr$, $^{28}Si + ^{124}Sn$, $^{12}C+^{197}Au$, $^{16}O+^{160}Gd$ and $^{22}Ne + ^{248}Cm$) ولكن باستخدام هدف مثار وقذيفة مثارة.

معامل الانتشار لهذه الأنظمة $^{28}Si+^{150}Nd$, $^{12}C+^{197}Au$, $^{6}Li+ ^{144}Sm$ يتوافق تمامًا مع القيمة القياسية fm (0.63) في حسابات القناة المقترنة.

في الجزء الثاني من الحسابات، لبعض الأنظمة المدروسة، كان تأثير تغيير عمق الجهد (V_0) على النسبة المحسوبة للتشتت شبه المرن إلى مقطع رذرفورد العرضي متفقاً مع عمق الجهد الذي تم اعتماده كقيمة قياسية أو بقيمة أقل منها.

جمهورية العراق
وزارة التعليم العالي والبحث العلمي
جامعة بابل
كلية التربية للعلوم الصرفة
قسم الفيزياء

حسابات الإستطارة شبه المرنة في بعض أنظمة الايونات الثقيلة

اطروحة مقدمة
الى مجلس كلية التربية للعلوم الصرفة جامعة بابل
كجزء من متطلبات نيل درجة الدكتوراه
فلسفة في التربية / الفيزياء

من قبل الطالبة

فرح جبار حمود عبد الحسين

بكالوريوس تربية فيزياء / جامعة بابل ٢٠٠٤ م
ماجستير تربية فيزياء / جامعة بابل ٢٠١٦ م

بأشراف

أ. د. خالد صالح جاسم

كلية التربية للعلوم الصرفة

قسم الفيزياء

١٤٤٥هـ **٢٠٢٣ م**